AN ABSTRACT OF THE DISSERTATION OF

Mark A. Matheson for the degree of Doctor of Philosophy in Atmospheric Sciences presented on December 13, 2005.

Title: Aerosol Indirect Radiative Forcing over the Northeastern Atlantic from AVHRR Observations.

Abstract approved:

Redacted for privacy

James A. Coakley, Jr.

Advanced Very-High Resolution Radiometer 4-km data were collected over the northeast Atlantic for May-August, 1995-1999. Aerosol optical depth was retrieved in cloud-free pixels. In pixels containing clouds from only single-layered, low-level systems, a retrieval scheme that accounts for partly-cloudy pixels was used to retrieve: cloud optical depth, droplet effective radius, cloud altitude, pixel-scale fractional cloud cover, liquid water path and column droplet concentration. Mean aerosol optical depths from 1° × 1° latitude-longitude regions were associated with mean cloud properties in the same region for the same satellite overpass. Results were composited for 5° latitude-longitude regions. As aerosol optical depth increased, droplet radius decreased and column droplet number concentration and cloud optical depth increased, consistent with the aerosol indirect effect. In many regions, liquid water path decreased as aerosol optical depth increased, contrary to the trends expected for drizzle suppression. The simultaneous increase in aerosol and cloud optical depths with increasing fractional

cloud cover might be mistaken for the aerosol indirect effect. The five-year data set was sorted into clean and polluted cases. Clouds in clean air had larger droplets and smaller cloud optical depths than clouds in polluted air, consistent with the aerosol indirect effect. Liquid water path increased as fractional cloud cover increased but no difference was found between clouds in clean and polluted air. Influences other than changes in aerosol burden may be controlling changes in liquid water. Observed changes in aerosol and cloud properties were used to estimate the aerosol indirect radiative forcing. Aerosol indirect forcing for overcast conditions was 1.4-2.2 times larger than the aerosol direct radiative forcing for cloud-free conditions. To simulate threshold retrievals, which do not account for partial cloud cover in partly-cloudy pixels, radiances in pixels that had a fractional cloud cover greater than 0.20 were used to recalculate cloud properties assuming the pixel was overcast. The decrease in droplet radii and increase in cloud optical depths for a given change in aerosol optical depth were larger using threshold retrievals than when using partly-cloudy retrievals. Threshold retrievals lead to a significant overestimation of the aerosol indirect radiative forcing.

Aerosol Indirect Radiative Forcing over the Northeastern Atlantic from AVHRR Observations

by

Mark A. Matheson

A DISSERTATION

submitted to

Oregon State University

in partial fulfillment of
the requirements for the
degree of

Doctor of Philosophy

Presented December 13, 2005

Commencement June 2006

Doctor of Philosophy dissertation of Mark A. Matheson presented on December 13, 2005

APPROVED:

Redacted for privacy

Major Professor, representing Atmospheric Sciences

Redacted for privacy

Dean of the College of Oceanic and Atmospheric Sciences

Redacted for privacy

Dean of the Graduate School

I understand that my dissertation will become part of the permanent collection of Oregon State University libraries. My signature below authorizes release of my dissertation to any reader upon request.

Redacted for privacy

Mark A. Matheson, Author

ACKNOWLEDGEMENTS

I offer my sincere thanks to everyone who helped and supported me during my time at Oregon State University. Without my friends and co-workers, this thesis would not have been possible.

I thank my advisor, Jim Coakley. Your insight and guidance were the driving force behind the science in this thesis. Your patience and your funding were also greatly appreciated.

Thanks to Bill Tahnk, my co-worker and co-author. Your help with science and your advice, based on your first-hand experience of earning a Ph.D., were invaluable.

I thank all my fellow students in Jim's lab: Matt S., Chris H., Chris W., Gunnar, Jason, Matt C., and Andrea. You made the lab a friendly place to come and work.

Thanks also to everyone else in Atmospheric Sciences for both your scientific assistance and your friendship, especially Nic and Craig. And thanks to all my friends outside of ATS, too numerous to mention.

Thanks to my parents who have always supported all my endeavors, including going back to school yet again.

I especially thank my partner, Reina Nakamura. Without you, I could not have made it through this process.

TABLE OF CONTENTS

LIST OF FIGURES

LIST OF FIGURES (Continued)

LIST OF TABLES

Chapter 1
Introduction

1.1 Background

In the last decade the scientific community has reached the consensus that human activity is warming the Earth's climate (IPCC, 2001), although the magnitude and regional variations of this warming are still being debated. The process in which the increase in greenhouse gases from anthropogenic sources warms the climate is well understood. In climate science, the Earth's climate sensitivity describes how much global mean temperature changes in response to a climate forcing. Climate forcing has units of Watts per square meter (W/m^2), a measure of the amount of energy per unit time per unit area that is entering or leaving the Earth-atmosphere system. Climate forcing is the net change in energy entering or leaving the Earth-atmosphere system that was caused by a change in a particular physical process. The increase in greenhouse gases since the start of the industrial revolution is estimated to cause a 2.5 W/m^2 warming, which, if that were the only change, would lead to approximately a 1.25 °C increase in the global, annual average surface temperature.

In addition to the greenhouse gases, aerosols also influence global climate. An aerosol is any solid or liquid particle suspended in the atmosphere. Aerosols can absorb and reflect incoming solar radiation. The direct interaction between aerosols and radiation can alter the energy budget of the Earth-atmosphere system, a process known as aerosol direct radiative forcing. Depending on the composition of the aerosol and the underlying surface, this interaction can either cause warming or cooling. Sulfate aerosols over a dark, oceanic surface will have a cooling effect. As a global average, aerosol direct radiative forcing is believed to be a cooling of about –0.5 W/m^2, much smaller in magnitude than the warming caused by the increase in greenhouse gases (IPCC, 2001).

Clouds have a major impact on global climate. It is estimated that the presence of clouds cools the Earth by approximately 10 °C (Ramanathan et al., 1989) and that a 5% increase in the amount of low-level clouds would offset the warming caused by a doubling of CO_2.

Cloud droplets do not form spontaneously, rather they form on a subset of aerosols known as cloud condensation nuclei (CCN). Increasing the number of CCN that enter a cloud will cause the cloud to have more cloud droplets than it would have had without the additional aerosols. Under the simplifying assumption that the amount of liquid water in the cloud does not change, adding more droplets to the cloud will cause the droplets to be smaller than they would have been and the cloud to be more reflective. The increase in the reflectivity of the cloud will cause the Earth to cool. The processes in which aerosols affect the radiative properties of clouds are collectively called the aerosol indirect radiative forcing. Because this process was first suggested by Twomey (1974) it is also called the Twomey Effect. Albrecht (1989) extended the idea of the Twomey Effect by noting that clouds with smaller droplets are less likely to form drizzle. Because clouds are not precipitating they may have longer lifetimes and cover larger areas. These effects will also cause the Earth to cool. According to the IPCC report on climate change (2001), uncertainty in the magnitude of aerosol indirect radiative forcing is the largest uncertainty in assessing human impact on climate. The IPCC states that the cooling due to aerosol indirect radiative forcing may be so large that it would nearly offset the warming caused by the buildup of greenhouse gases.

1.2 Using satellites to measure aerosol indirect radiative forcing

Clouds are highly variable, even when aerosol amounts are constant. A large data set is necessary to distinguish the signal of the Twomey Effect from this background variability. Taking measurements over a large area, as opposed to single-point measurements, aids in detecting the signal of the Twomey Effect as

well as providing information on its spatial variability. Satellite measurements are uniquely suited to provide such a data set.

Previous studies have used satellite data to investigate the aerosol indirect radiative forcing. Kaufman and Nakajima (1993) used Advanced Very High Resolution Radiometer (AVHRR) data to measure the reduction of cloud droplet size in the presence of smoke from biomass burning over the Amazon Basin. This study was later extended (Kaufman and Fraser, 1997) to estimate the radiative forcing of the effects of the smoke on the clouds. Han et al. (1994) performed a near-global survey of cloud droplet radii and found trends consistent with cloud-aerosol interaction, which include systematically smaller droplets in the Northern Hemisphere and also over land. In a later study (Han et al., 1998), similar evidence was found in a global survey of column droplet concentration. Wetzel and Stowe (1999) showed a decrease in droplet effective radius as aerosol optical depth increased for AVHRR data divided into seasonal and 10° zonal bands.

A variety of cloud-aerosol relationships were investigated by Nakajima et al. (2001), who showed that as aerosol burden increases: droplet effective radius decreases, cloud optical depth increases, liquid water path remains relatively constant, and droplet number concentration increases. Nakajima et al. (2001) found that the increase in cloud optical depth and of column number concentration only occurs after a critical value of aerosol burden has been exceeded. Sekiguchi et al. (2003) expanded on the study of Nakajima et al. (2001) by investigating the spatial and temporal scales of cloud-aerosol interaction and by estimating the radiative forcing caused by the changes in cloud properties.

A decrease in cloud droplet radius as aerosol burden increased was measured by Bréon et al. (2002) and Quass et al. (2004) using the POLDER (Polarization and directionality of the Earth's reflectances) instrument.

In this literature review, the focus has been on those studies that used exclusively satellite observations and omitted studies using in-situ measurements or satellite studies that relied on model results. These model-dependent studies combine satellite observations of cloud properties with model estimates of aerosol

burdens (Harshvardhan et al., 2002; Krüger and Grassl, 2002; Schwartz et al., 2002) or use satellite observations to validate the results of their atmospheric models (Lohmann and Lesins, 2002; Nakajima et al., 2003; Suzuki et al., 2004).

1.3 Outline of Thesis

This thesis presents the results of three papers that have been submitted or will be submitted to peer-reviewed scientific journals. These three papers share the common theme of using AVHRR observations to measure changes in clouds in response to different levels of aerosol burdens and to estimate the radiative forcing brought about by the changes to the clouds. There are three overarching themes to the research: to provide independent validation of previous studies of the Twomey Effect, to explore a refined methodology for measuring the Twomey Effect, and to illustrate situations in which correlations may erroneously indicate that the Twomey Effect is active.

All three studies in this thesis use data from the northeastern Atlantic during the months of May-August. This time and location is characterized by extensive fields of marine stratus and stratocumulus clouds, which are ideal clouds for performing cloud property retrievals. In addition, a wide range of aerosol optical depths is encountered due to frequent incursions of aerosol-laden air from the European continent into the relatively clean air over the Atlantic.

Chapter 2 introduces a refined methodology for studying the Twomey Effect. One improvement over previous studies is that aerosol and cloud properties are associated only when they are from the same satellite overpass and in the same $1° \times 1°$ latitude-longitude region. Previous studies have associated cloud and aerosol properties from different days or from large geographic distances. The constraints of simultaneity and relatively close geographic separation help to ensure that observed cloud properties might exhibit influences due to the observed aerosol burdens. Another way in which this study ensures that results accurately assess

cloud-aerosol interaction is by compositing results into relatively small 5° × 5° latitude-longitude geographic regions. Other studies have used larger, even global, scales for compositing their data.

The results of chapter 2 were drawn from a single year of observations. The methodology presented in chapter 2 is used on a five-year data set and the results of this study are presented in Chapter 3. Because the data set of chapter 3 is five times the size of that of chapter 2, greater statistical confidence in the results is possible. In addition, the greater volume of data allowed the observations to be divided into "clean" and "polluted" cases based on the 40^{th} and 60^{th} percentiles of the aerosol optical depth observed over the northeastern Atlantic during May-August. Changes in cloud properties associated with changes in fractional cloud cover can be made for both the "clean" and "polluted" clouds in order to compare the relative influences on cloud properties of changes in aerosol effect, which are attributable to the Twomey Effect, and changes in fractional cloud cover, which should not be attributed to the Twomey Effect.

The studies in chapters 2 and 3 made use of a new algorithm that retrieves cloud properties in imager pixels that are partially covered by clouds. All previous studies of the Twomey Effect have used cloud properties retrieved using a threshold retrieval, in which cloudy pixels are assumed to be overcast regardless of the actual cloud cover. Such retrievals are known to bias the cloud properties in partly cloudy pixels (Coakley et al., 2005). These biases make it appear as if cloud optical depth increases and droplet effective radius decreases as fractional cloud cover increases. It will be shown that aerosol optical depth also appears to increase as fractional cloud cover increases. The apparent increase in aerosol optical depth, increase in cloud optical depth and decrease in droplet effective radius as fractional cloud cover increases can be mistaken for the Twomey Effect. Chapter 4 presents a comparison of cloud property retrievals and radiative forcing results found using the partly cloudy pixel retrieval scheme and a threshold retrieval scheme.

Conclusions and suggestions for future work are found in Chapter 5.

Chapter 2
Aerosol and cloud property relationships for summertime stratiform clouds in the northeastern Atlantic from AVHRR Observations

2.1 Abstract

Advanced Very High Resolution Radiometer (AVHRR) 4-km data collected over the northeastern Atlantic off the coast of the Iberian Peninsula for May-August, 1995 were used to investigate the feasibility of empirically deriving estimates of the aerosol indirect radiative forcing. A retrieval scheme was used to derive cloud visible optical depth, droplet effective radius, cloud layer altitude, and pixel-scale fractional cloud cover. A 2-channel aerosol retrieval scheme was used to determine aerosol optical depth in cloud-free pixels. Mean aerosol optical depths derived from the cloud-free pixels in 1° × 1° latitude-longitude regions on a given satellite overpass were associated with mean cloud properties derived from the cloudy pixels in the same region for the same satellite overpass. The analysis was restricted to 1° regions that contained only single-layered, low-level cloud systems. Because aerosol and cloud properties are highly variable, results for the four-month period were composited into 5° × 5° latitude-longitude regions and averaged to obtain reliable trends in the cloud properties as functions of aerosol burden. Consistent with expectations for the aerosol indirect effect, in some 5° regions, droplet effective radii decreased and cloud visible optical depths increased as aerosol optical depths increased. The hypothesis that drizzle is suppressed in polluted clouds predicts that liquid water path should increase as aerosol burden increases. In three of the thirteen 5° regions studied, the liquid water path increased as aerosol optical depth increased but in none of the regions was the increase in cloud liquid water statistically significant. In the remaining regions cloud liquid water remained constant or even decreased with increasing aerosol optical depth. In many of the 5° regions, the retrieved aerosol optical depth

increased as the percentage of cloudy pixels increased. Consistent with expectations from adiabatic cloud parcel models, droplet effective radius, cloud optical depth, and cloud liquid water path also increased as fractional cloud cover increased. The simultaneous increase in retrieved aerosol and cloud optical depths with increasing fractional cloud cover might have been due to the aerosol indirect effect, but it might also have resulted from processes that affect both the cloud and aerosol properties as cloud cover changes. The dependence on fractional cloud cover suggests that some of the trends between aerosol optical depth and the cloud properties cannot be solely attributed to the effects of the aerosols. For comparison with previous studies, the simultaneous changes in aerosol and cloud properties were used to estimate the daily average aerosol indirect forcing for overcast conditions in the summertime northeastern Atlantic. The magnitude of the indirect forcing relative to that of the direct forcing reported here is smaller than estimates reported by others.

2.2 Introduction

The effect of particulates on clouds and their consequent effect on the sunlight reflected by clouds was first noted by Twomey (1974) and is known as the "Twomey Effect" or aerosol indirect radiative forcing. Starting with Kaufman and Nakajima (1993), several studies have used satellite imagery data to deduce the effect of aerosols on clouds by correlating aerosol and cloud properties within localized regions (Kaufman and Fraser, 1997; Wetzel and Stowe, 1999; Nakajima et al., 2001; Sekiguchi et al., 2003; Quaas et al., 2004). Among the goals of these studies were 1) provide evidence for cloud-aerosol interactions on regional and global scales, and 2) empirically derive estimates of the aerosol indirect effect which might limit the large uncertainty in model estimates of the aerosol indirect radiative forcing. Partly because they rely on climate model simulations of cloud properties, which are known to be poor (Randall et al., 2003; Potter and Cess,

2004), model estimates of the indirect forcing, are highly uncertain (Lohmann and Feichter, 1997; Rotstayn, 1999; Lohmann et al., 2000; Lohman and Lesins, 2002). The model estimates lead to the "poor confidence" and large uncertainty associated with the aerosol indirect radiative forcing as assessed by the Intergovernmental Panel on Climate Change (IPCC, 2001).

Here the strategy of correlating aerosol properties with collocated cloud properties to deduce the indirect effect of aerosols was re-examined by analyzing *NOAA-14* 4-km AVHRR observations of marine stratus and stratocumulus and aerosol burden in the northeastern Atlantic for the summer of 1995. The region and season were selected because 1) stratus and stratocumulus are the dominant cloud system and 2) the flow is sufficiently weak that frequent intrusions of polluted air from Europe encroach on the marine environment (Brengruier et al., 2000a). Also, the *NOAA-14* satellite was launched in December 1994 and the radiometric calibration of the AVHRR visible channel has been characterized for the summer of 1995 (Tahnk and Coakley, 2001ab). Although AVHRR has fewer spectral bands and coarser resolution than currently available with the Moderate Resolution Imaging Spectrometer (MODIS) (e.g. King et al., 2003), the AVHRR was used because of the multi-year length of its data record, which will be exploited in a forthcoming paper (Matheson et al., 2005b).

This satellite study differs from the previous satellite assessments in a variety of ways. First, the aerosols and the clouds were collocated at the same time in relatively small regions (1° × 1° latitude-longitude). This condition of simultaneity and collocation avoided the possibility of aerosols occurring on one day in one location being compared with cloud properties on another day in another location as was possible in some of the earlier studies (Wetzel and Stowe, 1999; Sekiguchi et al., 2003). Likewise, the relatively small region in which the clouds and aerosols were collocated also avoided attributing the appearance of a cloud response in one location to the effects of aerosols in another location (Sekiguchi et al., 2003; Quaas et al., 2004). Second, results from the simultaneous occurrence of clouds and aerosols were composited within relatively limited geographic regions (5° × 5°

latitude-longitude). Again, the restriction avoided comparisons of clouds in geographic regions subject to heavy aerosol burdens accompanied by one set of thermodynamic conditions with clouds in other geographic regions subject to light aerosol burdens accompanied by possibly distinctly different thermodynamic conditions as could have arisen in the global surveys performed by Nakajima et al. (2001) and Sekiguchi et al. (2003). Third, only regions with single-layered, low-level, maritime clouds were examined in order to avoid multi-layered cloud systems, which might have contaminated the results in the earlier studies.

In this study, the cloud properties were retrieved using a scheme that accounts for the partial cloudiness of the pixels (Coakley et al., 2005). While some earlier studies sought to avoid pixels that were partially covered (Wetzel and Stowe, 1999; Nakajima et al., 2001), the retrieval schemes relied on the assumption that the pixels used to obtain the cloud properties were overcast. Such retrievals generally lead to estimates for partly cloudy pixels of cloud droplet effective radii that are larger and optical depths that are smaller than would be obtained if the pixels were overcast (Han et al., 1994; Platnick et al., 2003). Consequently, as a region fills with clouds and the number of partly cloudy pixels decreases, cloud droplet effective radius might decrease while optical depth increases simply because of the biases in cloud properties associated with the assumption of overcast pixels. As aerosol optical depth has been found to increase with increasing cloud cover (Sekiguchi et al., 2003; Ignatov et al., 2005; Loeb and Manalo-Smith, 2005), correlations between aerosol burden and the biased retrieved cloud properties that arise as cloud cover increases could be misinterpreted as evidence of the Twomey Effect. The partly cloudy pixel retrieval scheme used here yields droplet radii and cloud optical depths that are both smaller, but only slightly so, for the clouds in the partly-cloudy pixels when compared with those of clouds in nearby overcast pixels and is therefore less susceptible to trends that would mimic those associated with the Twomey Effect. Nonetheless, as is shown in Section 2.4, cloud properties also vary systematically with regional cloud cover in ways that mimic expectations based on adiabatic cloud parcel models. Consequently, some of the trends between

cloud properties and aerosol burden might be attributable to the response of the clouds to thermodynamic processes.

2.3 Cloud and Aerosol Properties

Global Area Coverage (GAC) radiances, with a nominal nadir resolution of 4 km, measured by the Advanced Very High Resolution Radiometer (AVHRR) on board the National Oceanic and Atmospheric Administration (NOAA) satellite, *NOAA-14*, were analyzed for the months of May through August of 1995. All daytime satellite overpasses from the four months were used. The analysis area chosen for this study was in the northeastern Atlantic bounded by 35° – 55° N latitude and 20° W – 0° longitude. Although the region includes parts of Europe, cloud and aerosol properties were retrieved only over the ocean. The study region contained both coastal and open ocean regions. In addition, periods of both sustained onshore and offshore flow were observed in the NCEP reanalysis wind fields. These geographic and meteorological conditions allow for the analysis of a wide range of aerosol burdens and their effects on clouds. This region has also been studied in a variety of field campaigns such as the Atlantic Stratocumulus Transition Experiment (ASTEX) (Albrecht et al., 1995) and the Second Aerosol Characterization Experiment (ACE–2) (Raes et al., 2000).

Channel 1 (0.64 μm) of the AVHRR was calibrated in reference to the radiometrically stable ice sheets of Antarctica (Tahnk and Coakley, 2001ab). An on-board blackbody and deep-space views were used to calibrate channels 3 and 4 (3.7 and 11 μm) (Kidwell, 1995). Imager pixels containing land were identified by the latitude and longitude included in the AVHRR data stream and were removed from further analysis. Pixels which may be affected by sun glint are assumed to be those for which the angle of reflection is within 40° of that for specular reflection from a flat surface. Pixels in the sun glint were removed from the analysis. A

scene identification scheme was used to determine if the 4-km pixels were cloud-free, completely overcast by clouds in a single layer, partially covered by clouds, or overcast by clouds that were distributed in altitude (Coakley et al., 2005).

Aerosol optical depths at 0.55 μm were retrieved in the imager pixels identified as cloud-free using a two-channel method originally developed to obtain aerosol properties from AVHRR for the Indian Ocean Experiment (INDOEX) (Coakley et al., 2002). For the INDOEX aerosols, the bias and RMS error in the aerosol optical depth at 0.65 μm were 0.01 ± 0.06 when compared to surface sun photometer data. While the retrieval scheme for the aerosols differentiated between a fine mode aerosol, an average continental aerosol described by Hess et al. (1998), and a coarse mode aerosol, a marine aerosol, the correlations performed here were between cloud properties and total aerosol optical depth, which is given by the sum of the fine and coarse mode aerosol optical depths. The total aerosol optical depth yielded the strongest correlations with cloud droplet effective radius. As the fine mode fraction for the region was found to be 0.66, the fine mode optical depth and total aerosol optical depth produced much the same correlations with droplet effective radius, while the coarse mode optical depth produced little correlation. Nonetheless, in all but one of the 5° latitude-longitude regions for which the correlations were significant when using both the total aerosol optical depth and the fine mode optical depth, or using both the total optical depth and the coarse mode optical depth, the trends in the cloud properties with aerosol optical depth were in the same direction.

Cloud properties were retrieved using the method of Coakley et al. (2005). For pixels that the scene identification scheme identified as being overcast by optically thick single-layered clouds, radiances at 0.64, 3.7 and 11 μm were used to retrieve cloud optical thickness, droplet effective radius, and cloud layer altitude. For partly-cloudy pixels the clouds were assumed to be at the mean altitude retrieved for the nearby overcast pixels. In addition, the pixel radiances were assumed to have a linear mixture of the radiances that would be seen if the pixels were either completely overcast or completely cloud-free, so that,

$$I = (1 - A_c) I_s + A_c I_c(\tau_c, R_e, z_c)$$

where I is the radiance observed by the satellite instrument, A_c is the fractional cloud cover for the pixel, I_s is the average radiance for the cloud-free portion of the pixel, and $I_c(\tau_c, R_e, z_c)$ is the average radiance for the cloud-covered portion of the pixel and is a function of: τ_c, the cloud optical depth, R_e, the droplet effective radius, and, z_c, the cloud layer altitude. With z_c given by the altitude retrieved for nearby pixels that were overcast, radiances at 0.64, 3.7, and 11 μm were used to derive A_C, τ_C, and R_e. Radiances in the cloud-free portions of the partly-cloudy pixels were assumed to be equal to the mean of the radiances taken from nearby cloud-free pixels, or lacking sufficient nearby cloud-free pixels, from a monthly and regional climatology of cloud-free radiances.

An example of derived cloud and aerosol properties is shown in Figure 2.1. The region was covered largely by low-level clouds (Fig. 2.1a) but some high clouds were present on this day as indicated by their emission at 11 μm (Fig. 2.1b). As described below, 1° × 1° latitude-longitude regions that contain clouds that are not from single-layered, low-level systems were excluded from the data analysis . On this day, there was a high aerosol burden in the region off the Iberian Peninsula, but the air north of approximately 43° N was relatively clean (Fig. 2.1c). If the aerosol properties in the cloudy pixels are assumed to be similar to the aerosol properties in the nearby cloud-free pixels then the clouds off the coast of Iberia were in an environment with high aerosol burden, whereas the clouds further north were in an environment with a relatively low aerosol burden. The clouds in the north had larger droplet radii and the clouds near the coast of Iberia had smaller droplet radii (Fig. 2.1d). The relationship between droplet radius and aerosol burden illustrated in Fig. 2.1 is qualitatively consistent with that expected for the Twomey Effect.

The analysis in this study was limited to single-layered, low-level clouds. Regions off the western coast of most continents at mid-latitudes often contain marine boundary layer clouds and are regions likely to be susceptible to cloud-aerosol interaction (Nakajima et al., 2001). Screening rules were applied to the radiances and retrieved cloud properties within 1° × 1° latitude-longitude regions to identify regions in which all of the clouds were part of a single-layered, low-level system. If a cloud layer was present in the region, the mean cloud temperature and the 5th percentile of the 11-μm brightness temperature were required to be within 20 K of the mean surface temperature. In addition, to ensure that the clouds were in a well-defined layer, as opposed to being distributed in altitude, if the difference between the mean surface temperature and the mean cloud temperature was greater than or equal to 10 K then $(T_s - T_{5th})/(T_s - T_c) < 1.2$ and $\sigma_c/(T_s - T_c) < 0.2$, where, T_s is the mean surface temperature, T_{5th} is the 5th percentile of the 11-μm brightness temperature, T_c is the mean temperature associated with the layer at altitude z_c, and σ_c is the standard deviation of T_c, for the 1° latitude-longitude region. If $T_s - T_c < 10$ K then the requirements were $T_s - T_{5th} < 12$ K and $\sigma_c < 2$ K.

Figure 2.2 illustrates the average properties of single-layered, low-level clouds for the region under study. Satellite data for individual cloud or aerosol properties were averaged in 1° × 1° latitude-longitude regions for each orbital pass. In the case of the cloud properties, the averages were obtained by weighting the values by the pixel-scale fractional cloud cover. The means of each 1° latitude-longitude region were then averaged over all passes. For the summer of 1995, the air in the northeastern Atlantic was more polluted near the coast and cleaner over the ocean (Fig. 2.2a). The cloud droplet effective radius of single-layered, low-level clouds was small near the coast and large over the open ocean (Fig. 2.2b). Aerosol optical depth increased and cloud droplet effective radius decreased from west to east, as if the trends were manifestations of the Twomey Effect. On the other hand, the thinning and breakup of clouds as the continent is approached is typical of marine

stratus and may simply reflect the influence of incursions of dry continental air in the marine boundary layer and not the Twomey Effect. Regions closest to the coast were usually clear or contained broken clouds and more extensive cloud cover appeared further from shore (Fig. 2.2c).

Fractional cloud cover was relatively constant from south to north (Fig. 2.2c). Both aerosol optical depth and cloud droplet radius increased from south to north despite the supposition that cloud-aerosol interaction should result in smaller droplets where there is more aerosol. Droplet effective radius did not decrease as aerosol optical depth increased from south to north because there were south-north trends in cloud optical depth (Fig. 2.2d) and liquid water path (Fig. 2.2e), here calculated as $W = \frac{2}{3} R_e \tau_c \rho$, where $\rho = 1\,\mathrm{g\ cm^{-3}}$ is the density of water.

2.4 Relating Collocated Aerosol and Cloud Properties

Pixel-scale observations from each satellite overpass were mapped into 1° × 1° latitude-longitude regions. As stated earlier, all data was screened to ensure that 1° latitude-longitude regions that were either cloud-free ocean or partly covered by nothing but single-layered, low-level clouds were the only regions included in the analysis. The means of all cloud and aerosol properties were calculated in each 1° latitude-longitude region with the constraint that a minimum of 10 pixels or 5% of the pixels in the region (whichever was greater) for both aerosol and cloud properties were required. Because aerosol optical depth has an autocorrelation length of roughly 100 km (Anderson et al., 2003), the aerosol properties in the cloud-free pixels of the region were assumed to be well correlated with the aerosol properties in the cloudy pixels of the same region.

Within a geographic region, cloud properties and aerosol burden vary markedly from day to day. To detect reliable trends in cloud properties and aerosol burden the effects of the variability are reduced through averaging. In this study observations for the 1° latitude-longitude regions for each orbital pass were

averaged within their corresponding 5° × 5° latitude-longitude regions and then the pass averages were averaged for the four-month period. In addition, as was discussed in the previous section, there were large-scale trends in the 20° × 20° latitude-longitude region that could be interpreted as evidence for the Twomey Effect. The trends in cloud properties, on the other hand, may not be due to changes in aerosol burden but instead due to other factors such as the outflow of dry air from the continent. Averaging the collocated cloud and aerosol properties for the 1° latitude-longitude regions within the 5° latitude-longitude regions reduces somewhat the influence of the large-scale geographic gradients. Of course, gradients are still likely within the 5° latitude-longitude regions, but the 5° regions were the smallest studied because of the relatively small number of samples that fell into each region.

For each satellite overpass, the observations were segregated into 0.05 unit-wide bins in 0.55-μm aerosol optical depth. The means of the cloud properties and the corresponding aerosol optical depths were then calculated for each bin. After the means of each bin for each pass had been calculated, the bins were averaged over all passes. For example, Figure 2.3 shows the mean droplet effective radius calculated for every 0.05-unit wide bin of aerosol optical depth. In Fig. 2.3, and all subsequent figures, results for all sixteen 5° latitude-longitude regions are displayed simultaneously in their appropriate geographic location. Results for regions that contained land used data only from the pixels identified as being over ocean. In order to ensure that the values in each season-averaged bin were representative, means from at least five different passes for that bin were required. Linear least square fits were performed to quantify the trends in the cloud properties with aerosol optical depth. To improve the confidence in the least-squares fits, outlier data were removed by eliminating 1° latitude-longitude regions from individual satellite passes that had means that were outside the 5^{th} and 95^{th} percentiles for any property, except fractional cloud cover, in that 5° latitude-longitude region for the entire summer's collection of data. Fractional cloud cover is constrained between

0.0 and 1.0, so extremes were not considered outliers. Three of the sixteen regions had insufficient observations for calculating correlations. These regions are left blank in Figs. 2.3-2.9.

The error bars for each bin in Fig. 2.3 are given by the standard error of the bin, calculated as the standard deviation of the means of the individual satellite passes contributing to that bin divided by the square root of the number of satellite passes. Averages within a bin for each pass were taken to be statistically independent. As noted earlier, linear fits to the bin means were performed to determine the trends in the cloud properties with aerosol optical depth. In the fits, the means were inversely weighted by their estimated standard errors (Bevington, 1969). The slopes and estimates of their uncertainties were obtained from the distribution of the data about the trend lines (Press et al., 1994) and are reported in the figures. A slope is considered to be statistically significant if its magnitude is greater than twice the estimated uncertainty.

For the four-month period, 577 satellite overpasses were analyzed. There were 59,352 1° latitude-longitude regions that contained at least one pixel that was observed during daytime, over water, and away from sun glint, and was therefore suitable for attempting a retrieval. The number and percentage of 1° regions that passed the data screening algorithms described in this section are listed in Table 2.1. In order to maximize the signal of the aerosol indirect effect, data were tightly screened. Only 2.9% of the available 1° regions were used in the analysis. Despite the screening, the data were still rather noisy. The estimated uncertainties in the slopes of the associated cloud properties and aerosol optical depths were often larger than the slope estimates themselves. The highly variable nature of clouds makes determining reliable trends in cloud properties challenging.

As is shown in Fig. 2.3, in all but one of the 5° latitude-longitude regions droplet radius decreased as aerosol burden increased. Some regions showed an increase in cloud optical depth as aerosol burden increased while other regions showed no trend or even a decrease in cloud optical depth as aerosol burden

increased (Figure 2.4). Eight of the thirteen regions showed a decrease in droplet effective radius and an increase in cloud optical depth as aerosol burden increased. In only one of these eight regions, however, were the slopes significantly greater than twice the estimated error in the slopes and thus taken to be statistically significant. All but one region showed an increase in droplet number concentration, as given by τ_c / R_e^2, with increasing aerosol burden (not shown). Clouds in some regions were probably gaining CCN as aerosol burden increased and the clouds were probably responding to the aerosols consistent with the Twomey Effect.

None of the 5° latitude-longitude regions showed an increase in liquid water path as aerosol burden increased with an estimated slope that was significantly larger than the error estimate of the slope (Figure 2.5). Many regions showed a decrease in liquid water path as aerosol burden increased. Decreases in liquid water have also been observed for ship tracks (Platnick et al., 2000; Coakley and Walsh, 2002). Such trends might stand as evidence against the suppression of drizzle and increased cloud liquid water and cloud lifetimes for polluted clouds proposed by Albrecht (1989). On the other hand, high aerosol burdens in the coastal regions might have been associated with air originating over the continent, and thus the air was dryer. Clouds that formed in this dryer air might have been starved for water and quickly evaporated by entraining dry air from above the cloud, while clouds that formed far from the coast might have formed in moister, oceanic air with higher humidity and were less likely to dry out (Ackerman et al., 2004). Attempts to use humidity data from 2.5° × 2.5° latitude-longitude resolution NCEP reanalysis products to test this hypothesis were inconclusive. The decrease in cloud liquid water as aerosol burden increased might also be explained by the aerosol semi-direct effect; an increase in aerosol burden might lead to increased atmospheric heating which hinders cloud formation and augments cloud dissipation (Ackerman et al., 2000).

2.5 Dependence of Cloud Properties and Aerosol Optical Depth on Regional Cloud Cover

The previous section demonstrated that in some regions changes in cloud and aerosol properties were related in ways that are consistent with the Twomey Effect. Cloud properties, on the other hand, are also interrelated regardless of aerosol burdens. The possibility that the relationships among the cloud properties could have been incorrectly attributed to the Twomey Effect is explored.

Adiabatic cloud models provide a theoretical basis for relationships among cloud properties. Szczodrak et al. (2001) derive $R_e \propto \tau_c^{1/5}$ and give observational evidence for this relationship in maritime stratus off the west coast of North America. Brenguier et al. (2000b) describe aircraft observations showing liquid water content, $w \propto h$, where h is height above cloud base. By integration, the column water amount, $W \propto H$, where H is cloud geometric thickness. Brenguier et al. (2000b) also provide observational evidence for the derived relationship $R_e \propto h^{1/3}$, and find $\tau_c \propto H^{5/3}$. All of these relationships are for constant cloud droplet number concentration, and should therefore be observable for adiabatic conditions and a given aerosol burden. As cloud fields break up, however, fractional cloud cover decreases, mixing of dry air into clouds increases, and the relationships among cloud properties are likely to depart from those derived assuming adiabatic cloud parcels.

Figures 2.6 and 2.7 show trends in cloud properties as fractional cloud cover increased. Here binning procedures similar to those used in Figs. 2.3-2.5 were used but the bins are for every 0.05 in fractional cloud cover for the 1° regions. When associating aerosol and cloud properties, the 1° latitude-longitude regions used in the analysis were required to contain both cloud and aerosol retrievals. This restriction does not apply when comparing cloud properties to fractional cloud cover. Figs. 2.6 and 2.7 show data from both 1° latitude-longitude regions that were used in the cloud-aerosol associations (circles) and 1° latitude-longitude regions that passed the screening tests for single-layered, low-level clouds but

lacked sufficient numbers of aerosol retrievals to be included in the cloud-aerosol associations ('×'s). The data shown as circles in Figs. 2.6 and 2.7 are the same as used in the cloud-aerosol correlations (Figs. 2.3-2.5). As regions filled with clouds, the relationships among the cloud properties exhibited qualitatively the tendencies expected for adiabatic cloud parcels. Cloud optical depth increased as fractional cloud cover increased (Fig. 2.6). In all but the southern-most regions, droplet effective radius increased as fractional cloud cover increased (Fig. 2.7). For a given cloud cover fraction, cloud optical depths and droplet effective radii of the clouds associated with (circles) and not associated with aerosols ('×'s) showed little difference with the exception of droplet effective radius in the southern-most regions. There, clouds observed near aerosols (circles in Fig. 2.7) had larger droplet effective radii than clouds that were present with no collocated aerosol retrievals ('×'s in Fig. 2.7). Liquid water path, which is proportional to the product of cloud optical depth and droplet effective radius, increased as fractional cloud cover increased in all 5° latitude-longitude regions (not shown). Clouds observed near aerosols appeared to have higher cloud tops than clouds observed with no collocated aerosol retrievals (not shown). Cloud top height decreased with increasing fractional cloud cover in approximately half of the 5° latitude-longitude regions and was independent of fractional cloud cover in the other half of the regions (not shown).

Aerosol optical depth can be associated with both the fractional cloud cover and the cloudy pixel fraction, defined as the fraction of pixels in a 1° latitude-longitude region that were identified as having clouds (pixel-scale cloud fraction, $A_c > 0.2$). Because aerosol optical depth is not retrieved in partly cloudy pixels, cloudy pixel fraction was used as an index of regional cloud cover. Cloudy pixel fraction is similar to the fractional cloud cover derived using threshold cloud retrievals (Coakley et al., 2005). Retrieved aerosol optical depth increased as cloudy pixel fraction increased in many of the 5° latitude-longitude regions (Figure 2.8). This increase in aerosol optical depth as cloudy pixel fraction increased may

be due to cloud contamination. A single AVHRR GAC pixel is approximately 1 km × 4 km at nadir (Kidwell, 1995). Some pixels identified as being cloud-free may have contained subpixel resolution clouds. These unidentified clouds could cause the retrieved aerosol optical depths to be erroneously high. Presumably, subpixel scale clouds are more common in the presence of detectable clouds, explaining the trend toward larger aerosol optical depth as cloudy pixel fraction increased. Better algorithms for detecting subpixel scale resolution clouds and higher pixel resolution would both help alleviate this source of error.

The apparent increase in aerosol burden with increasing cloud cover could also be caused by the swelling of aerosol particles in the vicinity of clouds. Clouds form in environments with high relative humidity and aerosol particles swell as relative humidity increases (Seinfeld and Pandis, 1998; Clarke et al., 2002). Other causes for the apparent increase in aerosol optical depth as cloud cover increases include: increased illumination of the aerosols by sunlight leaving the sides of nearby clouds (Podgorny, 2003), increased particle production near clouds (Kütz and Dubois, 1997), and an increase in aerosol size due to in-cloud processing of CCN (Lelieveld and Heintzenberg, 1992). Clearly, characterizing how aerosols change and ensuring that cloud contamination of the "cloud-free" pixels remains unchanged as regions go from being largely cloud-free to largely overcast are hurdles which will have to be overcome before reliable assessments of the indirect effect of aerosols can be obtained empirically. Better cloud screening and better characterizations of aerosols in the vicinity of clouds are among the desired outcomes of the combination of lidar and imagery to come from *CALIPSO* and A-Train observations (Winker et al., 2003).

In all of the 5° latitude-longitude regions where aerosol optical depth increased as cloudy pixel fraction increased (Fig. 2.8), cloud optical depth also increased as fractional cloud cover increased (Fig. 2.6). The simultaneous increase in cloud and aerosol optical depth could be interpreted as an indication of the Twomey Effect, as suggested previously in this study (Fig. 2.4). On the other hand, both cloud and aerosol optical depth might have been changing in response to cloud cover,

indicating that at least some of the perceived correlation between cloud and aerosol optical depths may not be due to the Twomey Effect.

How can aerosol optical depth (Fig. 2.8) and droplet effective radius (Fig. 2.7) both increase with increasing cloud cover fraction, yet droplet effective radius decreases with increasing aerosol optical depth (Fig. 2.3)? The results shown for all of the parameters in Figs. 2.3-2.8 are means drawn from widely dispersed distributions. Aerosol and cloud optical depths have highly skewed distributions. Both have long tails stretching to large optical depths at low frequencies. Droplet radius, on the other hand, has a more compact distribution owing to bounds constrained by droplet formation at the low end and by precipitation at the high end. The full range of cloud properties is exhibited under average aerosol conditions while the clouds that appear with the infrequent occurrence of large aerosol burdens tend to have smaller than average droplets and, for the most part, larger than average optical depths. The fact that droplet radius decreases with increasing aerosol optical depth despite the countering trends of increasing droplet radius and aerosol optical depth with increasing cloud cover fraction suggests that the clouds are likely responding to the increased particle loading. On the other hand, since the number of partly cloudy pixels generally decreases and the number of overcast pixels increases as regional cloud cover increases, and since droplet radius is generally overestimated when the partly cloudy pixels are assumed to be overcast, the downward trend in droplet radius with increasing aerosol optical depth may also arise from misidentifying some partly cloudy pixels as being overcast (Coakley et al., 2005). Because of the natural trends in cloud properties with changing cloud fraction, the potential errors in the cloud property retrievals, and the observed increase in aerosol optical depth as the cloudy pixel fraction increases, caution must clearly be used in attributing observed correlations of cloud and aerosol properties to the Twomey Effect.

2.6 Radiative Forcing Estimates

Section 2.3 demonstrated that cloud microphysical properties might have been changing in response to changes in aerosol optical depth. Section 2.4 explained that the correspondence between aerosol optical depth and cloud properties is more complicated than suggested by section 2.3. Because of the great interest in determining the magnitude of aerosol indirect radiative forcing, this section estimates the forcing using the trends calculated in section 2.3. These results must, of course, be viewed skeptically in light of the discussion of section 2.4.

A broadband radiative transfer model that accounts for scattering and absorption by gases, aerosols, and clouds (Coakley et al., 2002) was used to calculate top of the atmosphere fluxes in each of the 5° latitude-longitude regions. For the calculations, an equal mix of continental and marine aerosols as described by Hess et al. (1998) was assumed. The mean fraction of continental aerosol type for the 1° latitude-longitude regions containing both cloud and aerosol retrievals was 0.66 ± 0.30. In this study, an arbitrary change in 0.55-μm aerosol optical depth of 0.1 was used to produce the radiative effects. The "background" level was chosen to be an aerosol optical depth of 0.15, and the "polluted" level was chosen to be an aerosol optical depth of 0.25. When a cloud was inserted in the model it was placed above the aerosol layer and the optical depth of the cloud was taken from the linear fits in Fig. 2.4 associated with the aerosol optical depths set at 0.15 and 0.25.

Calculations were performed for five different cases: 1) cloud-free and a "background" 0.55-μm aerosol optical depth of 0.15, 2) overcast with a cloud optical depth given by that associated with a "background" 0.55-μm aerosol optical depth of 0.15 as given in Fig. 2.4 combined with an underlying aerosol with the same optical depth, 3) cloud-free and a "polluted" 0.55-μm aerosol optical depth of 0.25, 4) overcast with a cloud optical depth associated with a "polluted" 0.55-μm aerosol optical depth of 0.25 as given in Fig. 2.4 combined with an underlying

aerosol with the same optical depth, and 5) overcast with a cloud optical depth associated with a "polluted" 0.55-μm aerosol optical depth of 0.25 as given in Fig. 2.4 but combined with an underlying aerosol with the "background" 0.55-μm optical depth of 0.15. The difference between cases 1 and 3 is the aerosol direct radiative forcing and is the same in all 5° latitude-longitude regions. The difference between cases 2 and 4 is here reported as the aerosol indirect radiative forcing. Changes in cloud cover associated with changes in aerosol optical depth were not considered in these calculations. The aerosol indirect radiative forcing reported here is not comparable to the forcing between pre-industrial and current times, but is rather the forcing that results from an arbitrary 0.1 change in the 0.55-μm aerosol optical depth for overcast conditions. Cases 2 and 5 had the same amount of aerosol, but the optical depths of the clouds were different. The difference between cases 2 and 5 was used to investigate the relative contributions of changes in cloud properties and changes in aerosol burden in the calculation of aerosol indirect radiative forcing.

The direct radiative forcing for cloud-free oceans is the same in all 5° latitude-longitude regions, -3.94 W/m^2 (shown as dashed lines in Figure 2.9). This forcing is the 24-hour average forcing for an increase of 0.1 in the aerosol 0.55-μm optical depth for cloud-free oceans during the summer months in the northeastern Atlantic. The indirect radiative forcing varied from -14.60 W/m^2 to 2.43 W/m^2 (shown as black bars in Fig. 2.9). In approximately half the regions, the indirect radiative forcing was found to provide more cooling than the direct radiative forcing. In two of the regions, the indirect radiative forcing was found to be warming. In these two regions, cloud optical depth decreased with increasing aerosol optical depth (Fig. 2.4).

Case 5 gives the top of the atmosphere forcing for "polluted" clouds over "background" aerosols. The difference between case 2 and case 5 is shown as gray bars in Fig. 2.9 and was compared to the aerosol indirect radiative forcing (the difference between case 2 and case 4) as an indication of how much of the aerosol

indirect forcing was solely the result of the changes in cloud properties. In all regions, the aerosol indirect radiative forcing and the forcing by changes in cloud properties alone were similar, within 1.5 W/m^2, indicating that changes in the overcast regions due to the scattering and absorption by the increased burden of aerosols was relatively minor.

The radiative forcing calculations were repeated, but instead of calculating cloud optical depth using the trends shown in Fig. 2.4, cloud optical depth was calculated using the observed changes in droplet effective radius as aerosol optical depth increased (Fig. 2.3) and an assumption of fixed liquid water. The indirect radiative forcing calculated in this manner was always cooling and varied from –7.78 to –0.68 W/m^2 (shown as white bars in Fig. 2.9). The average value of the radiative forcing calculated for constant liquid water, weighting the 13 regions equally, was –4.69 W/m^2, which is smaller than the average forcing calculated using observed changes in cloud optical depth, -5.22 W/m^2. In ten of the regions the forcing calculated by assuming fixed liquid water is more than 3 W/m^2 different from the forcing calculated by using observed changes in cloud optical depth. In one region, the assumption of fixed liquid water gives a forcing that is 10.48 W/m^2 smaller than the value calculated using the observed changes in cloud optical depth. Many climate model simulations show an increase in cloud water content with increasing aerosols (e.g. Feichter et al., 2004) whereas the results presented here show that a decrease in liquid water path is clearly possible (Fig. 2.5).

The mean value of the aerosol indirect radiative forcing for overcast conditions, weighting the 13 regions equally, was –5.22 W/m^2 for a 0.1 change in aerosol 0.55-μm optical depth. The change in albedo for overcast conditions per unit change in aerosol optical depth, calculated using a solar constant of 1365 W/m^2 and the diurnal average of the cosine of the solar zenith angle for July for the North Atlantic of 0.354, was $\Delta r / \Delta \tau_a = 0.11$. Kaufman and Fraser (1997), studying the effect of smoke on low-level clouds over the Amazon, observed a similar value, $\Delta r / \Delta \tau_a = 0.12 \pm 0.08$.

Sekiguchi et al. (2003), using AVHRR data, estimated the global mean aerosol indirect radiative forcing, not including changes in cloud fraction, as between –0.7 and –0.9 W/m^2. Their fractional cloud cover was between 0.3 and 0.4, indicating an indirect radiative forcing for overcast conditions of –1.75 to –3.0 W/m^2. They also calculated an aerosol direct radiative forcing of –0.4 W/m^2, indicating a radiative forcing for cloud-free conditions of –0.57 to –0.67 W/m^2. Therefore, Sekiguchi et al. (2003) calculated an indirect forcing for overcast conditions that was 3 to 4.5 times greater than the direct forcing for cloud-free conditions. In the current study, the mean value of the aerosol indirect radiative forcing for overcast conditions was only slightly larger than the direct forcing for cloud-free conditions (–5.22 and –3.94 W/m^2 respectively). When holding cloud liquid water constant, Sekiguchi et al. (2003) calculated an indirect radiative forcing (–0.64 or –0.16 W/m^2) that was 30 or 76% less than the indirect forcing calculated for observed changes in cloud optical depth (–0.91 or –0.68 W/m^2). The current study calculates an indirect radiative forcing assuming constant liquid water that was 10% less than the forcing calculated from observed changes in cloud optical depth (–4.69 and –5.22 W/m^2 respectively). Both Sekiguchi et al. (2003) and the current study indicate that the assumption of fixed liquid water can lead to estimates of the aerosol indirect radiative forcing that are different from the indirect forcing that is estimated for the observed changes in cloud optical depth.

Rotstayn and Penner (2001) used a global climate model to estimate the global average direct radiative forcing between the pre-industrial and current eras as –0.75 W/m^2 and the indirect forcing as –2.57 W/m^2. Because their model included multiple cloud layers (approximately 40% low-cloud cover and 32% high-cloud cover), it is difficult to translate these numbers into forcings for cloud-free and overcast conditions. Nevertheless, their estimate of indirect forcing was substantially larger than their estimate of direct radiative forcing. A major difference between the current study and those of Sekiguchi et al. (2003) and Rotstayn and Penner (2001) is that their studies were global averages whereas the current study was limited to a 20° × 20° latitude-longitude region in the

northeastern Atlantic. In addition, the current study used collocated simultaneous observations of aerosol and cloud properties as discussed earlier.

2.7 Conclusions

AVHRR imagery data with a nominal nadir resolution of 4 km were collected over the northeastern Atlantic for May-August, 1995. Within each satellite overpass, mean cloud properties deduced from the cloudy pixels in 1° × 1° latitude-longitude regions were associated with simultaneous mean aerosol properties deduced from the cloud-free pixels in the same 1° latitude-longitude regions. The observations were screened so that 1° latitude-longitude regions that contained only single-layered, low-level clouds and had sufficient numbers of cloud-free pixels yielding aerosol retrievals were used in the analysis. In pixels that contained clouds, a retrieval scheme was used to derive: cloud visible optical depth, droplet effective radius, cloud layer altitude, and pixel-scale fractional cloud cover. Aerosol optical depth was retrieved in cloud-free pixels. Results were composited in 5° × 5° latitude-longitude areas. The conditions of simultaneity and close spatial proximity were adopted to ensure that the observed properties of the clouds were in response to the observed aerosol burden, that is, comparisons of clouds from one day and location to aerosols from a different day or different location were avoided.

Clouds in some areas of the study region appeared to respond to aerosols as predicted by the Twomey Effect: as aerosol optical depth increased, cloud droplet number concentration increased, droplet effective radius decreased, and cloud optical depth increased. Strong evidence for trends consistent with the Twomey Effect was lacking in many of the 5° latitude-longitude regions. Many regions exhibited no change or even a decrease in cloud liquid water as aerosol burden increased. The incursion of dry, polluted continental air in the marine environment

is suggested as a possible explanation for the decrease in cloud water associated with the increase in aerosol optical depth.

As regional fractional cloud cover increased, droplet effective radius, cloud optical depth, and cloud liquid water path all increased. Aerosol optical depth increased as the percentage of pixels identified as containing clouds (pixel-scale cloud fraction, $A_c > 0.2$) increased. The increase in retrieved aerosol optical depth as cloud fraction increased might have been due to 1) cloud contamination in the retrievals of the aerosol properties, 2) the swelling of aerosols in the high humidity cloudy environments, 3) the increased illumination of the cloud-free columns by the scattering of sunlight reflected from nearby clouds, 4) the increased particle production by photochemical processes in the vicinity of clouds, and 5) the chemical processing within cloud droplets leading to larger particles when the droplets evaporate. The simultaneous increase in cloud optical depth and aerosol optical depth as fractional cloud cover increased might be interpreted as the aerosol indirect effect. On the other hand, cloud and aerosol optical depth were both responding to an increase in cloud cover and some of the correlation between the cloud and aerosol optical depths might not have been due to the Twomey Effect.

An assumption intrinsic to all satellite studies of cloud-aerosol interaction is that clouds observed near aerosols are influenced by aerosols similar to those observed nearby. The current study was limited to single-layered, low-level clouds. It was assumed that most of the aerosols were in the boundary layer and affected the microphysical properties of the low-level clouds. The region off the coast of Europe was chosen, in part, because aerosol plumes coming from the continent are often in the boundary layer (Johnson et al., 2000). A vertical profiling instrument such as GLAS (Abshire et al., 1998) or the lidar to be flown on the *CALIPSO* satellite (Winker et al., 2003) is required to determine whether the observed clouds and aerosols are actually at the same altitude and thus likely to be interacting, or a substantial fraction of the aerosol is in a lofted layer above the clouds, as presumably would be the case for the long range transport of windblown dust.

For comparison with other studies, a broadband radiative transfer model was used to calculate the direct and indirect radiative forcing for an arbitrary change of 0.1 in the aerosol 0.55-μm optical depth. The 24-hour average summertime indirect radiative forcing calculated for overcast conditions in the 5° latitude-longitude regions ranged from –14.60 to 2.43 W/m^2. The majority of this forcing was due to changes in the cloud properties and not to the increased reflectivity caused by increased aerosol burden beneath the clouds. When averaged over all regions, the aerosol indirect effect for overcast conditions was –5.22 W/m^2, which was only slightly larger than the direct radiative forcing of –3.94 W/m^2 for cloud-free regions. Rerunning the forcing calculations using the observed changes in droplet effective radius and assuming fixed liquid water resulted in an aerosol indirect radiative forcing that was 10% less (–4.69 W/m^2) than the forcing calculated from observed changes in cloud optical depth. The indirect forcing obtained here is similar to that found by Kaufman and Fraser (1997). The indirect forcing when compared with the direct forcing is smaller than similar comparisons reported by Sekiguchi et al. (2003) and by Rotstayn and Penner (2001). Here no account was made for changes in fractional cloud cover which may be associated with the effects of the aerosols because, as noted earlier, many alternative physical processes might explain the correlations observed between aerosol burden and cloud cover fraction.

Table 2.1. Number and percentage of 1° × 1° latitude-longitude regions that survived successive data screening tests. Percentages are based on 59,352 1° latitude-longitude regions from 577 satellite overpasses that contained at least one pixel that was observed during daytime, over water, and away from sun glint, and were therefore suitable for attempting a retrieval.

Screening	Aerosol		Cloud	
	Number	%	Number	%
At least 10 pixels or 5% (whichever was greater) of all pixels in region has cloud (aerosol) retrievals	11,806	19.9	30,286	51.0
Region contained only cloud-free pixels or clouds from single-layered, low-level cloud systems	9,620	16.2	16,820	28.3
Region contained cloud and aerosol properties that were within the 5th and 95th percentile for that 5° latitude-longitude area	7,963	13.4	11,697	19.7
Region contained both cloud and aerosol retrievals that passed previous data screening tests	1,930	3.3	1,930	3.3
At least 5 cloud retrievals per 0.05 unit-wide bin of aerosol optical depth in at least 3 separate bins for that 5° latitude-longitude area	1,741	2.9	1,741	2.9

a)

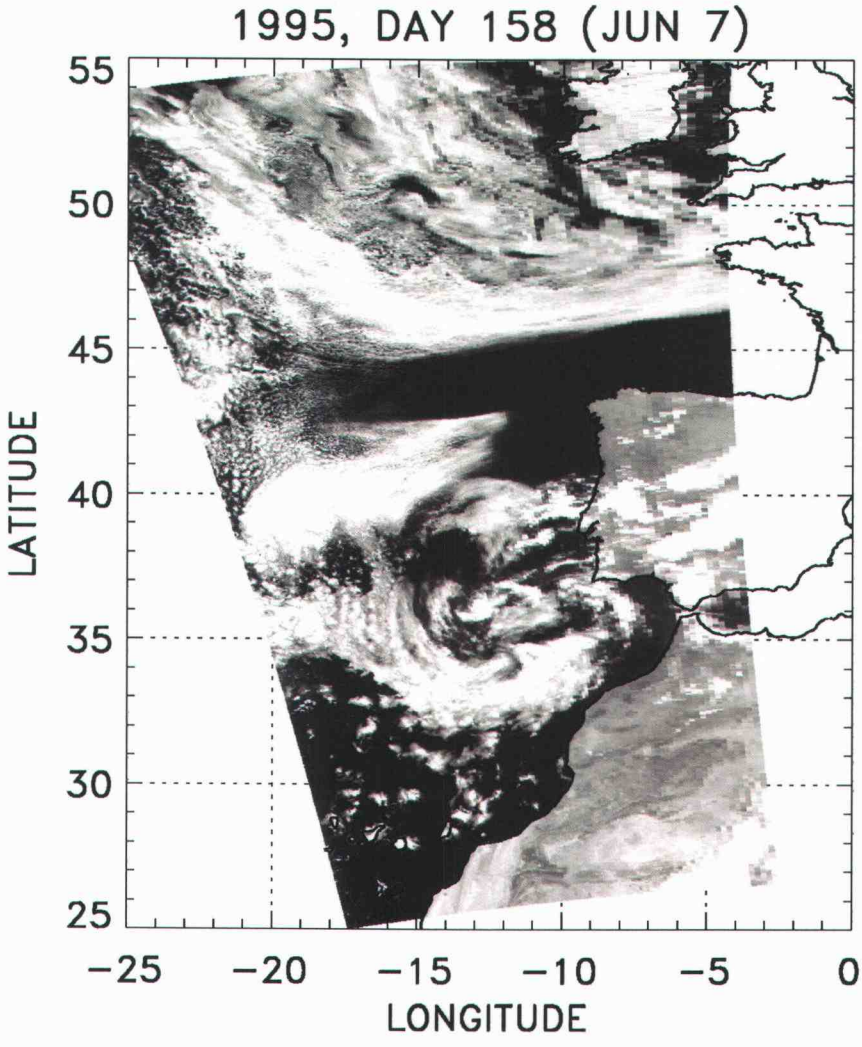

Figure 2.1. Images of the study region on June 7, 1995, dominated by low-level, single-layered stratocumulus off the west coast of Europe. a) 0.84-μm 4-km AVHRR reflectances. b) 11-μm radiances. Upper-level clouds (light objects) overlie a portion of the low-level clouds. c) Same as a), but overlain with 0.55-μm aerosol optical depth. d) Same as a), but overlain with droplet effective radius (μm).

b)

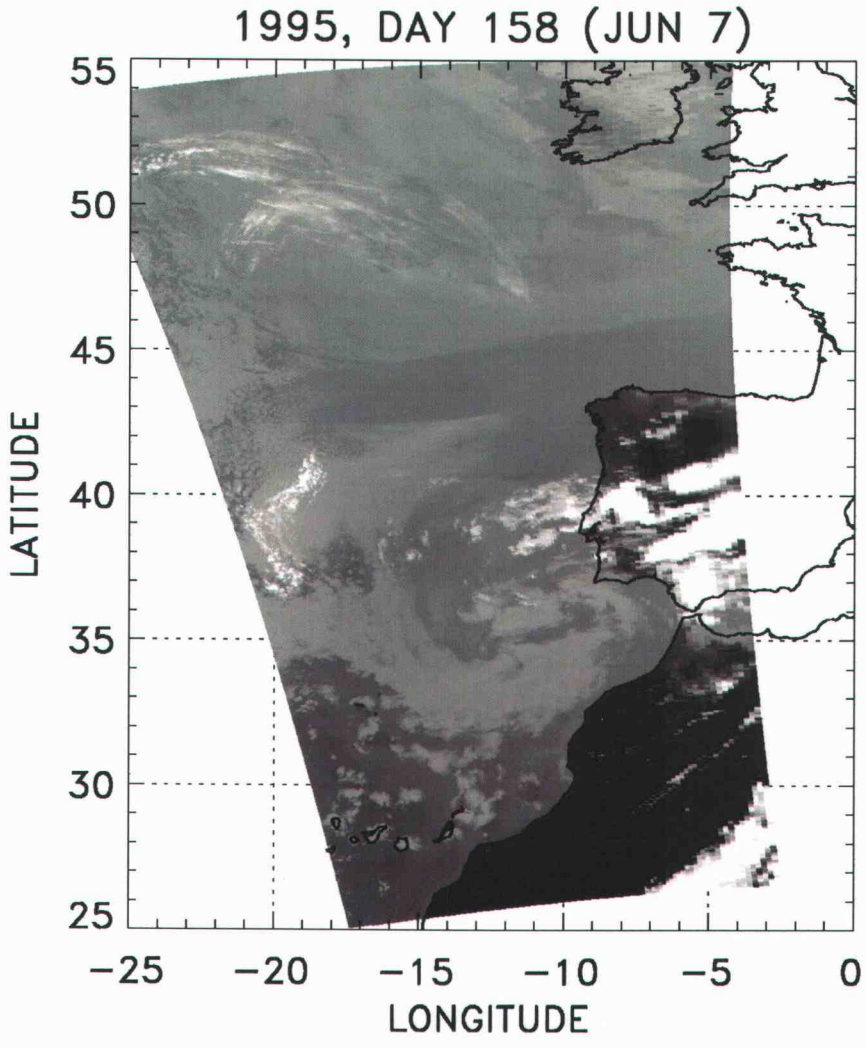

Figure 2.1 (Continued)

c)

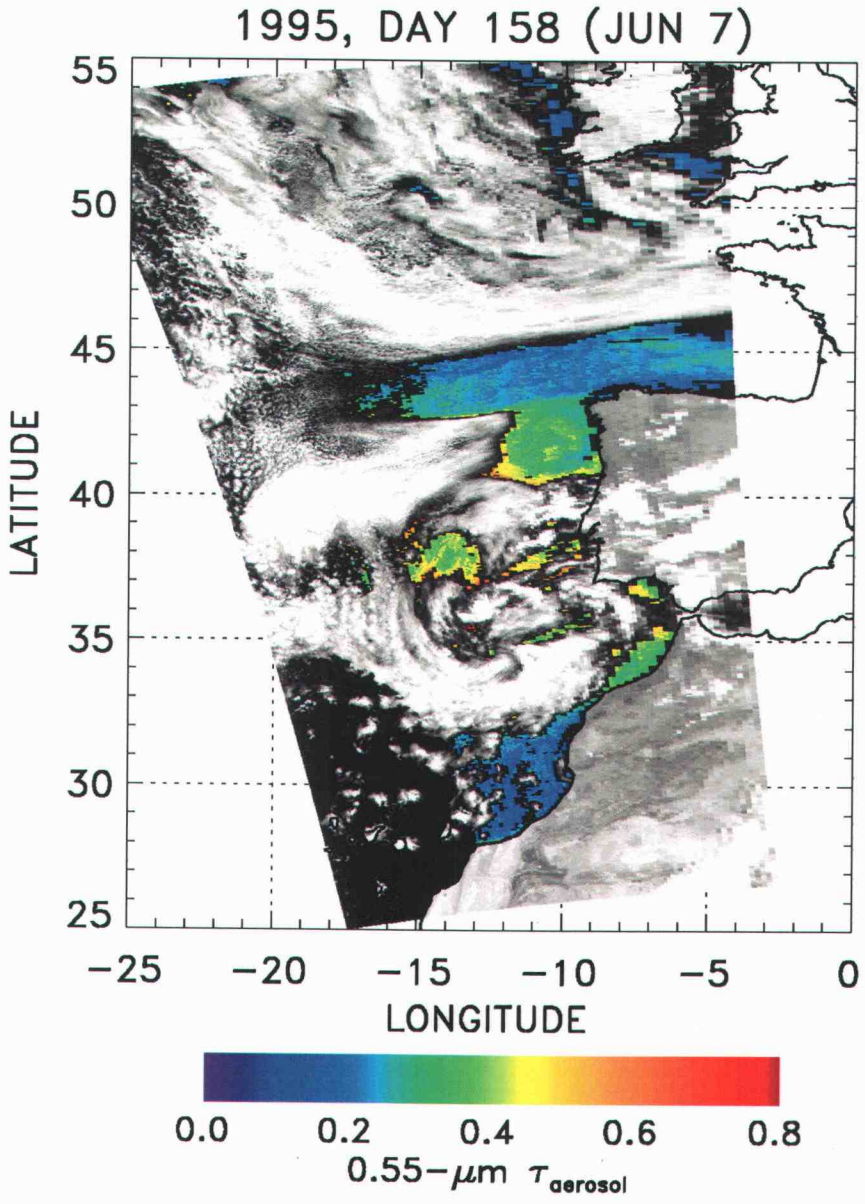

Figure 2.1 (Continued)

d)

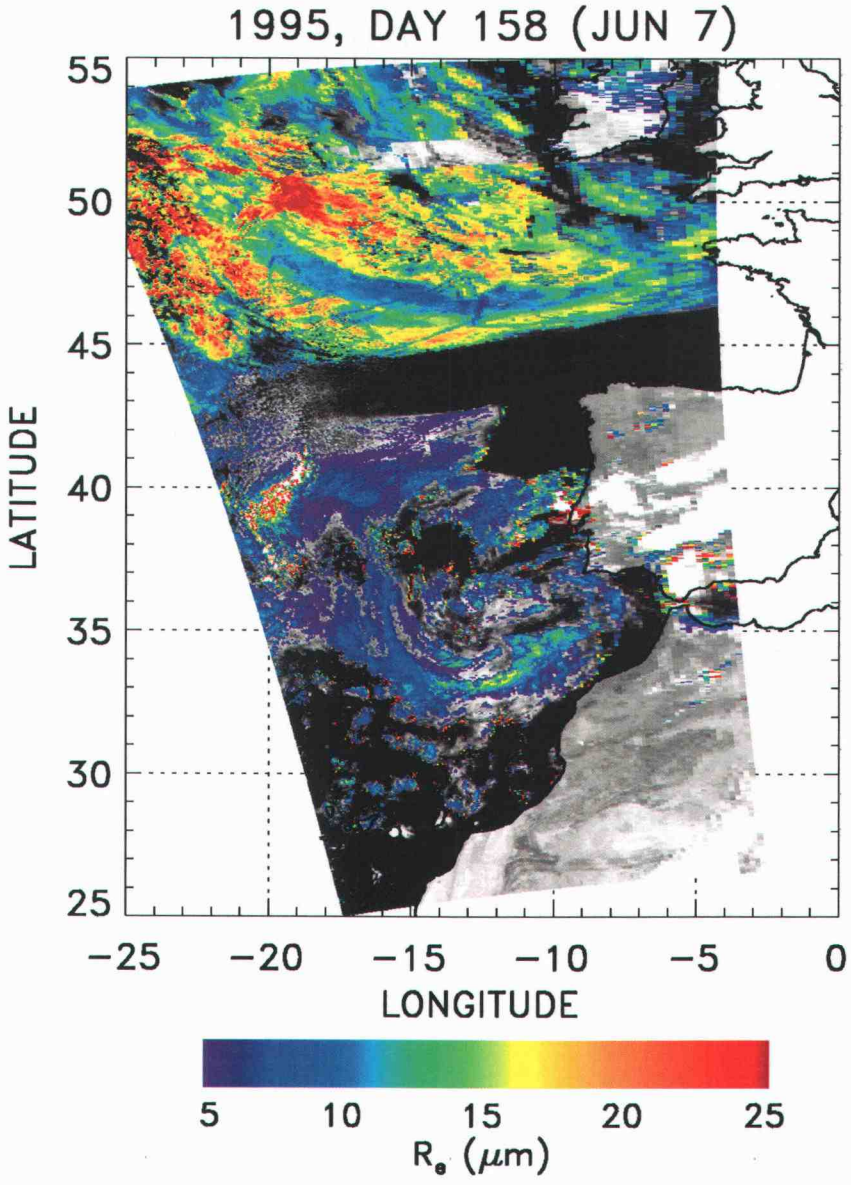

Figure 2.1 (Continued)

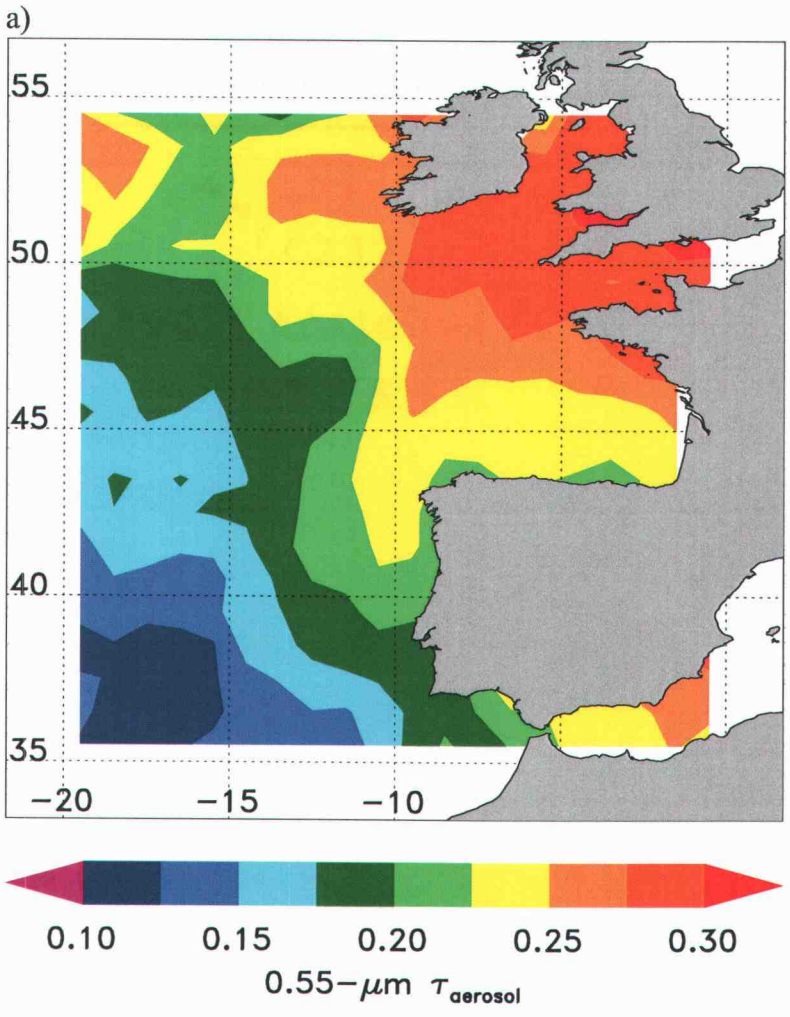

Figure 2.2. Summertime (May-Aug, 1995) average properties of single-layered, low-level clouds and aerosols. Contour data has been smoothed to show large-scale trends. a) 0.55-μm aerosol optical depth. Aerosol data from 1° × 1° latitude-longitude regions that contained clouds that were not part of a single-layered, low-level cloud system were not included in the analysis. b) Droplet effective radius (μm). c) Fractional cloud cover. d) 0.64-μm cloud optical depth. e) Liquid water path (g/m^2). In parts b-e, data were limited to 1° latitude-longitude regions that contained only low-level, single-layered cloud systems. In calculating the pass averages within a region, cloud properties were weighted by the pixel-scale fractional cloud cover.

b)

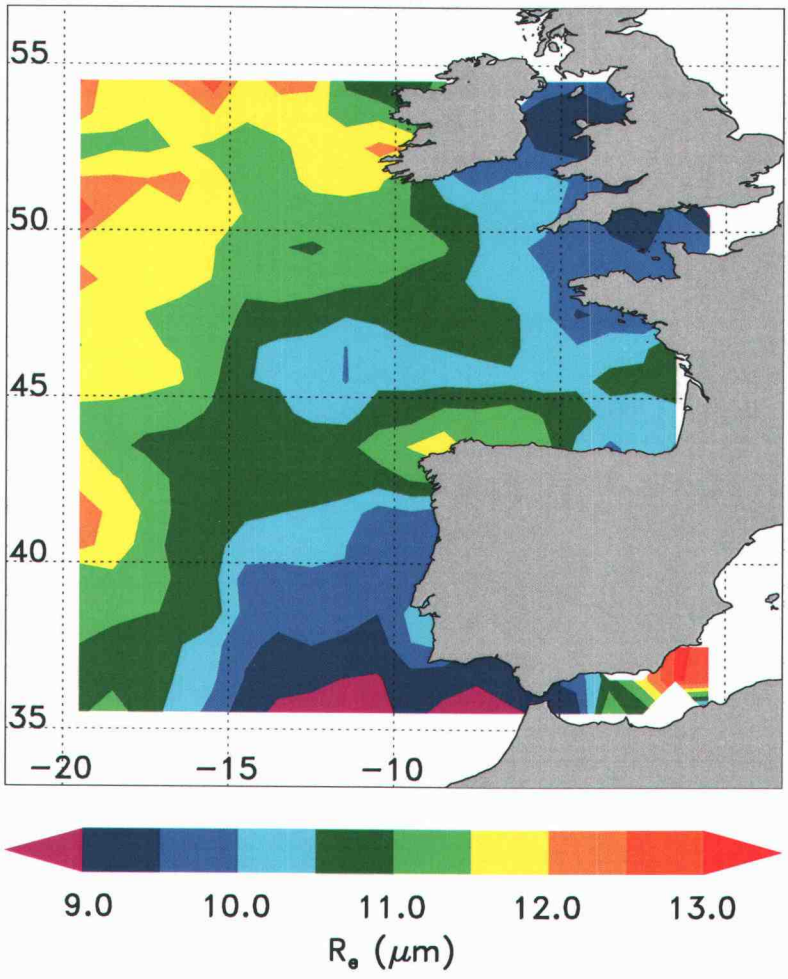

Figure 2.2 (Continued)

c)

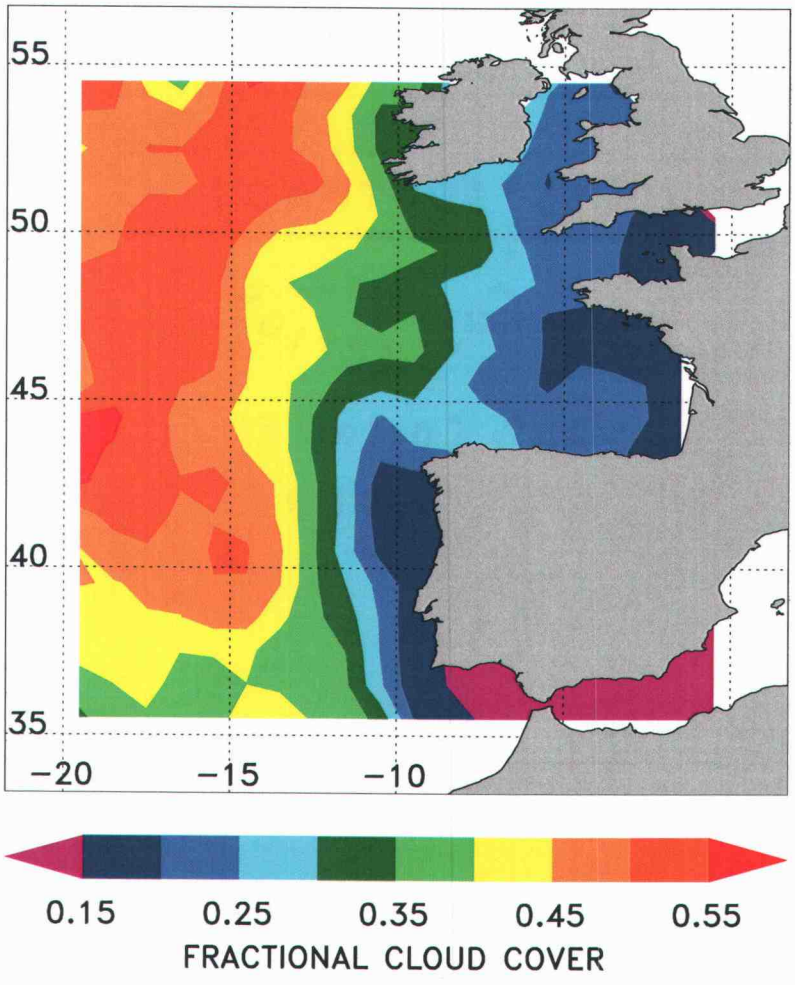

Figure 2.2 (Continued)

d)

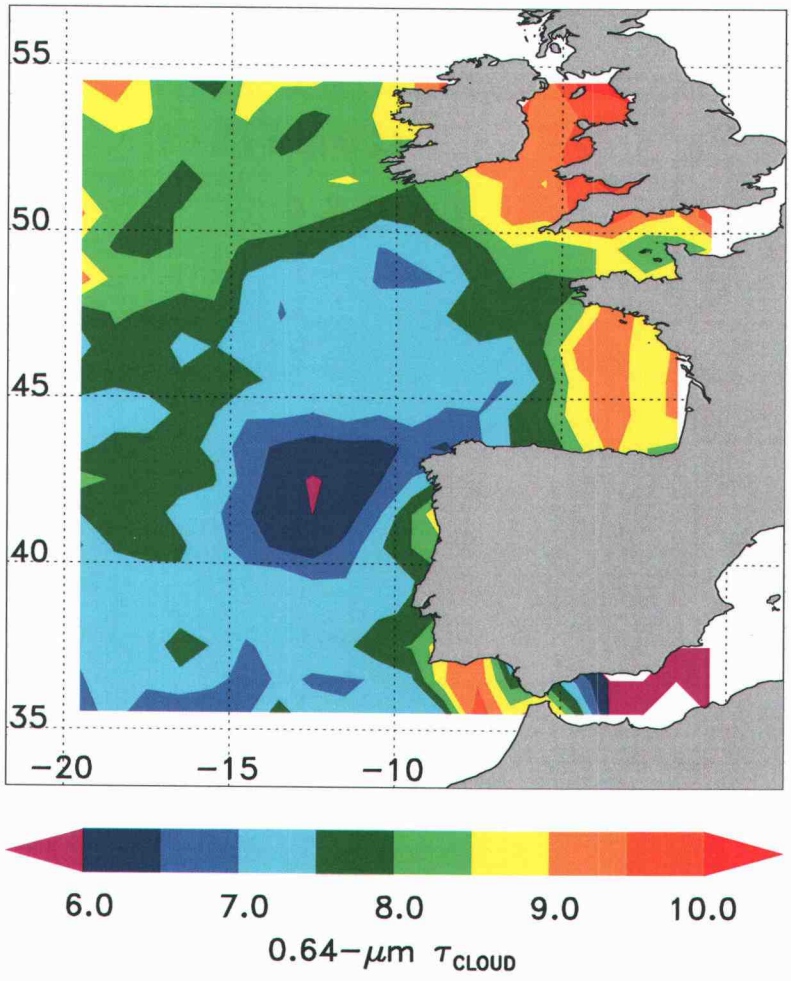

Figure 2.2 (Continued)

e)

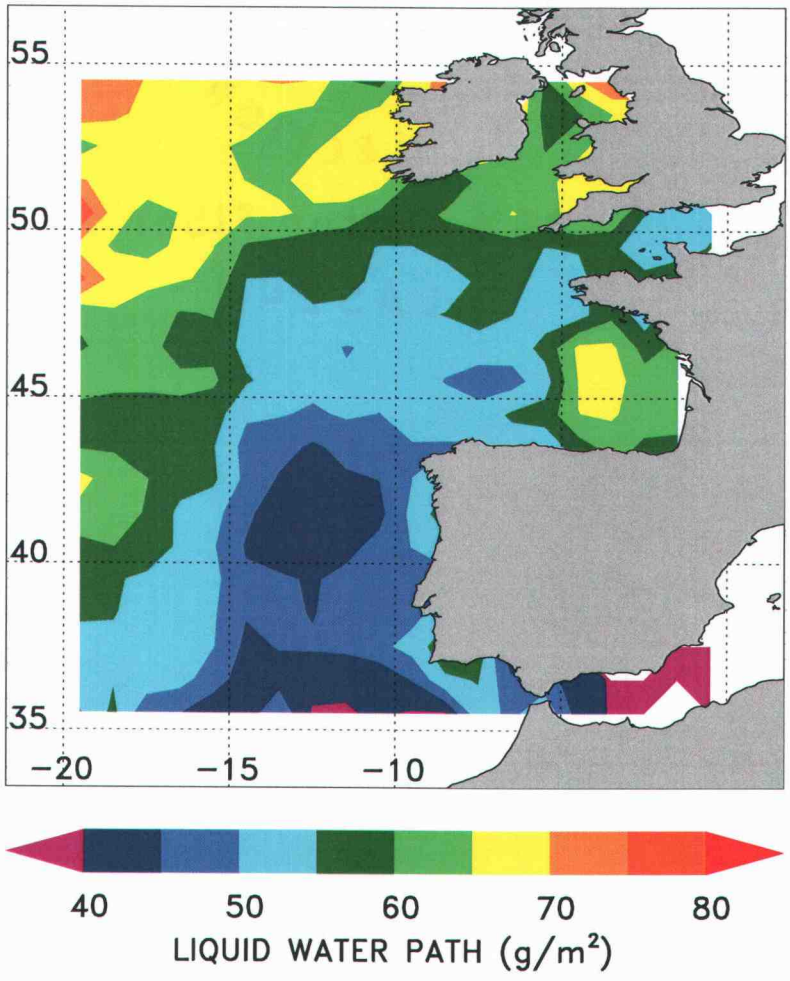

Figure 2.2 (Continued)

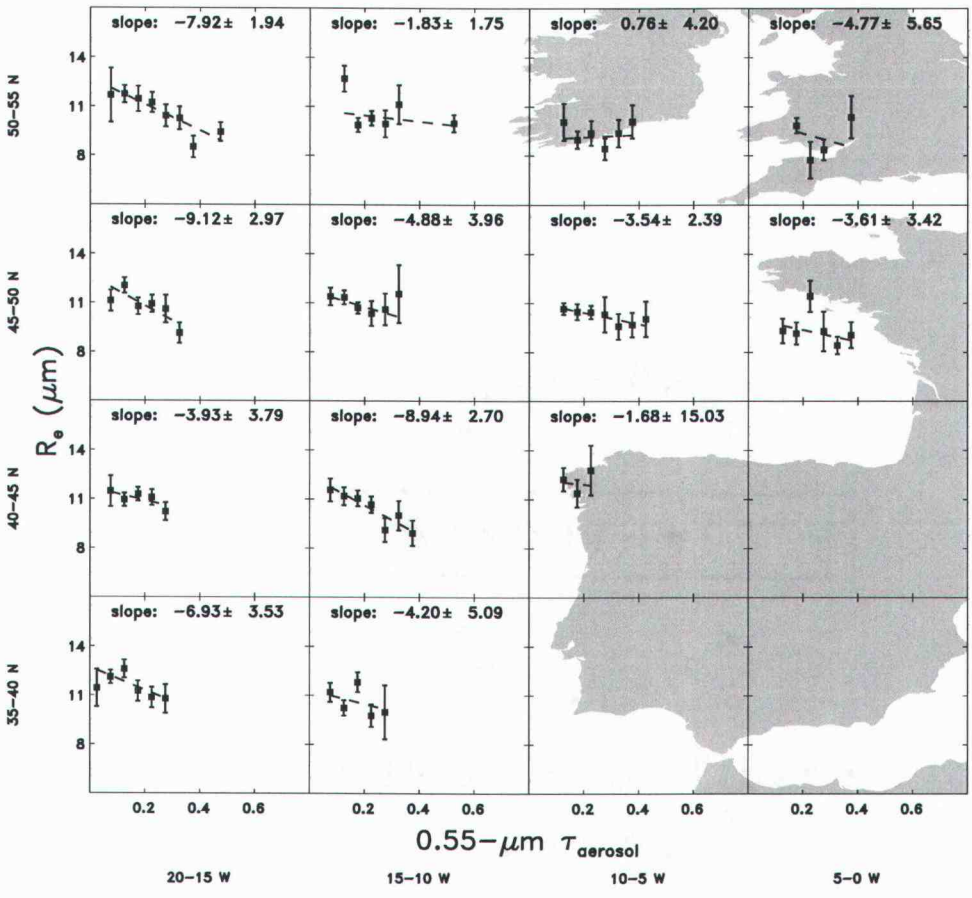

Figure 2.3. Means of daily averaged droplet effective radius (μm) for 1° latitude-longitude regions binned for each 0.05 interval of aerosol optical depth. Each sub-panel contains data from that 5° × 5° latitude-longitude region. Error bars represent the standard error, given by the standard deviation of the means from individual days for that bin divided by the square root of the number of days that contributed observations to that bin. The dashed line is a linear fit to the bin means inversely weighted by the standard error. Also given are the mean and standard deviation estimated for the slope of the linear fit.

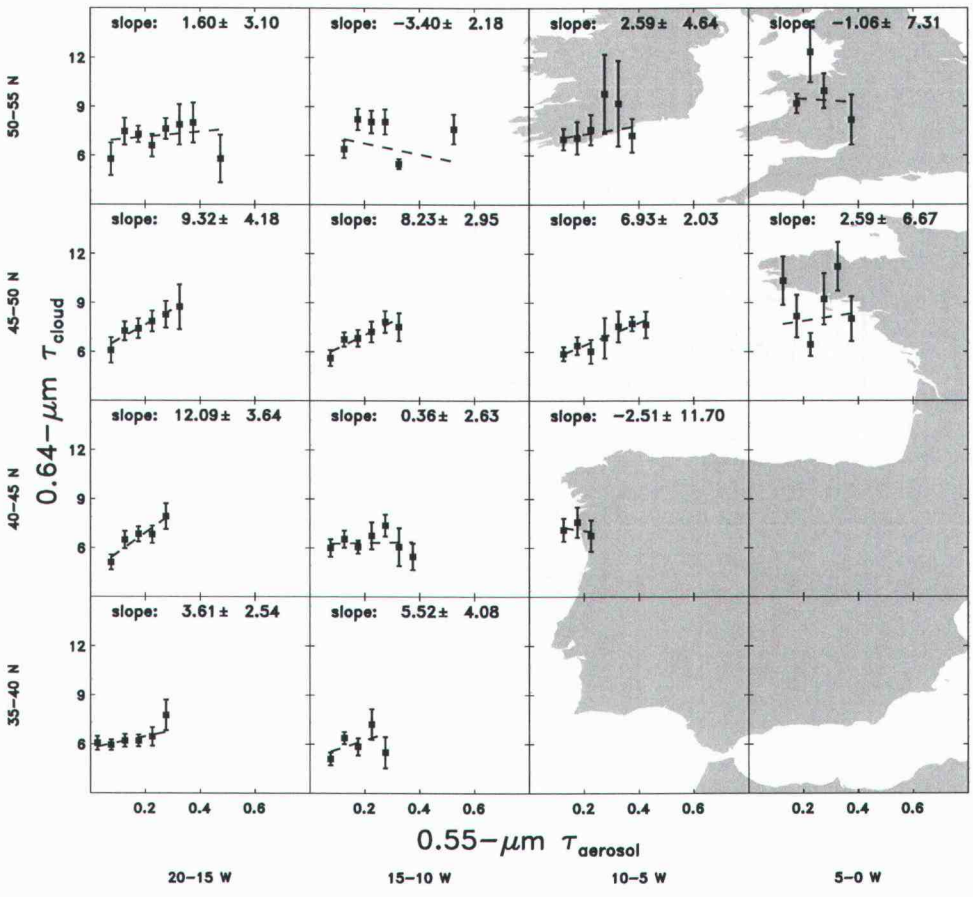

Figure 2.4. Same as Fig. 2.3, but for 0.64-μm cloud optical depth and 0.55-μm aerosol optical depth.

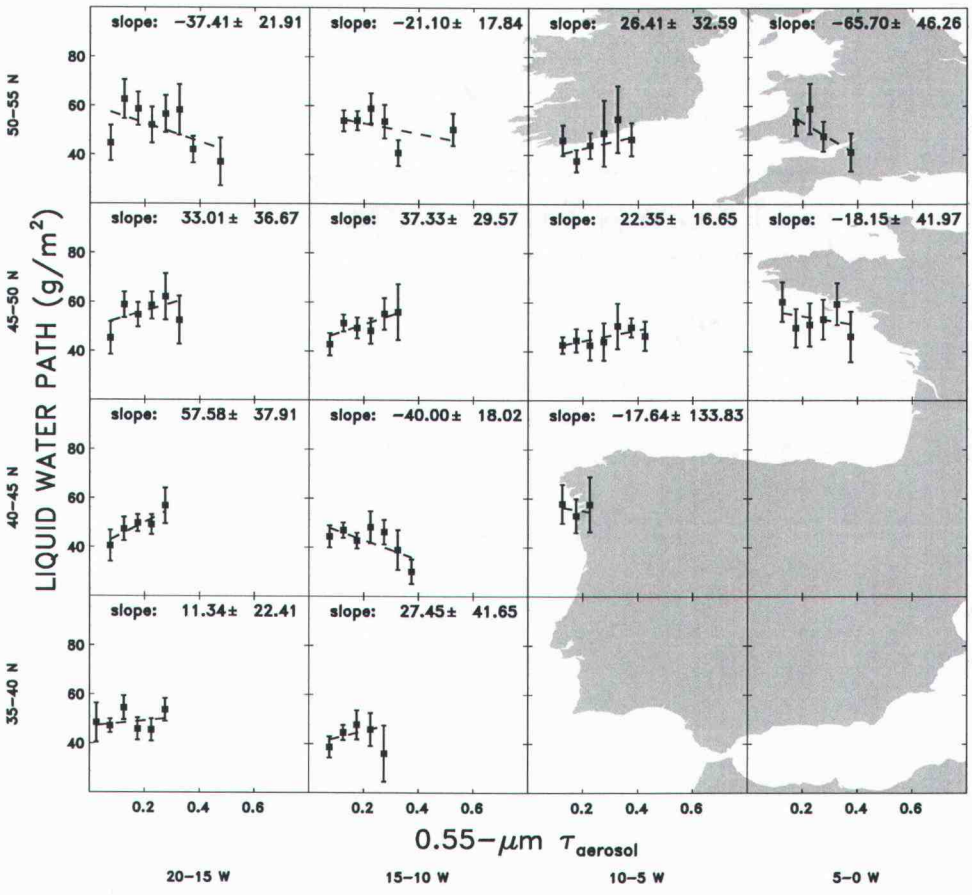

Figure 2.5. Same as Fig. 2.3, but for cloud liquid water path (g/m^2) and 0.55-μm aerosol optical depth.

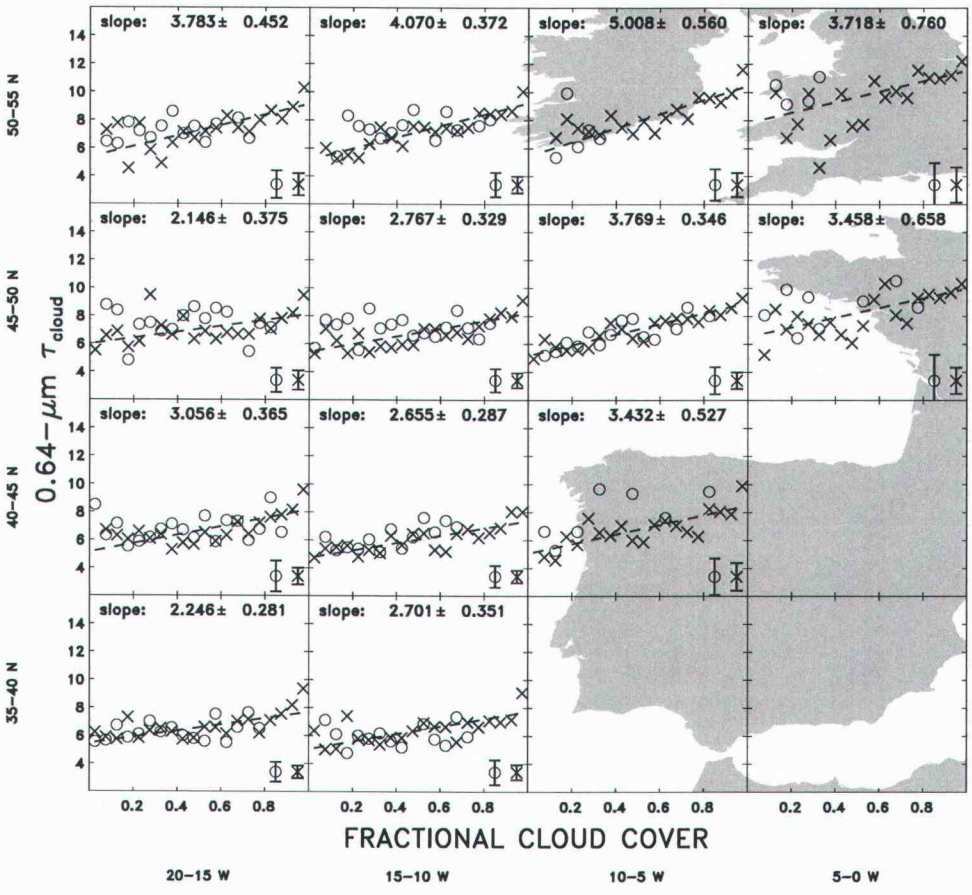

Figure 2.6. Means of daily averaged 0.64-μm cloud optical depth for 1° latitude-longitude regions binned for each 0.05 interval of fractional cloud cover. Each sub-panel contains data from that 5° × 5° latitude-longitude region. Circles are data for 1° regions that contained sufficient observations of both aerosol and cloud properties to be included in Figs. 2.3-2.5. '×'s are data from 1° latitude-longitude regions that passed the screening tests for single-layered, low-level clouds but lacked a sufficient number of aerosol retrievals to be included in the aerosol-cloud associations. The root-mean-square of the standard error (as described in Fig. 2.3) for the two data sets are shown in the lower right corner of each panel. The dashed line is a linear fit to the bin means of the combined data sets inversely weighted by the standard errors of the combined data sets. Also given are the mean and standard deviation estimated for the slope of the linear fit.

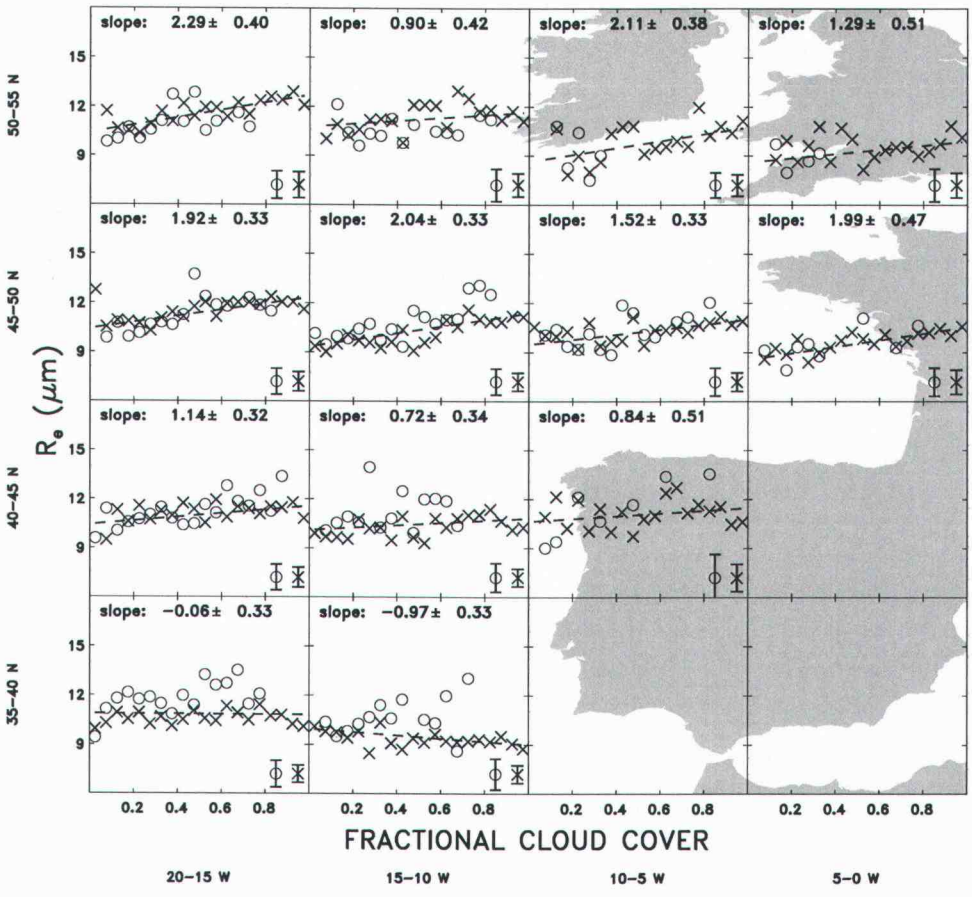

Figure 2.7. Same as Fig. 2.6, but for droplet effective radius (μm) and fractional cloud cover.

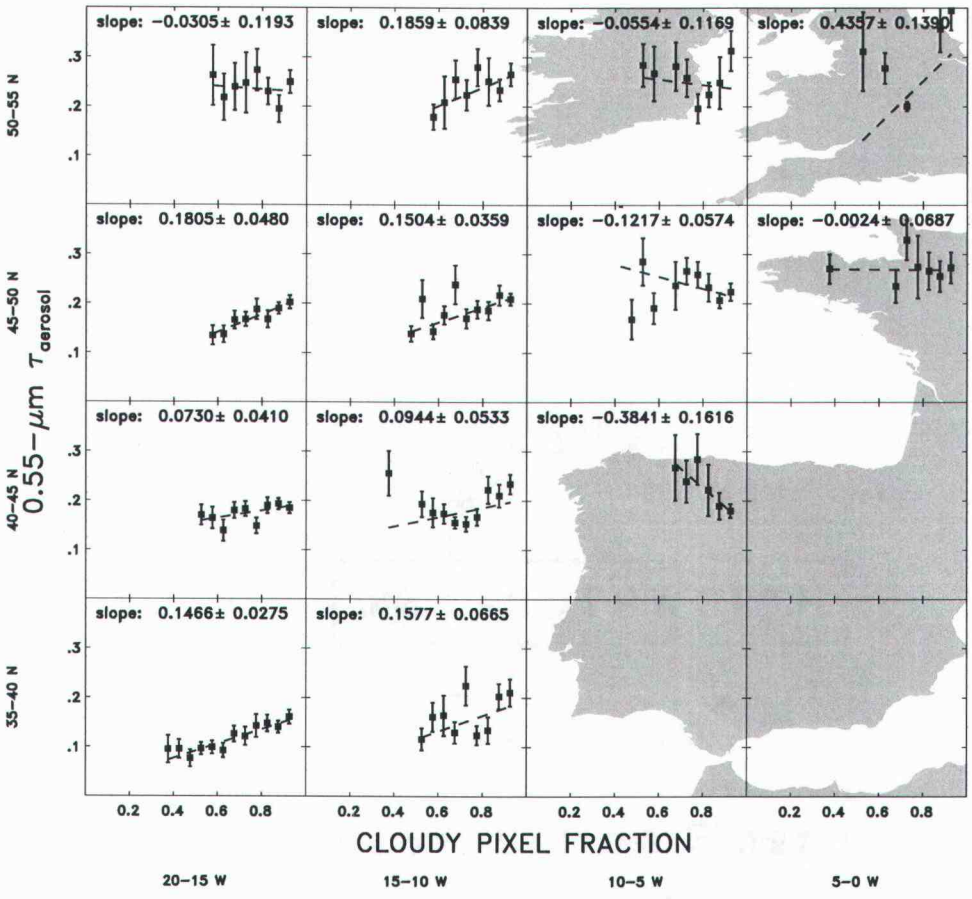

Figure 2.8. Same as Fig. 2.3, but for 0.55-μm aerosol optical depth and cloudy pixel fraction. Cloudy pixel fraction is the fraction of pixels within a 1° latitude-longitude region that were identified as containing clouds (pixel-scale cloud fraction, $A_c > 0.2$).

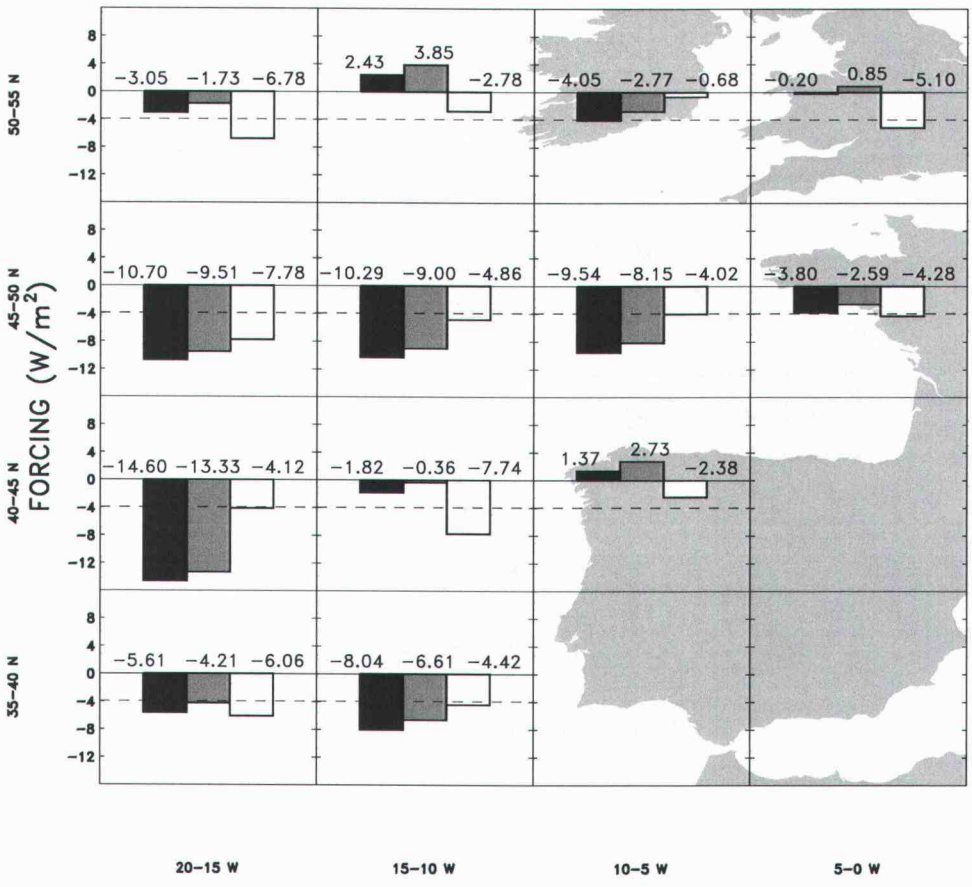

Figure 2.9. Radiative forcing estimates (W/m^2) for an arbitrary increase of aerosol 0.55-μm optical depth of 0.1 (from 0.15 to 0.25). Black bars are the forcings for overcast conditions calculated using the changes in cloud optical depth taken from the linear fits in Fig. 2.4 and an increase of the aerosol optical depth below the cloud. Gray bars are the same forcing as the black bars except the aerosol optical depth was held at the "background" level. White bars are the forcings for overcast conditions calculated using the changes in droplet effective radius taken from the linear fits in Fig. 2.3 and assuming a constant liquid water path. The dashed line is the aerosol direct radiative forcing for cloud-free conditions (-3.94 W/m^2).

Chapter 3
Multiyear AVHRR observations of summertime stratocumulus collocated with aerosols in the northeastern Atlantic

3.1 Abstract

Advanced Very High Resolution Radiometer (AVHRR) 4-km data were collected over the northeast Atlantic for May-August, 1995-1999. Aerosol optical depth at 0.55 μm was retrieved in pixels identified as being cloud free. In pixels identified as containing clouds from single-layered, low-level cloud systems, the following cloud properties were retrieved: 0.64-μm cloud optical depth, droplet effective radius, cloud top height, pixel-scale fractional cloud cover, liquid water path and column droplet concentration. Properties of aerosols and single-layered, low-level clouds were averaged in 1° × 1° latitude-longitude regions for each pass. Cloud and aerosol properties were compared for 1° latitude-longitude regions in which there existed a sufficient number of both single-layered, low-level cloud and aerosol retrievals in a single overpass. The comparisons were composited in 5° × 5° latitude-longitude regions to determine trends. Within each 5° latitude-longitude region the cloud properties were similar from year to year, permitting the data to be composited for all five years. Aerosol optical depth decreased systematically with time, probably as a result of the increase in solar zenith angle due to the precession of the satellite orbit. Within the 5° regions, as aerosol optical depth increased, droplet effective radius decreased and column number concentration and cloud optical depth increased, qualitatively consistent with the trends expected for the aerosol indirect effect. In many regions, liquid water path decreased as aerosol optical depth increased, contrary to the trends expected for the suppression of drizzle. Droplet effective radius increased as fractional cloud cover increased for clouds associated with both small and large aerosol burdens. Within each of the 5° latitude-longitude regions, clouds in clean air had larger droplets and smaller cloud

optical depths than clouds in polluted air, likewise consistent with trends expected for the aerosol indirect effect. Liquid water path increased as fractional cloud cover increased but no difference was found between clouds in relatively clean and relatively polluted air. Changes in the liquid water may be more strongly influenced by factors other than aerosol burden, such as the water vapor concentration in the air mass containing the aerosols. On average, the aerosol indirect radiative forcing for overcast conditions was 1.4 to 2.2 times larger than the aerosol direct radiative forcing for cloud-free conditions depending on whether the cloud liquid water was allowed to vary or was held fixed as the clouds responded to changes in aerosol burden.

3.2 Introduction

Seeking evidence for aerosol indirect radiative forcing and using observations to empirically derive estimates of the forcing has proven elusive. In a previous paper (Matheson et al. 2005a), hereafter referred to as MCT, a methodology was suggested and results presented for *NOAA-14* 4-km Advanced Very High Resolution Radiometer (AVHRR) imagery analyses of the response to variations in aerosol loading of the 1995 summertime marine stratus and stratocumulus in the northeastern Atlantic. As MCT noted, signs of the effects of the aerosols on the clouds, namely the decrease in droplet radius, the increase in the visible optical depth, and the increase in the column droplet number concentration, were consistent with what has become known as the "Twomey Effect" (Twomey, 1974). The findings were qualitatively consistent with many of the findings of other studies in which regional and even global scale cloud and aerosol properties were similarly associated in attempts to estimate the aerosol indirect radiative forcing (Kaufman and Nakajima, 1993; Kaufman and Fraser, 1997, Wetzel and Stowe, 1999; Nakajima et al. 2001; Seikiguchi et al. 2003; Quass et al. 2004). But, as MCT also noted, correlations of cloud properties with measures of aerosol

concentrations are unlikely to reveal just the effects of the particles on the clouds because there are physical processes that are likely to affect the aerosols as well as the retrievals of aerosol properties in the vicinity of clouds. The physical processes may also affect the clouds. In particular, MCT found that the low-level marine clouds near the European continent appeared to lose liquid water as the aerosol burden rose, in contrast to climate model predictions of the aerosol indirect forcing which indicate that cloud liquid water increases in polluted clouds and that this increase has a substantial impact on estimates of the forcing (Lohmann et al. 2000; Lohmann and Lesins, 2002). Twohy et al. (2005) also found liquid water path decreased as droplet number concentration increased, but the results tended not to be statistically significant due to high variability of liquid water and the small number of cases. The loss in liquid water might be explained by the drying of the clouds and boundary layer through the enhanced entrainment in the polluted clouds of dry continental air overlying the marine boundary layer (Ackerman et al. 2004). Harshvardhan et al. (2002) also noted the competition between the response of the clouds to aerosols and their response to the thermodynamics of their environment.

MCT also found that as regional cloud cover fraction increases cloud optical depth and droplet effective radius also increase. At the same time, the retrieved aerosol optical depth also increases as the regional cloud cover increases. Yet, droplet effective radius decreases as aerosol optical depth decreases. The increase of both aerosol optical depth and droplet radius with fractional cloud cover and the decrease in droplet radius with increasing aerosol optical depth were explained in terms of the widely dispersed distributions exhibited by the aerosol optical depth and the cloud properties. A wide range of cloud properties was observed within each range of aerosol loading. The trend in the mean of those properties was towards clouds with smaller droplets when the aerosol loading was high. Given the large dispersions of the distributions associated with the aerosol optical depth and the cloud properties, such trends might be influenced by the cases selected for analysis, and in particular, to the number of statistically independent cases used in the analysis.

Here, the number of cases included in the analysis is greatly expanded by incorporating the summertime observations for five years (1995-1999) of *NOAA-14* AVHRR observations. The cloud properties and aerosol optical depth for the five-year period were examined to determine year-to-year variations. The regional-scale year-to-year variations proved to be small compared with estimates of the statistical uncertainty in the means of the cloud properties and substantially smaller than the daily variability that these properties exhibited within each region studied (section 3.3). The similarity of the cloud properties and aerosol optical depths throughout the period justified the grouping of all observations into a single ensemble. The trends reported in MCT were then examined for their stability in the face of the larger ensemble of cases (section 3.4). The larger ensemble also allowed the separation of cloud data into those that occurred on relatively unpolluted "clean" days and those that occurred on relatively "polluted" days. Such comparisons facilitated estimates of the aerosol indirect radiative forcing for overcast conditions, normalized to the aerosol direct radiative forcing for cloud-free conditions. Radiative forcing was also estimated from the correlation of the cloud properties with collocated aerosol optical depths, as was done in MCT and in many of the earlier studies (section 3.5).

3.3 Data and Methodology

Global Area Coverage (GAC) radiances form the AVHRR on the *NOAA-14* satellite were analyzed for all daytime satellite passes over the northeastern Atlantic during May through August for the years 1995 – 1999. The region of analysis was bounded by 35° – 55° N latitude and 0° – 20° W longitude. Pixels over land were not used. NCEP reanalysis data showed periods of sustained onshore and offshore flow which gives rise to a wide range of aerosol burdens mixing with the marine stratus and stratocumulus that frequently cover this region during the summer.

The analysis methodology was described in MCT and is summarized briefly here. The shortwave reflectivities for the *NOAA-14* AVHRR were calibrated following Tahnk and Coakley (2001ab) and the 3.7 and 11-μm radiances were calibrated using standard methods (Kidwell 1995). Pixels that were within 40° of the sun's reflection, assuming specular reflection from a flat surface, were assumed to have been affected by sun glint and were removed from further analysis. A scene identification scheme was used to identify 4-km pixels as cloud-free, partially covered by clouds, completely overcast by clouds in a single layer, or overcast by clouds distributed in altitude. For cloud-free pixels, a two-channel scheme developed for retrieving aerosol properties for the Indian Ocean Experiment (INDOEX) was used to retrieve the 0.55-μm aerosol optical depth and apportion the fraction of the optical depth associated with a marine aerosol, which was made up of large non-absorbing particles, and an average continental aerosol, which was made up of small absorbing particles (Coakley et al. 2002). The aerosol models are described by Hess et al. (1998). Following Coakley et al. (2005), in pixels that contained clouds that were part of a single-layered, low-level system, a partly cloudy pixel retrieval scheme was used to obtain the 0.64-μm cloud optical depth, τ_c, droplet effective radius, R_e, cloud top altitude, and pixel-scale fractional cloud cover. In turn, these retrieved properties were used to derive cloud liquid water path, $W = \frac{2}{3} R_e \tau_c \rho$, where $\rho = 1$ g cm^{-3} is the density of water, and column droplet concentration, $N_c = \frac{\tau_c}{Q \pi R_e^2}$, where Q is the scattering efficiency, here taken to be 2.

Pixel-scale observations for each satellite pass were mapped into 1° × 1° latitude-longitude regions. The cloud screening rules described in MCT were used to ensure that the clouds in the 1° latitude-longitude regions accepted for analysis were all part of a single-layered, low-level cloud system. The mean of all cloud and aerosol properties were calculated for each satellite overpass for each 1° latitude-longitude region. For the cloud properties, the pixel-scale values were

weighted by the pixel-scale fractional cloud cover to calculate the means. For the aerosol optical depths, the means of the fine-mode optical depth, associated with the continental aerosol, the coarse-mode optical depth, associated with the marine aerosol, and the total optical depth, which is the sum of the fine and coarse-mode optical depths, were calculated. To ensure adequate sampling, a minimum of 10 pixels or 5% of all pixels in the 1° region, whichever was larger, was required for both cloud-free and cloudy pixels that yielded aerosol and cloud property retrievals for the region to be included in further analysis.

The observations for the 1° latitude-longitude regions were gathered into 5° × 5° latitude-longitude regions for individual years and the 5th and 95th percentiles of the 1° latitude-longitude overpass means of all cloud and aerosol properties were calculated. With the exception of fractional cloud cover, if the mean value of an aerosol or cloud property for a 1° region from a single satellite overpass was outside the 5th and 95th percentiles for a particular year and 5° latitude-longitude region, that 1° mean was considered to be an outlier and all aerosol and cloud properties for that 1° region and from that overpass were eliminated. Fractional cloud cover ranges between 0 and 1, so extremes in fractional cloud cover were not considered outliers.

The average of each cloud and aerosol property was calculated in 5° × 5° latitude-longitude regions for each satellite overpass. These overpass means for each 5° latitude-longitude region were in turn used to calculate means and standard deviations for each year. In addition, the standard errors, defined as the standard deviation of the individual pass means divided by the square root of the number of satellite overpasses were calculated. The standard errors serve as estimates of the uncertainty of the means.

Figure 3.1 shows the standard deviations of the passes within the years (outer range of error bars), and standard errors (inner range of error bars) for the 0.55-μm aerosol optical depth and selected cloud properties in each 5° latitude-longitude region for each of the five years. The means of the quantities lie midway between the inner error bars associated with the standard errors. Clearly, the variability of

the quantities within each year is substantially larger than the year-to-year variability in the means. While the yearly averages of droplet effective radius, cloud optical depth, cloud altitude, fractional cloud cover, liquid water amount, and column droplet concentration fluctuated about their five-year mean values, the fluctuations were small, often smaller than the standard error estimated for the yearly means. Only aerosol optical depth shows a trend toward smaller values as time progresses. The retrieved aerosol optical depths were dependent on the satellite viewing geometry, and in particular, aerosol optical depth decreased as the solar zenith angle increased. The year-to-year decrease in retrieved aerosol optical depth was likely caused by the satellite equator crossing times occurring later in the day as the years progressed due to the precession of the satellite's orbit. The bias introduced over the range of solar zenith angles was small and comparable in size to the errors reported for aerosol optical depths retrieved for the Indian Ocean (Coakley et al. 2002). Some of the decrease in aerosol optical depth might also arise from errors in the calibration of the AVHRR shortwave reflectivities, which are expected to be within 5% (Tahnk and Coakley, 2001ab). That similar trends were not found for the retrieved cloud optical depths suggests that the calibration errors were not a major factor in the aerosol optical depth trends, although the variability in cloud optical depths would all but mask the effects of a 5% error in calibration.

Because of the year-to-year consistency in the averages and standard deviations of the cloud and aerosol properties within each of the 5° latitude-longitude regions, all five years of data were composited into a single ensemble of observations. Hereafter, the removal of outlier data was performed by calculating the 5^{th} and 95^{th} percentiles based on the 5-year composite of data within each of the 5° latitude-longitude regions rather than on individual years as was done for the analysis presented in Fig. 3.1.

Cloud or aerosol retrievals were attempted in a total of 271,301 1° latitude-longitude regions that contained pixels that were observed during daytime, away from sun-glint, and over water. Table 3.1 indicates that only 3.4% of the candidate

regions passed the screening process that ensured that all clouds in the region were part of a single-layered system and the region had sufficient numbers of both cloud and aerosol retrievals to enable a comparison of cloud and aerosol properties. This percentage of usable 1° latitude-longitude regions is similar to the 2.9% found for 1995 (MCT). The 5 years of data provided 5.3 times the number of samples used in MCT, thereby facilitating analyses that could not be performed with the 1995 observations alone and also providing greater statistical confidence in the results.

Figure 3.2 shows the geographical distributions for aerosol optical depth, column droplet concentration, droplet effective radius, cloud optical depth, cloud cover fraction, and liquid water amount. The data in each satellite overpass was averaged in 1° latitude-longitude regions and then all overpass means in that 1° region were averaged over the five years to produce the climatology. The aerosol optical depths were retrieved in cloud-free pixels within the 1° regions and the cloud properties were accumulated only for cases in which all clouds within the 1° region were part of a single-layered, low-level cloud system. Smoothing was applied to the observations to emphasize the large-scale trends.

The geographical distributions shown in Fig. 3.2 are similar to those found for 1995 in MCT. During the summer months of 1995-1999, aerosol optical depth was, on average, highest near the coast (Fig. 3.2a). Column droplet concentration was also highest near the coast (Fig. 3.2b) consistent with an increase in the number of cloud condensation nuclei as aerosol optical depth increases. Cloud droplet effective radii were smallest and cloud optical depths were largest near the coast (Figs. 3.2c and d). That regions with larger aerosol optical depths had larger column droplet concentrations, smaller droplet radii, and larger cloud optical depths may be a manifestation of the Twomey Effect. On the other hand, it is possible that air flowing off the continent was more polluted and dryer than marine air at the same location. Continental air may have given rise to a drying of the clouds and marine boundary layer leading to smaller cloud droplets, cloud liquid water amounts, and cloud fractions (Figs. 3.2e and f). Clearly, the clouds may be

responding to the thermodynamics of the environment in which they are imbedded as well as to the aerosol burden.

3.4 Collocated aerosol optical depths and cloud properties

Figures 3.3-3.7 show various properties of low-level, single-layered clouds associated with aerosol optical depth. For each satellite overpass, the mean of the aerosol optical depth and all cloud properties were calculated for 1° × 1° latitude-longitude regions in which all the clouds were part of a single-layered, low-level cloud system and the region contained sufficient numbers of pixels yielding retrievals of cloud properties and aerosols to be included in the analysis. Cloud properties were associated only with aerosol optical depths from the same 1° region on the same satellite overpass. The 1° latitude-longitude averages were then composited in the associated 5° × 5° latitude-longitude regions in order to minimize the effects of the large scale trends evident in Fig. 3.2. Smaller regions would have been preferable, but even at 5° the number of cases were sometimes insufficient to achieve high levels of statistical confidence in the results. The cloud properties in each 5° latitude-longitude region were divided into 0.05 wide bins of aerosol optical depth. The mean and standard error of the overpass means were calculated for each aerosol bin. Bins with overpass means from fewer than 10 separate satellite overpasses were excluded. The estimated slope and standard deviation of the slope were estimated from a linear fit to the bin means weighted by the inverse of the standard errors of the bin means (Bevington, 1969). 5° latitude-longitude regions with bin-means from fewer than five bins were considered to have insufficient data for calculating trends and were left blank in the figures.

As was done in MCT, the cloud properties in Figs. 3.3-3.7 were correlated with the total optical depth, as opposed to the fine or coarse mode optical depths, as the total optical depth had the greatest correlation with the cloud properties. As most of the aerosol was in the fine-mode, associated with an average continental aerosol,

the total optical depth was well-correlated with the fine-mode optical depth. Neither the total optical depth nor the cloud properties were well-correlated with the coarse mode optical depth. Nonetheless, when significant trends were obtained with both the total and coarse mode optical depths, as for example, changes in cloud optical depth with aerosol optical depth, the changes were in the same direction with the exception of one 5° latitude-longitude region for the correlation between cloud altitude and aerosol optical depth.

In most of the 5° latitude-longitude regions, droplet effective radius decreased as aerosol optical depth increased (Fig. 3.3). Similar trends were found in MCT, but the greater number of cases contributed by the multiyear observations allowed for an investigation of additional 5° latitude-longitude regions surrounding the Iberian Peninsula and also larger ranges of aerosol optical depth in many of the regions. Column droplet concentration (Fig. 3.4) and cloud optical depth (Fig. 3.5) both increased with increasing aerosol optical depth in the majority of the 5° latitude-longitude regions. Cloud altitude stayed constant with changing aerosol burden in many regions but tended to decrease as aerosol burden increased around the Iberian Peninsula (Fig. 3.6).

Twomey's original estimates of the aerosol indirect radiative forcing invoked fixed cloud liquid water amounts (Twomey, 1974). Albtrecht (1989) suggested that cloud liquid water would increase with increasing aerosol burden owing to the suppression of drizzle. In six of the fifteen regions, the slope of the liquid water amount was greater than twice the estimated error, thereby indicating statistically significant trends (Fig. 3.7). Five of the six regions exhibited a decrease in cloud liquid water as aerosol burden increased. Air masses with larger aerosol burdens probably originated over the continent and were therefore dryer than less polluted, oceanic air masses. Ackerman et al. (2004) suggest that when the air in the free troposphere above the clouds is sufficiently dry, polluted clouds should lose liquid water as appears to occur in the results shown in Fig. 3.7.

The results shown in Figs. 3.3-3.5 are consistent with the Twomey Effect. Clouds in regions with larger aerosol burdens had larger column droplet

concentrations, smaller droplets and higher optical depths. Nonetheless, cloud properties are highly variable, and changes in cloud properties may arise from many factors. Many changes are surely not solely dependent on effects due to aerosols. As was noted in MCT and as is shown in Figure 3.8, aerosol optical depth appeared to increase as the percentage of cloudy pixels within a 1° × 1° latitude-longitude region increased for many of the 5° latitude-longitude regions. This increase in aerosol optical depth could have been caused by cloud contamination in the cloud-free pixels used to retrieve the aerosol properties. Undetected subpixel scale clouds in the cloud-free pixels cause the retrieved aerosol optical depths to be erroneously high. As cloud fraction increases, the degree of cloud contamination is likely to increase. In addition to cloud contamination, the increase in aerosol optical depth could have resulted from the swelling of aerosol particles in the higher humidity environments near clouds (Seinfeld and Pandis, 1998; Clarke et al., 2002). Increased particle production near clouds (Kütz and Dubois, 1997) and an increase in aerosol size caused by in-cloud processing (Leliveld and Heintzenberg, 1992) are also possible explanations for the increase in aerosol optical depth near clouds. Likewise, sunlight reflected by nearby clouds enhances the illumination of the adjacent cloud-free pixels thereby causing the aerosol optical depth to be overestimated (Podgorny, 2003). With both aerosol and cloud optical depths increasing with increasing cloud cover (Figure 3.10), the apparent correlation between cloud and aerosol optical depths (Fig. 3.5) cannot be solely the result of the Twomey Effect. The changes in retrieved aerosol and cloud properties may arise from changes in the cloud environment that affect both cloud and aerosol properties as well as fractional cloud cover.

In an attempt to identify changes in cloud properties attributable to changes in aerosol burden, the cloud properties were divided into two sets, one set that included those 1° latitude-longitude regions with mean 0.55-μm aerosol optical depths less than 0.13, the 40th percentile of aerosol optical depths for the entire 20° latitude-longitude domain, and another set that contained those 1° latitude-longitude regions with aerosol optical depths greater than 0.17, the 60th percentile

of the aerosol optical depths. For convenience, these two sets will be referred to as "clean clouds" and "polluted clouds." Cloud properties associated with the midrange of aerosol optical depths were excluded from this analysis. Figures 3.9-3.13 show the trends in cloud properties binned for each 0.05 increment in the 1° latitude-longitude regional fractional cloud cover for both the clean clouds (circles) and polluted clouds (crosses). Bin means are shown only for bins that had at least ten samples. Trends were not calculated in regions that did not have at least 5 bins for both the clean and polluted clouds.

Droplet effective radius increased as fractional cloud cover increased for both the clean clouds (circles in Fig. 3.9) and the polluted clouds (crosses in Fig. 3.9) indicating that at least some of the observed changes in droplet radius were due to factors other than the change in aerosol optical depth. Nonetheless, with the exception of one of the 5° × 5° latitude-longitude regions, the clean clouds had larger droplets than the polluted clouds, regardless of regional cloud cover, indicating that some of the change in droplet size could be associated with changes in aerosol burden.

Clean clouds had lower optical depths than polluted clouds (Fig. 3.10). For the clean clouds, cloud optical depth remained constant with fractional cloud cover in all but the southernmost regions. For the polluted clouds 6 of the 9 regions showed an increase in cloud optical depth as fractional cloud cover increased and had a slope larger than the error in the slope. In four of these regions, the slope was twice the error. Not only was cloud optical depth sensitive to aerosol burden, but the presence of large amounts of aerosol also seemed to influence the relationship between cloud optical depth and fractional cloud cover.

Cloud altitude remained constant or decreased with increasing fractional cloud cover (Fig. 3.11). The tendency for cloud altitude to decrease with increasing fractional cloud cover was more pronounced in the clean clouds than in the dirty clouds.

Despite the weak dependence of cloud optical depth on fractional cloud cover (Fig. 3.10) liquid water path increased as fractional cloud cover increased in most

regions (Fig. 3.12). A few of the regions showed a separation in the liquid water amounts for the clean and polluted clouds, but in most regions increases in aerosol burdens had no significant impact on the relationship between cloud liquid water and fractional cloud cover. Increased aerosol burden may decrease cloud liquid water (Fig. 3.7) but the effects of the aerosol appear to be minor compared with the changes in cloud liquid water associated with changing fractional cloud cover. As mentioned earlier, the amount of water vapor in the air mass may have a larger effect on cloud liquid water amounts than does the aerosol burdens and cloud condensation nuclei concentrations.

With the exception of one of the 5° latitude-longitude regions, polluted clouds consistently had more cloud droplets than clean clouds (Fig. 3.13). Interestingly, column droplet concentrations decreased as fractional cloud cover increased. Regions with higher cloud cover fractions contained clouds that were probably more mature and thus had more time for collision-coalescence processes, which may have reduced the number of cloud droplets.

3.5 Radiative Forcing Estimates

Top of the atmosphere fluxes were calculated in each of the 5° latitude-longitude regions using a broadband radiative transfer model that accounts for scattering and absorption by gases, aerosols, and clouds (Coakley et al., 2002). The radiative transfer model was run twice without clouds, once with a small amount of aerosols and once with a larger amount of aerosols. The difference in the top of the atmosphere fluxes between these two cases is the direct radiative forcing. The radiative transfer model was then run twice more with overcast clouds overlying the aerosol, once with a cloud optical depth for clean clouds overlying the small amount of aerosols and again for polluted clouds overlying the larger amount of aerosol. The difference in the top of the atmosphere fluxes between these cases is

the aerosol indirect radiative forcing for overcast conditions. The ratio of the indirect radiative forcing to the direct radiative forcing is shown in Figure 3.14.

Four methods were used to calculate the cloud and aerosol optical depths to be used as inputs to the radiative transfer model. 1) The aerosol 0.55-μm optical depths were chosen to be 0.15 and 0.25, in order to measure the response of the system to a 0.1 change in aerosol optical depth. The cloud optical depths were calculated from the trend lines in Fig. 3.5 for the given aerosol optical depths. This method was used in MCT. Results from this method are shown as the left-hand black bar in each sub-panel of Fig. 3.14. 2) In the second method, cloud liquid water was assumed to be fixed. The same aerosol optical depths as used in the previous method, 0.15 and 0.25, were used. Droplet effective radii were calculated from the trend lines of Fig. 3.3, given these aerosol optical depths. The assumption of constant liquid water amount was used to arrive at cloud optical depths. This method was also used in MCT. Results from this method are shown as the right-hand black bar in each sub-panel of Fig. 3.14. 3) The next two methods used the results obtained by dividing the cases into clean and polluted conditions. The trend of aerosol optical depth as a function of fractional cloud cover was calculated for both the clean and polluted data sets. The average cloud cover for the clean and polluted conditions was used with these trends to establish the clean and polluted aerosol optical depths. The average fractional cloud cover was also used in conjunction with Fig. 3.10 to determine the cloud optical depth for the clean and polluted clouds. The results of the radiative forcing calculations for this method are shown in Fig. 3.14 as the left-hand gray bar in each sub-panel. 4) In the fourth method, cloud liquid water was assumed to be fixed. The aerosol optical depths were the same as used in the previous method. The average fractional cloud cover for the clean and polluted clouds were used with Fig. 3.9 to calculate the droplet effective radii. The assumption of fixed liquid water was invoked to calculate cloud optical depths. The results of the radiative forcing calculations for this method are shown as the right-hand gray bar in each of the sub-panels of Fig. 3.14. Also shown in Fig. 3.14 are the results from MCT, the left-hand white bars are

from trends in cloud optical depth, and the right-hand white bars are from the assumption of fixed liquid water. The MCT results were calculated in the same manner as the first two methods described above.

The ratio of the aerosol indirect radiative forcing for overcast conditions to the direct radiative forcing for cloud-free conditions calculated by MCT ranged from –0.62 to 3.71. The range found in the current study from all four methods was –1.20 to 3.83 and the largest range of any individual method was –1.20 to 2.69 for the correlation of cloud optical depth with aerosol optical depth. If the ratio of –1.20 for the southeast corner of the study area is omitted, the range of ratios from this method reduces to 0.30 to 2.69. The increased stability of the forcing estimates in the current study results from the five-fold increase in data used. For the four methods used to calculate radiative forcing, the mean of the ratio of indirect to direct forcing, weighting all 5° latitude-longitude regions that contained data equally, ranged from 1.35 to 2.17. For comparison, MCT found the ratio of indirect forcing to direct forcing to be 1.33. These estimates of the strength of the indirect forcing relative to the direct forcing are substantially less than Sekiguchi et al. (2003), who found the indirect forcing for overcast conditions was 3 to 4.5 times greater than the direct forcing for cloud-free conditions.

MCT found that the assumption of fixed liquid water led to a slight underestimation of the indirect forcing. The results of the current study also indicate that assuming fixed liquid water may lead to an underestimation of the indirect radiative forcing. For the first two methods, based on the correlation of cloud properties with aerosol optical depths, the ratios of the direct to indirect forcing were nearly identical, 1.35 based on trends of cloud optical depth and 1.36 based on the assumption of fixed liquid water. For the latter two methods, however, based on comparisons of clean and polluted clouds, the ratio of forcings based on changes in cloud optical depth was 2.17 and that based on the assumption of fixed liquid water was 1.57.

Table 3.2 gives the cloud and aerosol properties used in the calculation of radiative properties for the clean and polluted clouds (gray bars on Fig. 3.14). The

trend lines calculated for aerosol and cloud properties as a linear function of fractional cloud cover, such as those shown in Figs. 3.9-3.13, were used along with the mean fractional cloud cover for the clean and polluted clouds in each of the 5° latitude-longitude regions to calculate the cloud and aerosol properties listed in Table 3.2.

Although not included in the ratios of the indirect to direct aerosol radiative forcing reported here, changes in cloud cover represent changes in cloud liquid water that might be attributed to the increased aerosol burden (Ackerman et al. 2003). Here the ratios are for the aerosol indirect forcing for overcast conditions to the aerosol direct radiative forcing for cloud-free conditions. Cloud droplet effective radius and cloud optical depth were affected by the change in cloud cover, as shown in Figs. 3.9 and 3.10, but the effects of the additional cloud cover on radiative fluxes was not included in the radiative forcing calculations. Increased aerosol optical depth was associated with increased cloud cover for all regions. Of course, some of the increase in aerosol optical depth accompanying the increase in cloud cover, as shown in Fig. 3.8 and as previously discussed, may be due to processes that have little relevance for the aerosol indirect radiative forcing.

3.6 Conclusions

Cloud and aerosol properties were retrieved in 1° × 1° latitude-longitude regions in which all the clouds were part of a single-layered, low-level system. Only regions that contained sufficient numbers of cloud-free pixels for aerosol retrievals and sufficient numbers of cloudy pixels for cloud retrievals were used in the analysis. The means of the cloud and aerosol properties for each satellite pass were composited in the associated 5° × 5° latitude-longitude region. 1° latitude-longitude regions containing outliers, beyond the 5^{th} or 95^{th} percentiles for a 5° latitude-longitude region for the five-year period, were excluded. The year-to-year variations in the means and standard deviations of the cloud and aerosol properties in each 5° × 5° latitude-longitude region were examined for the five-year period.

Annual mean aerosol optical depths appeared to decrease slowly, but systematically with time. The decrease was probably the result of the precession of the satellite's orbit and consequent increase in the average solar zenith angle. The annual mean cloud properties showed no systematic variations and changes in the annual means were often smaller than the standard error in the mean and considerably smaller than the standard deviation of the overpass means within each year. The uniformity of the cloud and aerosol properties for all five years justified the combination of the observations into a single ensemble. Each satellite pass within the ensemble was taken to be an independent sample.

Links between aerosol and cloud properties were analyzed in each of the 5° regions. The size of the region was chosen to minimize effects of geographic trends in the cloud and aerosol properties. Smaller regions would have reduced the effects of the geographic trends, but they would also have had smaller numbers of cases thereby reducing the confidence levels of any trends. The conditions of simultaneity and close spatial proximity were designed to ensure that the changes in cloud properties were linked to changes in aerosol burdens. The restrictions on the size of the region analyzed and on the simultaneity of the cloud and aerosol observations ensured that comparisons between clouds and aerosols on different days or in different locations were avoided. For some of the analyses, the data were segregated into "clean" clouds, those for which the average 0.55-μm aerosol optical depth for a 1° latitude-longitude region was less than 0.13, the 40^{th} percentile of the aerosol optical depths within the 20° domain for the five-year period, and "polluted" clouds, those for which the average aerosol optical depth was greater than 0.17, the 60^{th} percentile of the aerosol optical depths.

The results presented here suggest that clouds are affected by increased burdens of aerosols, but they also suggest that other factors can affect the clouds and how they respond to increased aerosol burdens. In addition, the results also suggest that both clouds and aerosols may be affected by the thermodynamic environment in which they are imbedded and behave in ways that could be

interpreted as evidence for the indirect effect of aerosols, but may have nothing to do with cloud-aerosol interactions. As would be expected on the basis of the Twomey effect, in general, column droplet concentration and cloud optical depth rose and droplet radii fell as aerosol optical depth increased. This behavior was found not only when the cloud properties were correlated with the aerosol optical depth but also when clean clouds were compared with polluted clouds. At the same time, droplet effective radius, cloud optical depth, and aerosol optical depth all increased as the regional scale fractional cloud cover increased. Clearly, in order to determine how aerosols affect droplet effective radius and cloud optical depth, correlations between aerosol optical depth and the cloud properties, such as shown in Fig. 3.3, should be performed while holding the remaining cloud parameters that affect droplet radius and optical depth, such as fractional cloud cover and cloud altitude, constant.

The tendency for both cloud and aerosol optical depths to increase as fractional cloudiness increased suggests that correlations between aerosol and cloud optical depths are not solely due to the Twomey Effect. Instead, both aerosol and cloud optical depths change in response to thermodynamic fields that also affect the fractional cloud cover. Several processes, including, for example, cloud contamination in the cloud-free pixels used to determine the aerosol burdens, were suggested as possible reasons for the increase in aerosol optical depth as cloudy pixel fraction increased. Interestingly, when polluted clouds were compared to clean clouds, the polluted clouds were more likely than clean clouds to show an increase in cloud optical depth with increasing fractional cloud cover. For both polluted and clean clouds, the column droplet number concentration seemed to fall with increasing cloud cover. The fall in column droplet number concentration may reflect the maturity of systems that heavily cover the 1° latitude-longitude regions studied here. In a few of the 5° latitude-longitude regions, cloud altitude decreased as both aerosol optical depth and fractional cloud cover increased.

Liquid water path generally decreased or remained constant as aerosol optical depth increased. Liquid water path increased as fractional cloud cover increased

and the liquid water paths were essentially the same for clean and polluted clouds within the 5° regions. Evidently, clean clouds are associated with moist oceanic air and polluted clouds are associated with dry continental air. For dry conditions, liquid water path can decrease as aerosol optical depth increases (Ackerman et al. 2004). As Fig. 3.2e appears to suggest, dry continental air is associated with small regional fractional cloud cover and moist maritime air is associated with large fractional cloud cover. Clearly, the effects of aerosols on clouds need to be disentangled from the effects of the moisture, or lack of moisture, delivered with the aerosols.

Depending on the method used to calculate changes in cloud optical depth, whether from differences between clean and polluted clouds, or from allowing cloud liquid water to change or forcing the liquid water to remain constant, the aerosol indirect radiative forcing for overcast conditions was found to be 1.4 to 2.2 times larger than the corresponding aerosol direct radiative forcing for cloud-free conditions. The range of the ratio of indirect to direct forcing was less in this study than in MCT. This reduction in the range of the radiative forcing estimates was due to the increased volume of data that resulted from compositing five years of observations. The additional observations also made possible the separation into clean and polluted conditions.

Table 3.1. Number and percentage of 1° × 1° latitude-longitude regions that survived successive data screening tests. Percentages are based on 271,301 1° latitude-longitude regions from 2499 satellite overpasses that contained at least one pixel that was observed during daytime, over water, and away from sun glint, and was therefore suitable for attempting a retrieval.

Screening	Aerosol		Cloud	
	Number	%	Number	%
At least 10 pixels or 5% (whichever was greater) of all pixels in region had either cloud or aerosol retrievals	59,063	21.8	131,541	48.5
Region contained only cloud-free pixels or clouds from single-layered, low-level cloud systems	47,745	17.6	70,641	26.0
Region contained cloud and aerosol properties that were within the 5th and 95th percentile for that 5° latitude-longitude area	39,579	14.6	47,714	17.6
Region contained both cloud and aerosol retrievals that passed previous data screening tests	9,247	3.4	9,247	3.4

Table 3.2. Aerosol and cloud properties used in radiative forcing calculations based on the correlations with fractional cloud cover (gray bars in Fig. 3.14). Properties are: 0.55-μm aerosol optical depth, $\tau_{aerosol}$, fractional cloud cover, fcc, 0.64-μm cloud optical depth, τ_{cloud}, droplet effective radius, R_e (μm), column droplet concentration, N_c (10^6 cm^{-2}), liquid water path, LWP (g/m^2), and cloud altitude, Z_c (km).

		20-15 W		15-10 W		10-5 W	
50-55 N		clean	polluted	clean	polluted		
	$\tau_{aerosol}$	0.117	0.248	0.152	0.241		
	fcc	0.32	0.44	0.38	0.45		
	τ_{cloud}	7.93	8.02	7.06	8.27		
	R_e	11.1	11.4	11.8	11.0		
	N_c	1.34	1.29	0.94	1.47		
	LWP	61.1	65.2	57.3	64.1		
	Z_c	1.88	1.87	1.75	1.91		
45-50 N		clean	polluted	clean	polluted	clean	polluted
	$\tau_{aerosol}$	0.105	0.230	0.105	0.241	0.104	0.256
	fcc	0.38	0.45	0.39	0.40	0.36	0.41
	τ_{cloud}	6.83	7.81	6.41	7.89	6.82	7.79
	R_e	11.8	10.9	11.4	10.6	11.0	9.8
	N_c	0.97	1.43	1.08	1.60	1.13	1.87
	LWP	55.8	59.3	50.0	56.4	49.3	52.5
	Z_c	1.71	1.92	1.70	1.83	1.63	1.63
40-45 N		clean	polluted	clean	polluted		
	$\tau_{aerosol}$	0.094	0.224	0.093	0.243		
	fcc	0.36	0.42	0.34	0.38		
	τ_{cloud}	6.17	6.79	6.06	7.06		
	R_e	12.1	11.2	12.0	10.1		
	N_c	0.94	1.34	0.98	1.57		
	LWP	49.8	50.2	48.7	45.3		
	Z_c	1.71	1.67	1.55	1.60		
35-40 N		clean	polluted	clean	polluted		
	$\tau_{aerosol}$	0.089	0.215	0.095	0.232		
	fcc	0.34	0.38	0.33	0.35		
	τ_{cloud}	6.23	7.05	5.86	6.29		
	R_e	12.4	11.4	11.6	10.3		
	N_c	0.95	1.32	0.95	1.62		
	LWP	51.0	52.4	44.1	40.1		
	Z_c	1.79	1.82	1.56	1.48		

a)

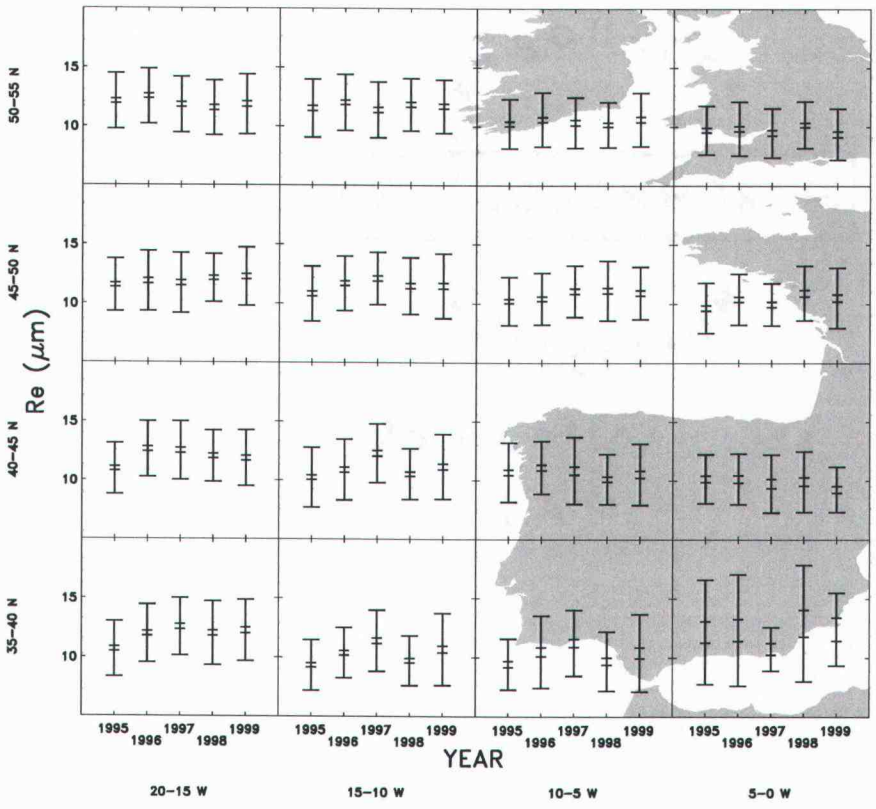

Figure 3.1. Standard deviation (outer range of error bars) and standard error (inner range of error bars) for a) droplet effective radius (μm), b) 0.64-μm cloud optical depth, c) cloud altitude (km), d) fractional cloud cover, e) liquid water path (g/m^2), f) column droplet concentration (10^6 cm^{-2}), and g) 0.55-μm aerosol optical depth. The standard error is given by the standard deviation divided by the square root of the number of samples, in this case, the number of satellite overpasses that contributed observations. All cloud properties are for single-layered, low-level clouds. Means are calculated for every daytime satellite overpass in 1° × 1° latitude-longitude regions. In calculating the pass averages within a region, cloud properties were weighted by the pixel-scale fractional cloud cover. These pass-means were then averaged for May-August in the 5° × 5° latitude-longitude regions. Data from individual years, 1995-1999, are shown in their respective 5° latitude-longitude region.

b)

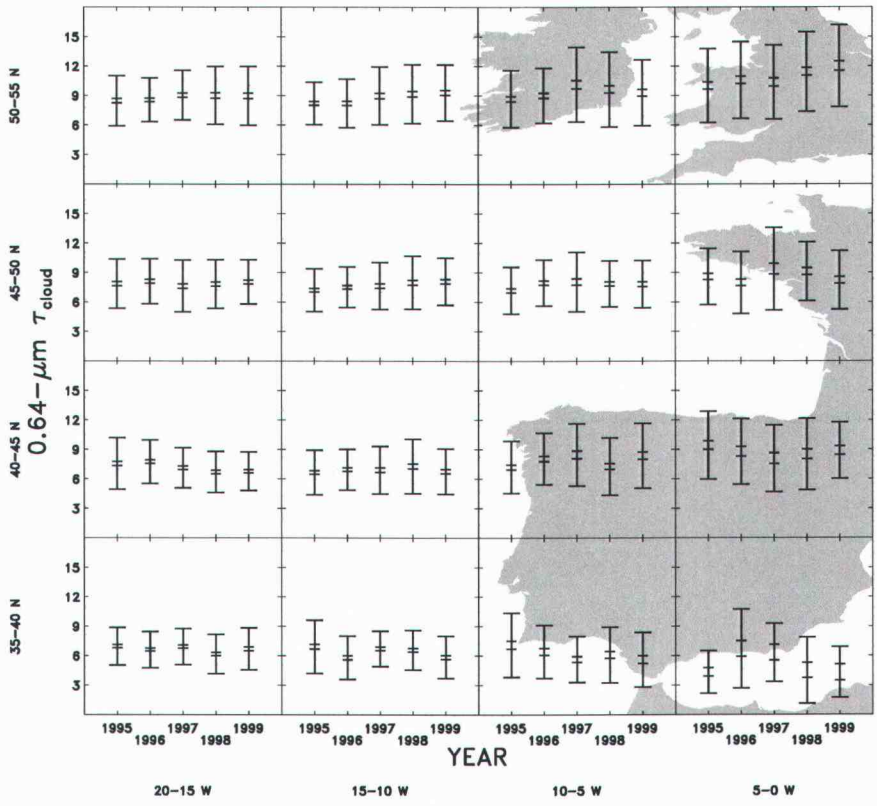

Figure 3.1 (Continued)

c)

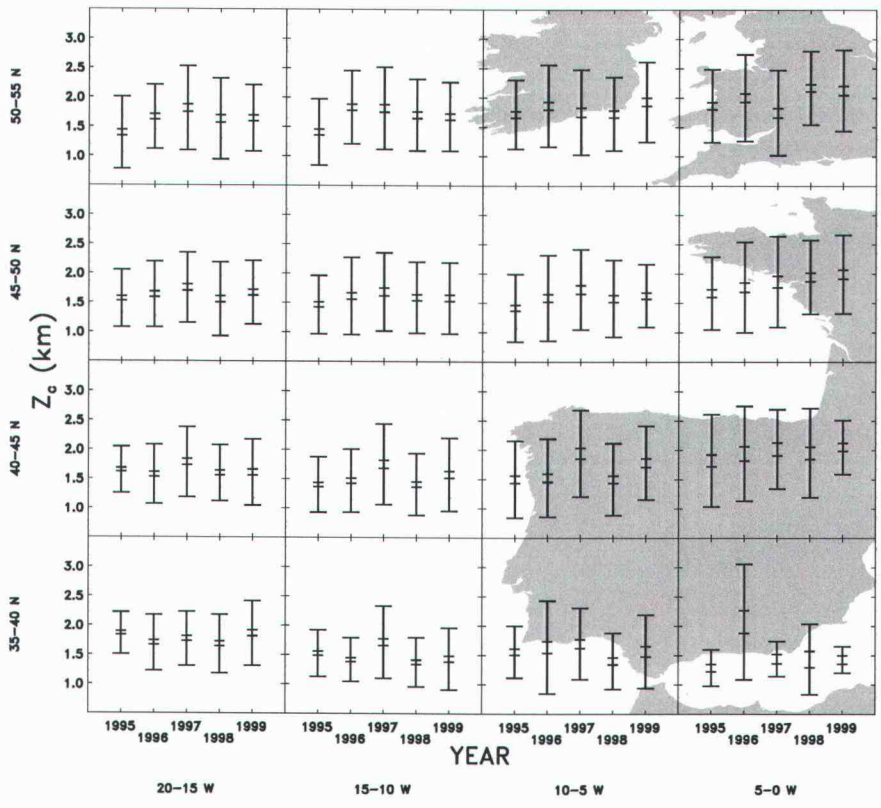

Figure 3.1 (Continued)

d)

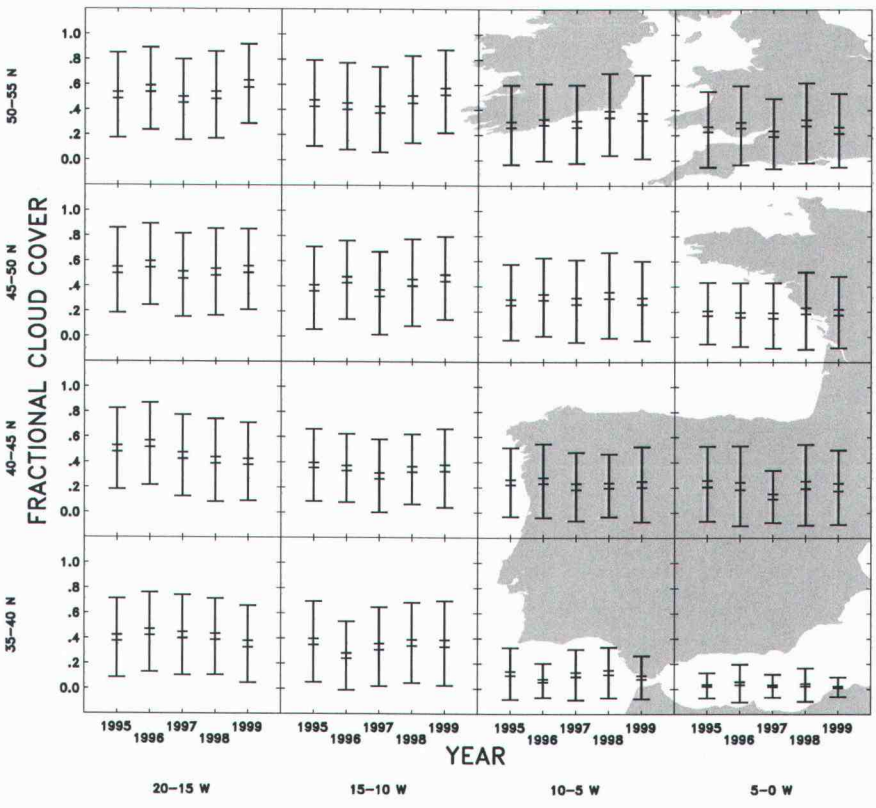

Figure 3.1 (Continued)

e)

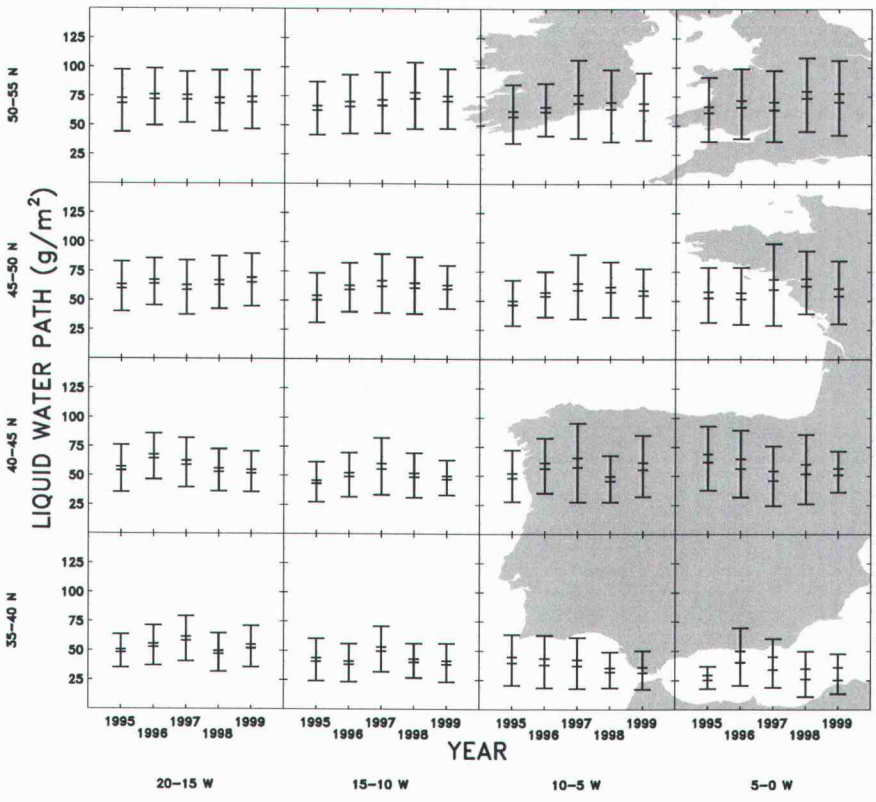

Figure 3.1 (Continued)

f)

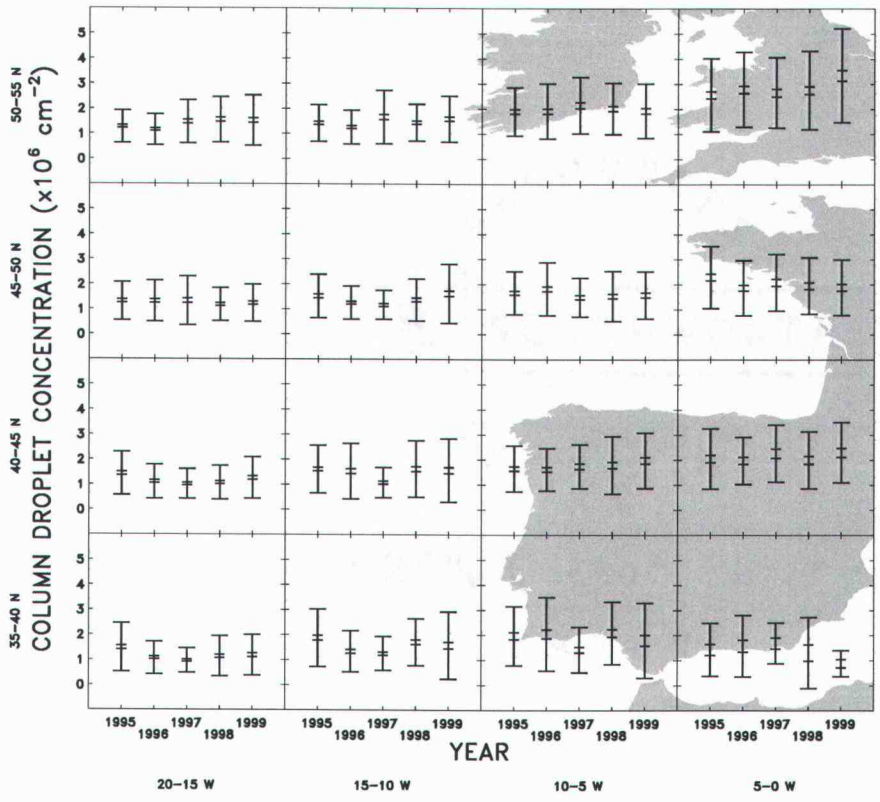

Figure 3.1 (Continued)

g)

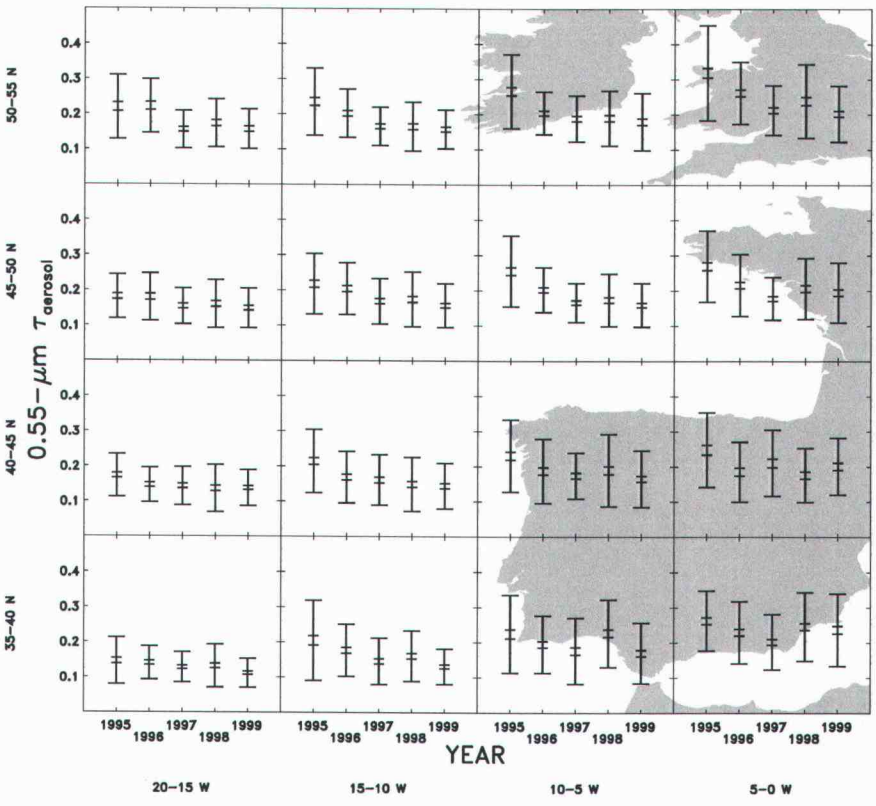

Figure 3.1 (Continued)

a)

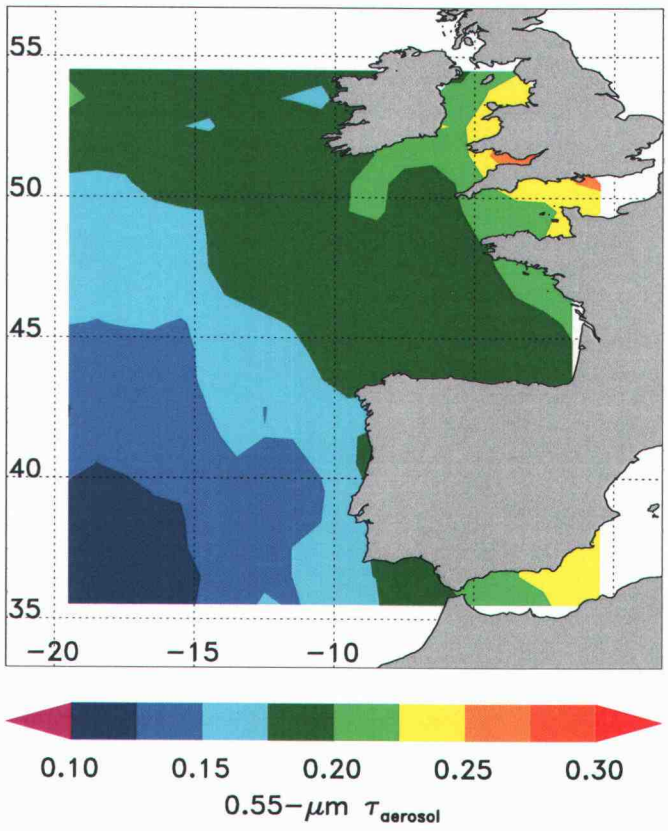

Figure 3.2. Mean properties of single-layered, low-level clouds and 0.55-μm aerosol optical depth for May-August, 1995-1999: a) 0.55-μm aerosol optical depth, b) column droplet concentration (10^6 cm^{-2}), c) droplet effective radius (μm), d) 0.64-μm cloud optical depth, e) fractional cloud cover, and f) liquid water path (g/m^2). The contours have been smoothed to show the large-scale trends. The aerosol optical depths are from 1° × 1° latitude-longitude regions in which all of the clouds in the region were part of a single-layered, low-level system or were cloud-free. In calculating the overpass averages within a region, cloud properties were weighted by the pixel-scale fractional cloud cover.

b)

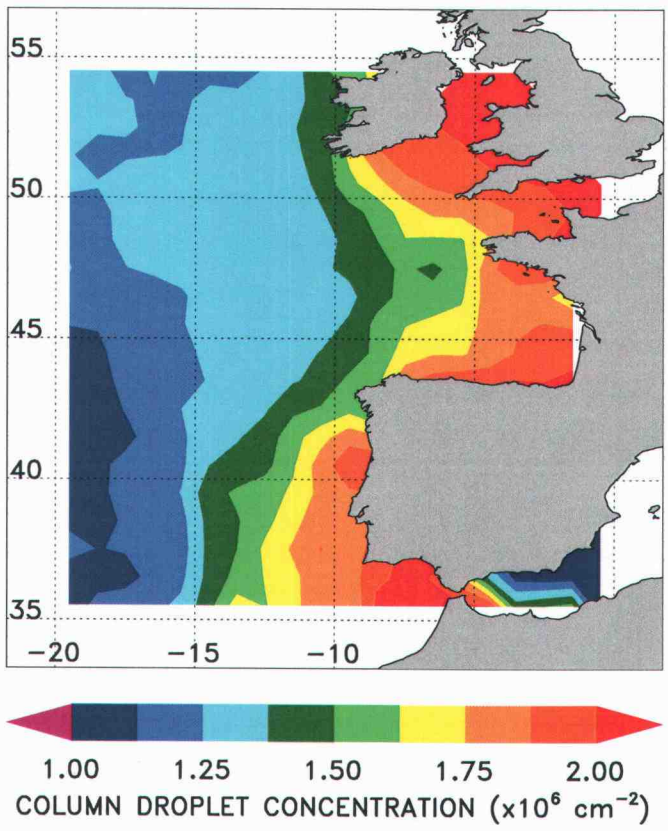

Figure 3.2 (Continued)

c)

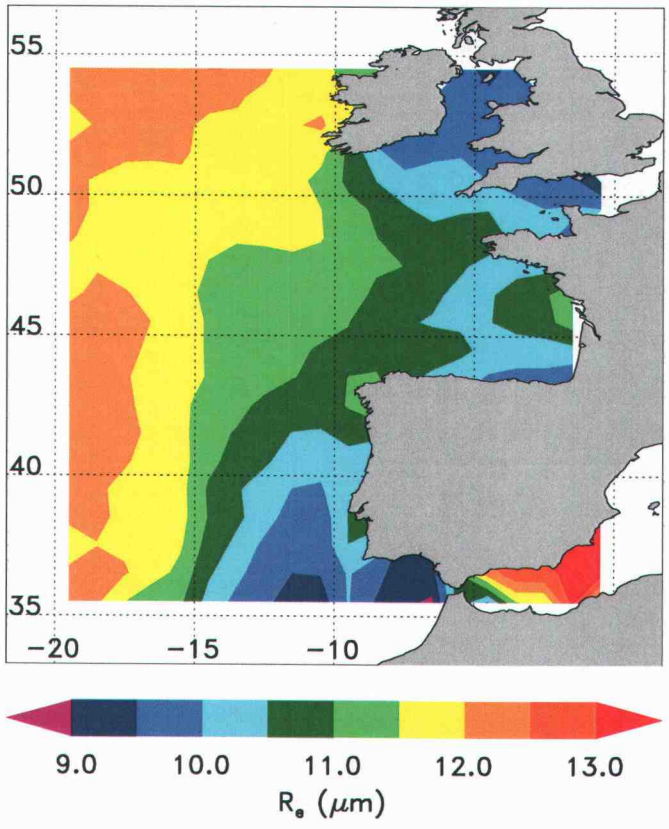

Figure 3.2 (Continued)

d)

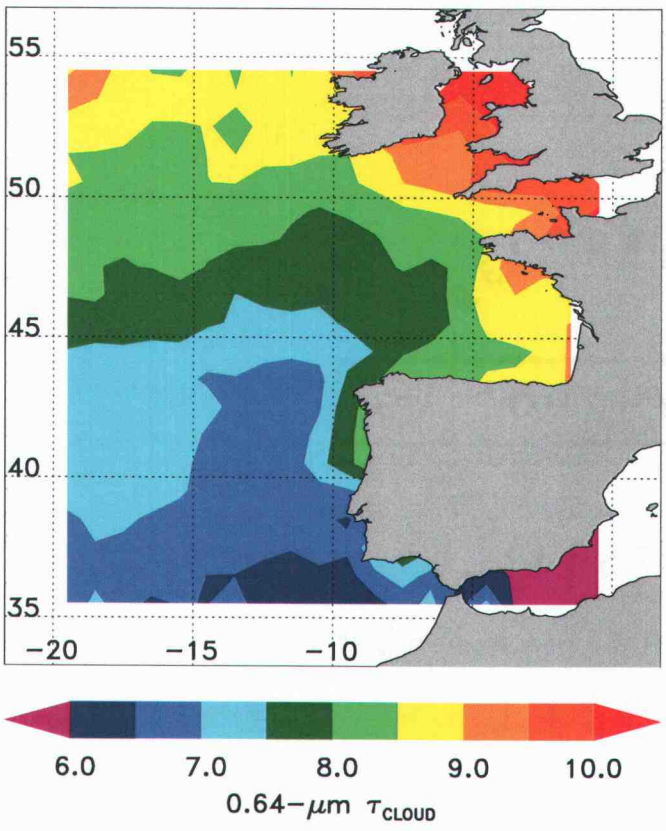

Figure 3.2 (Continued)

e)

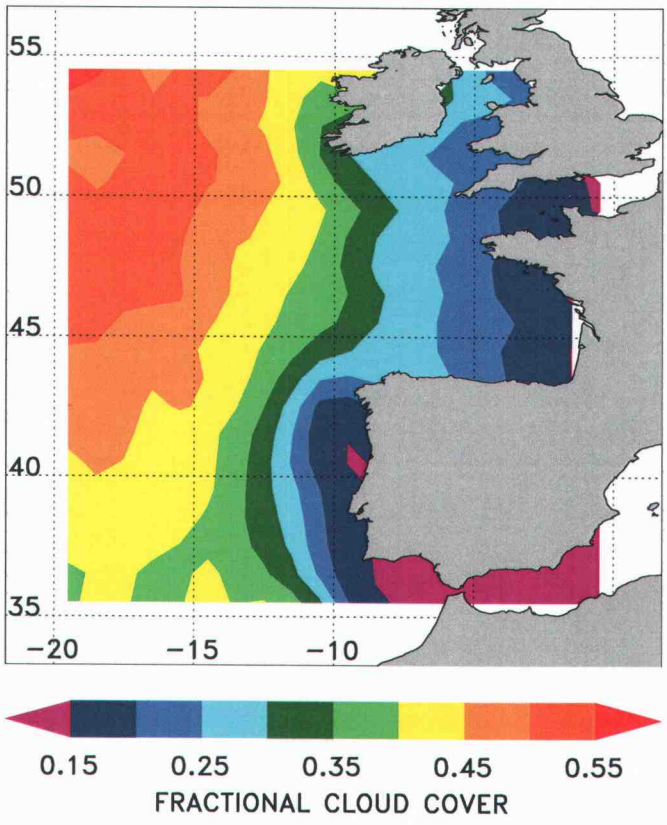

Figure 3.2 (Continued)

f)

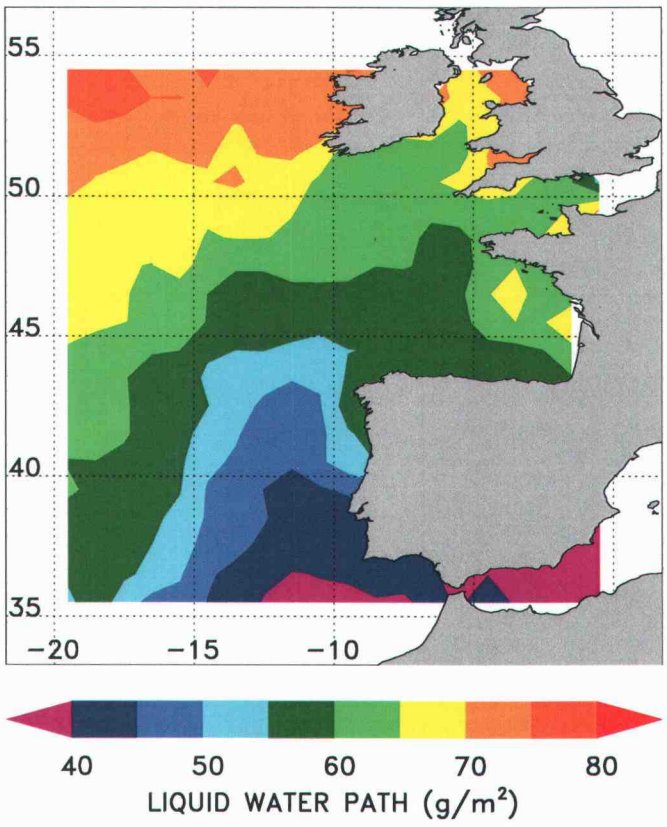

Figure 3.2 (Continued)

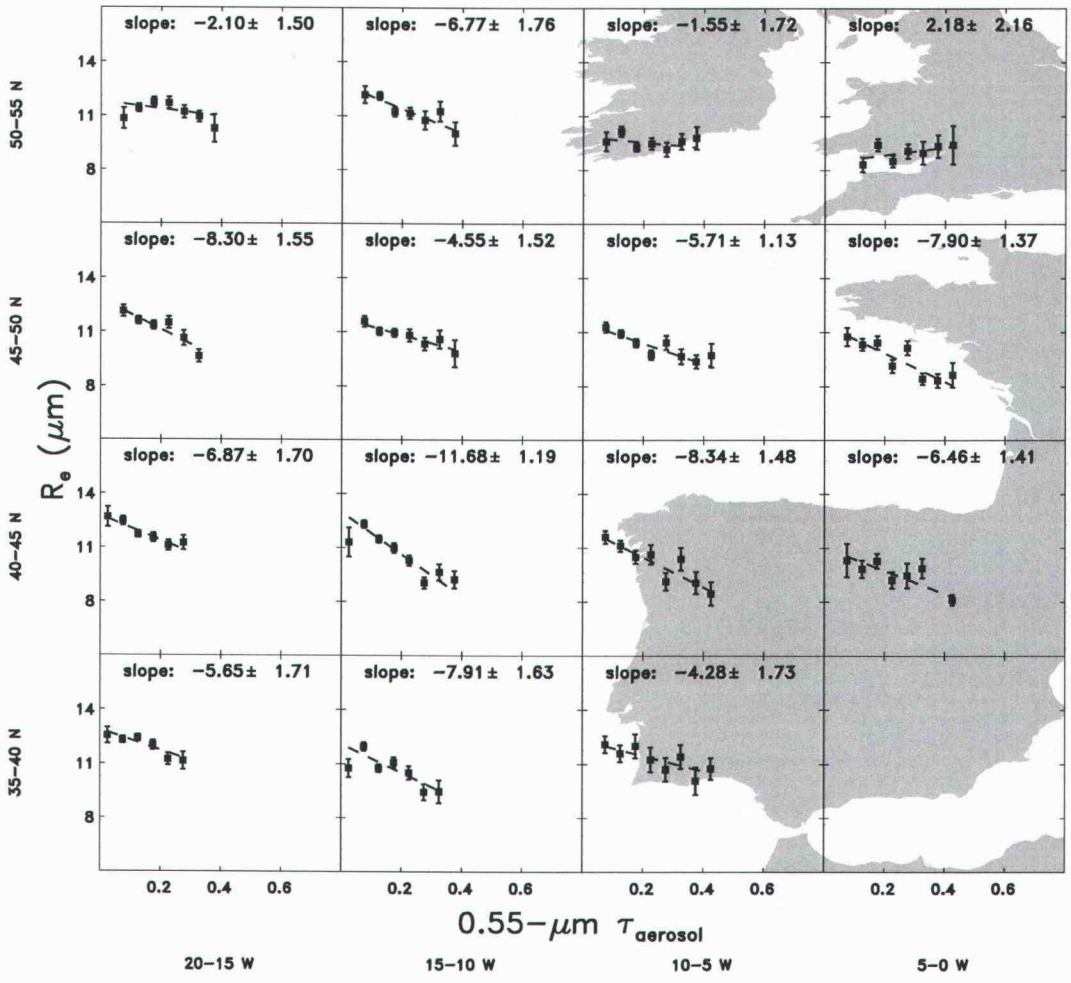

Figure 3.3. Means of overpass averaged droplet effective radius (μm) for 1° latitude-longitude regions binned for each 0.05 interval of aerosol optical depth. Each sub-panel contains data from that 5° × 5° latitude-longitude region. Error bars represent the standard error, given by the standard deviation of the means from individual passes for that bin divided by the square root of the number of passes that contributed observations to that bin. The dashed line is a linear fit to the bin means inversely weighted by the standard error. Also given are the mean and standard deviation estimated for the slope of the linear fit.

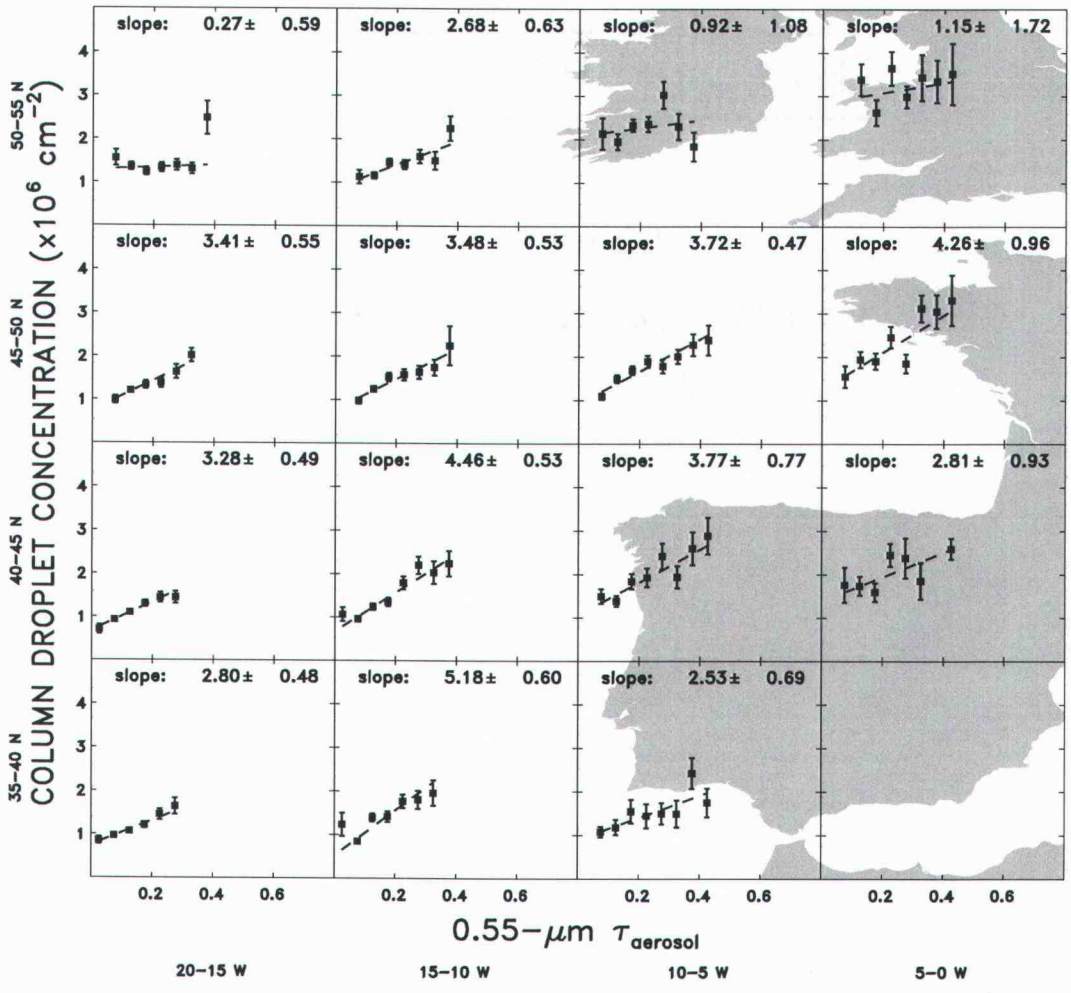

Figure 3.4. Same as Fig. 3.3, but for column droplet concentration (10^6 cm^{-2}).

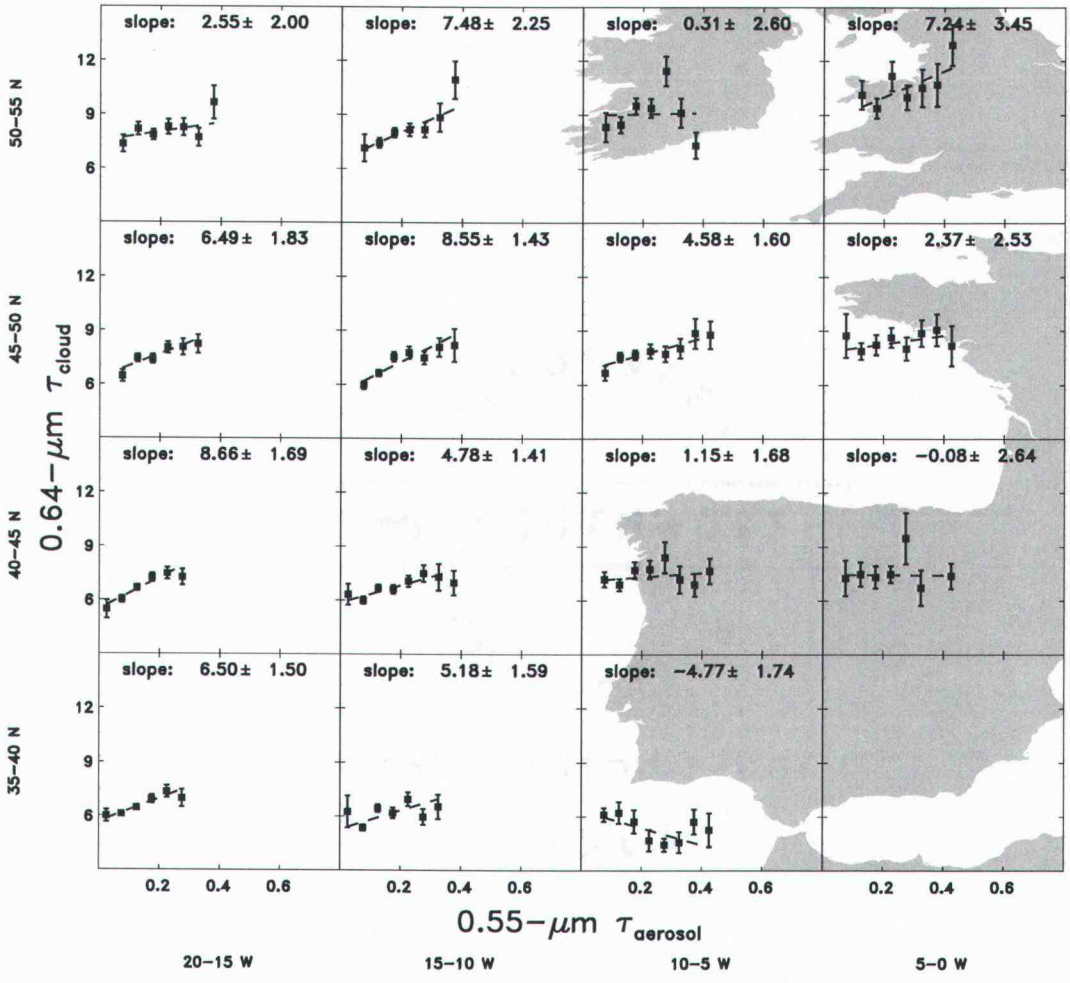

Figure 3.5. Same as Fig. 3.3, but for 0.64-μm cloud optical depth.

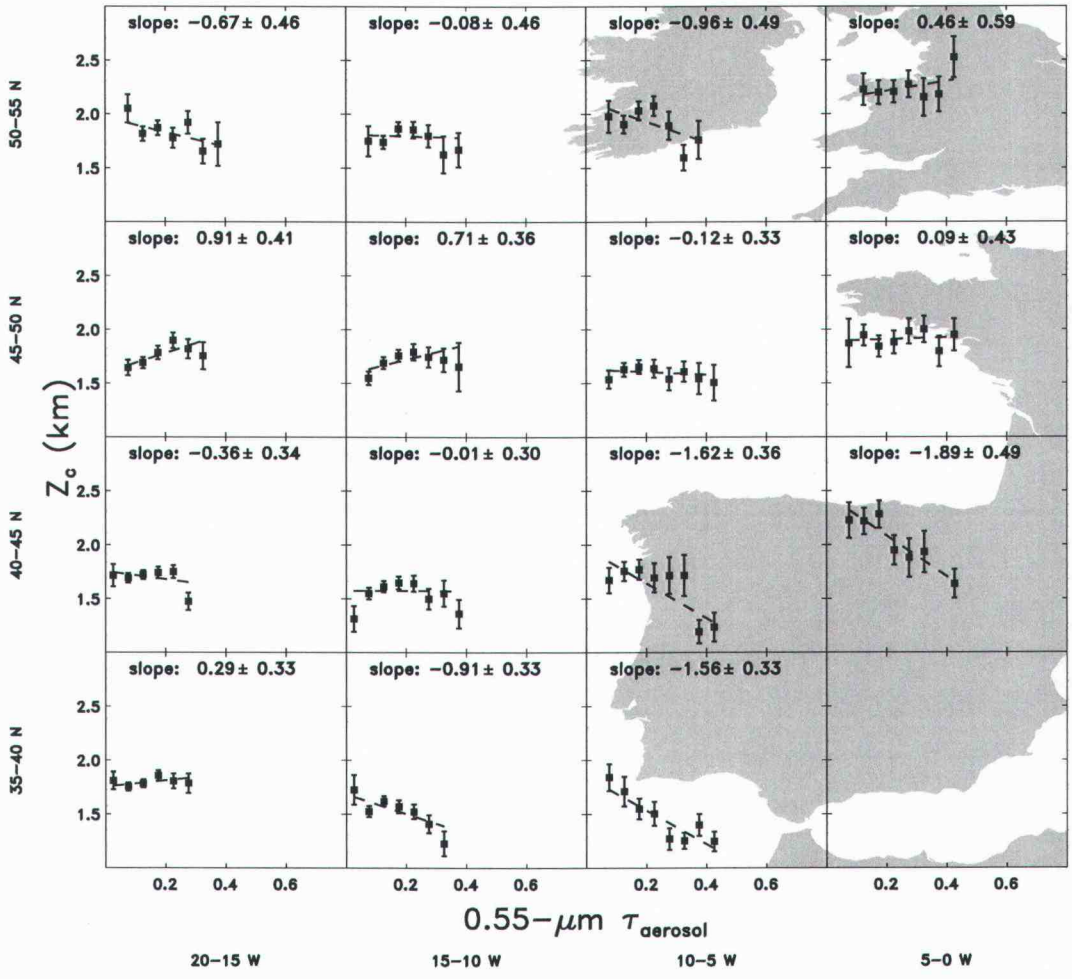

Figure 3.6. Same as Fig. 3.3, but for cloud altitude (km).

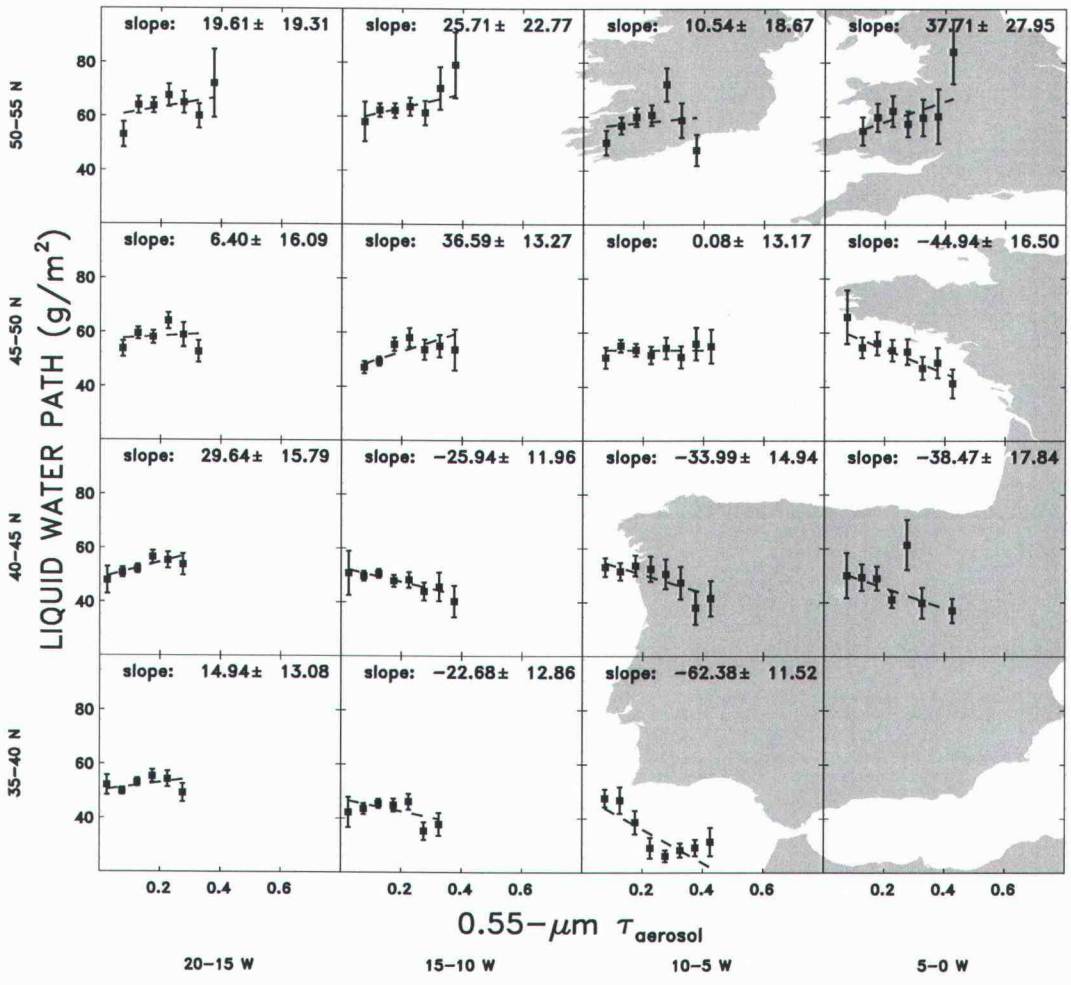

Figure 3.7. Same as Fig. 3.3, but for liquid water path (g/m^2).

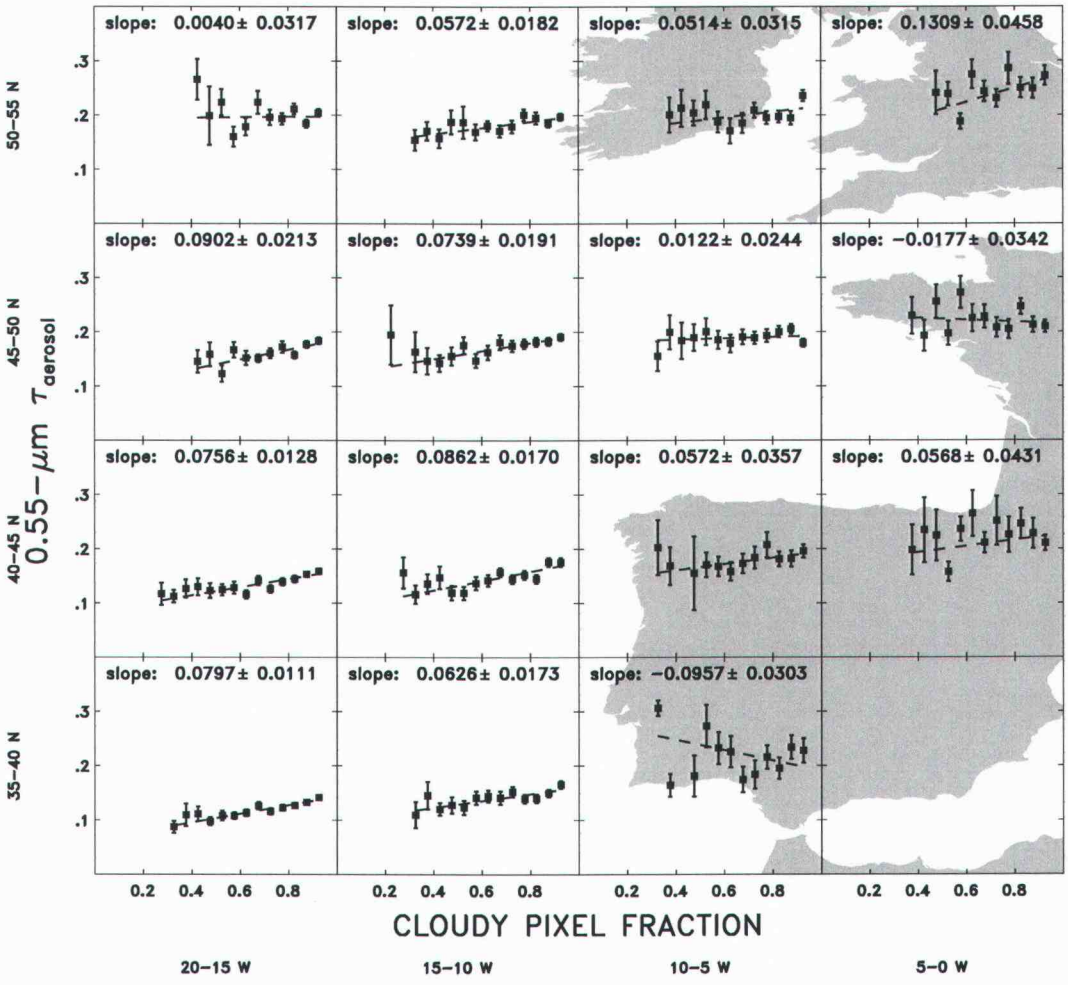

Figure 3.8. Same as Fig. 3.3, but for 0.55-μm aerosol optical depth and cloudy pixel fraction. Cloudy pixel fraction is the fraction of pixels within a 1° × 1° latitude-longitude region identified as containing clouds (pixel-scale cloud fraction > 0.2). Only the 1° × 1° latitude-longitude regions that also contained a sufficient number of cloud retrievals for which the properties are presented in Figs. 3.3-3.7 are included.

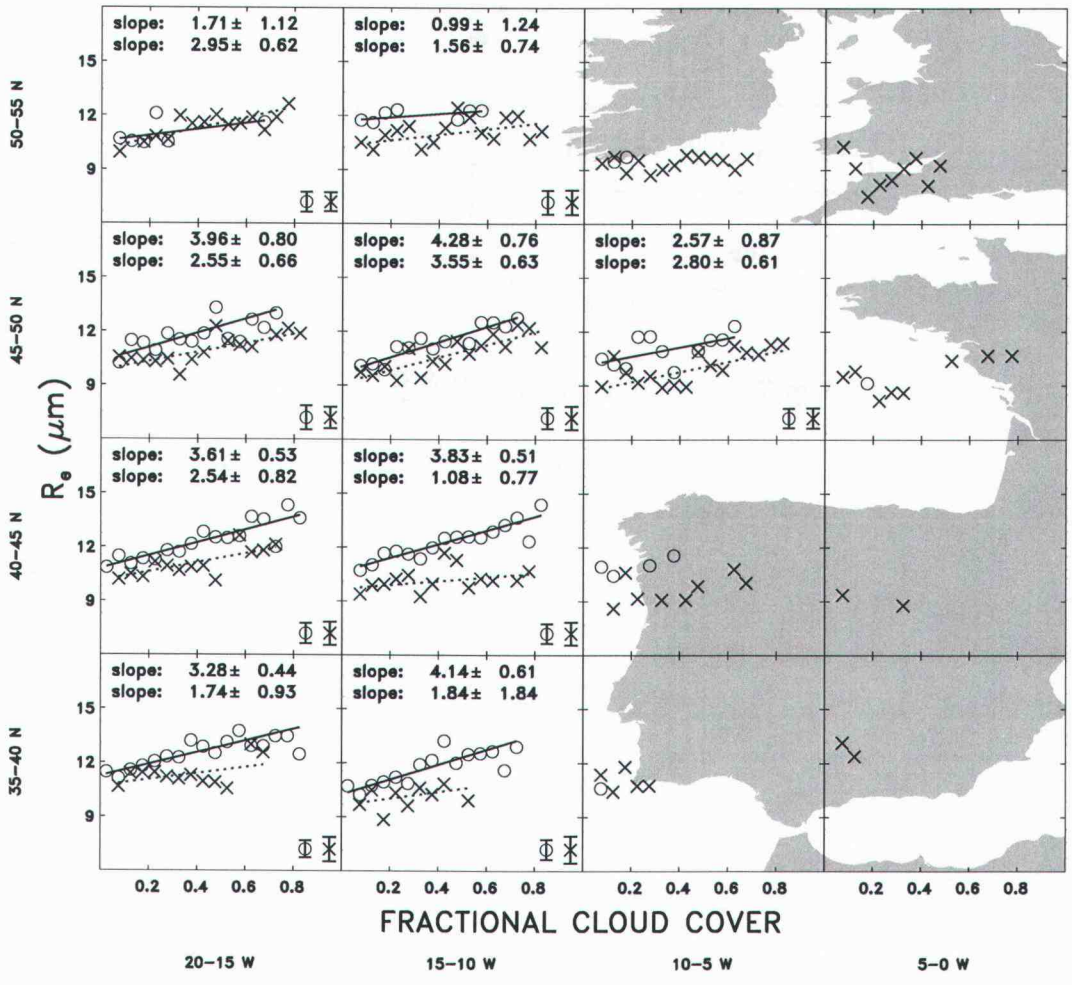

Figure 3.9. Means of overpass averaged droplet effective radius (μm) for 1° latitude-longitude regions binned for each 0.05 interval of fractional cloud cover. Circles are for 1° latitude-longitude regions that had a mean aerosol optical depth less than 0.13, the 40th percentile of aerosol optical depth of all 1° latitude-longitude regions. Crosses are for 1° latitude-longitude regions that had a mean aerosol optical depth greater than 0.17, the 60th percentile of aerosol optical depth. Error bars plotted in the lower right corner are the RMS of the standard error for the data points. The solid (dashed) line is a linear fit to the bin means of the circles (crosses) inversely weighted by the standard error. Also given are the mean and standard deviation estimated for the slope of the linear fit to the circles (upper) and crosses (lower).

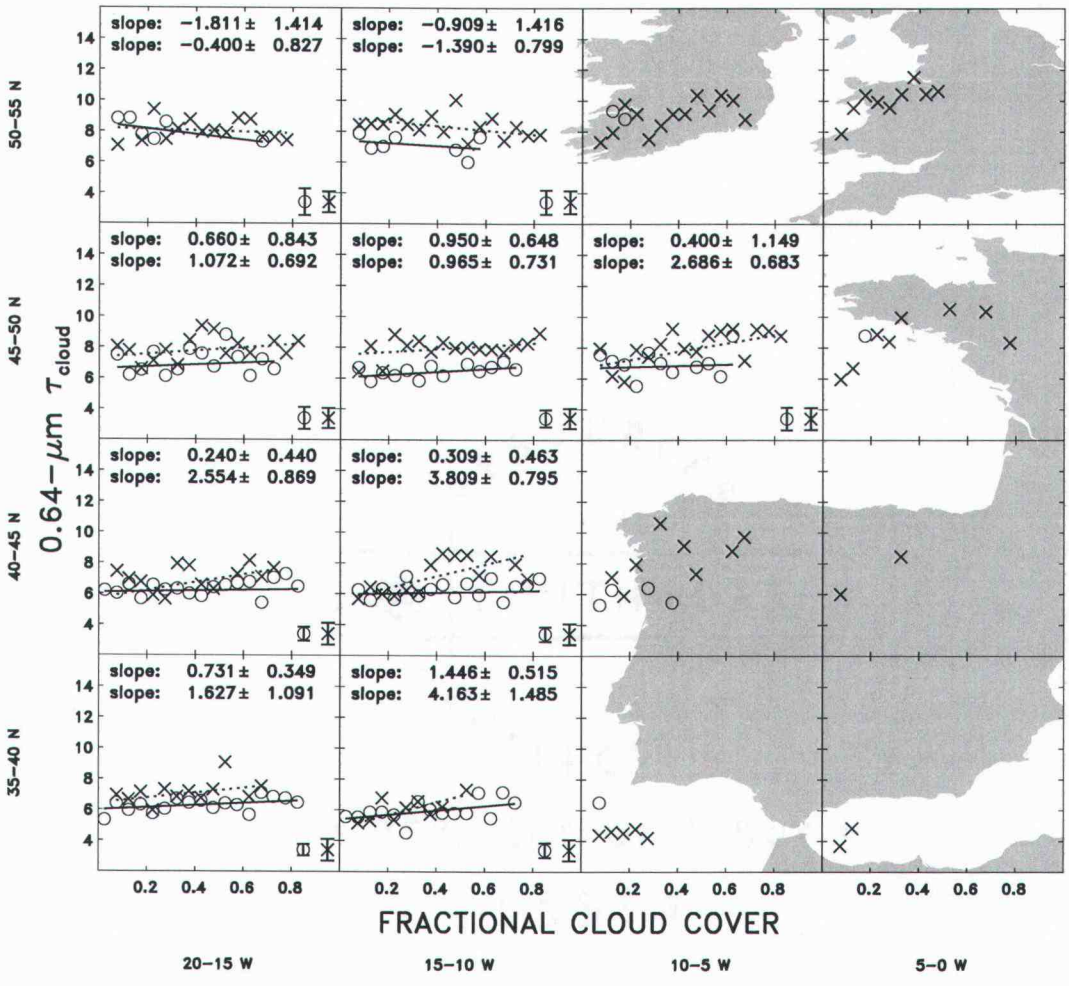

Figure 3.10. Same as Fig. 3.9, but for 0.64-μm cloud optical depth.

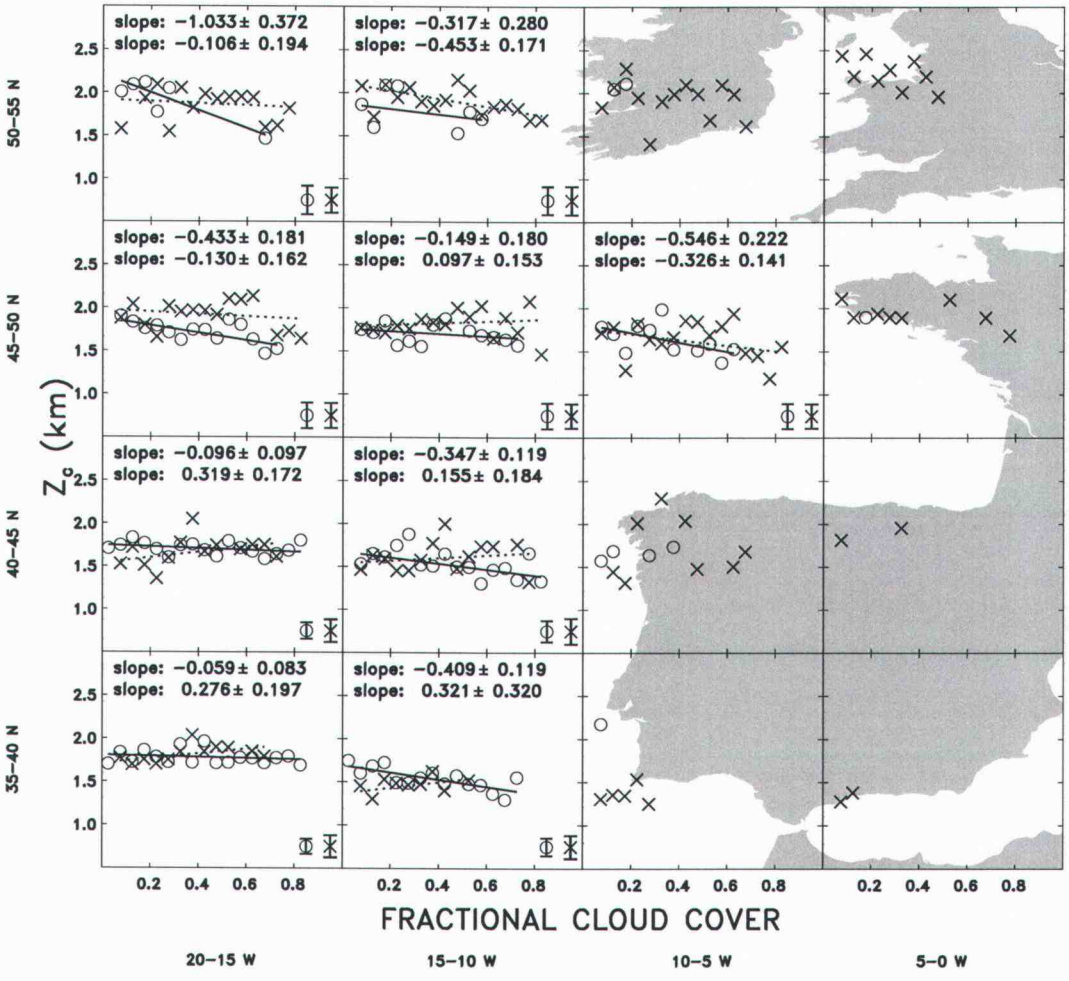

Figure 3.11. Same as Fig. 3.9, but for cloud altitude (km).

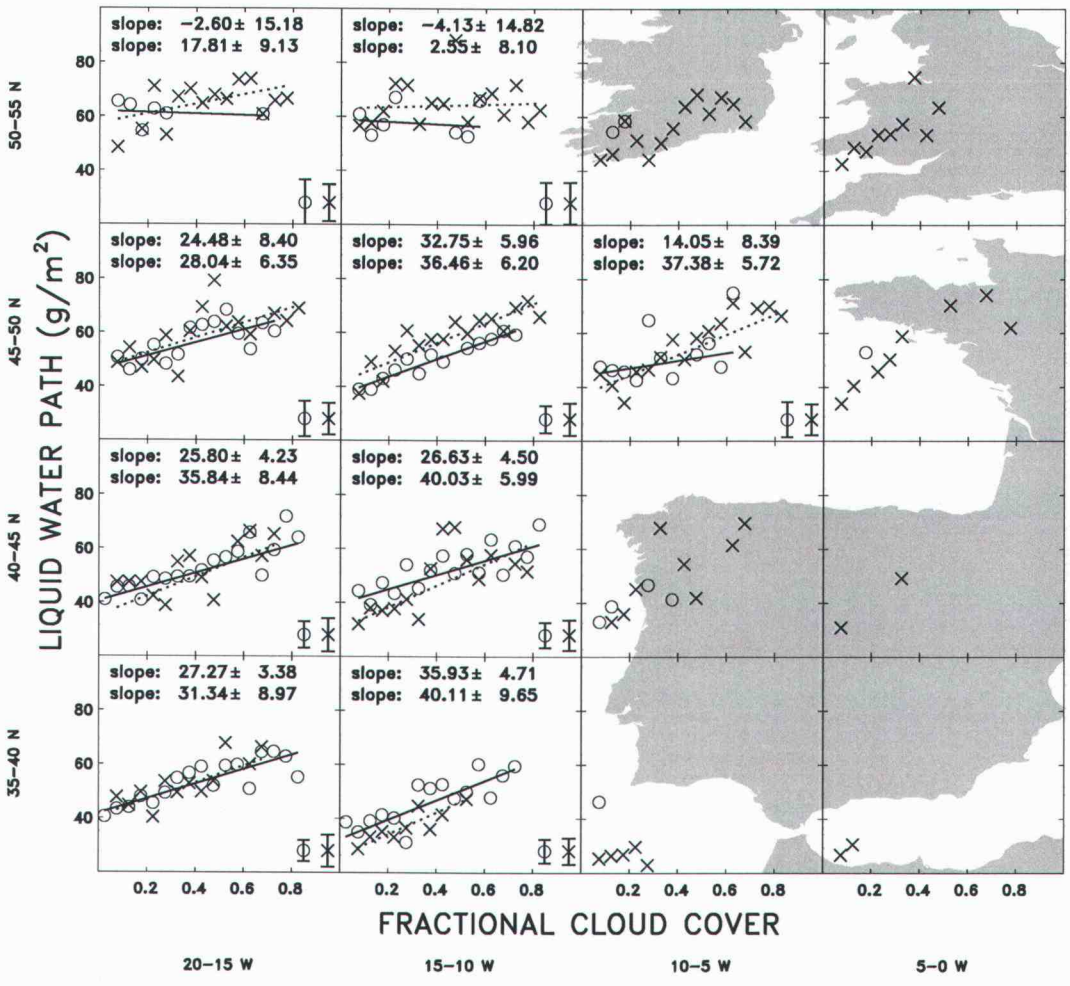

Figure 3.12. Same as Fig. 3.9, but for liquid water path (g/m^2).

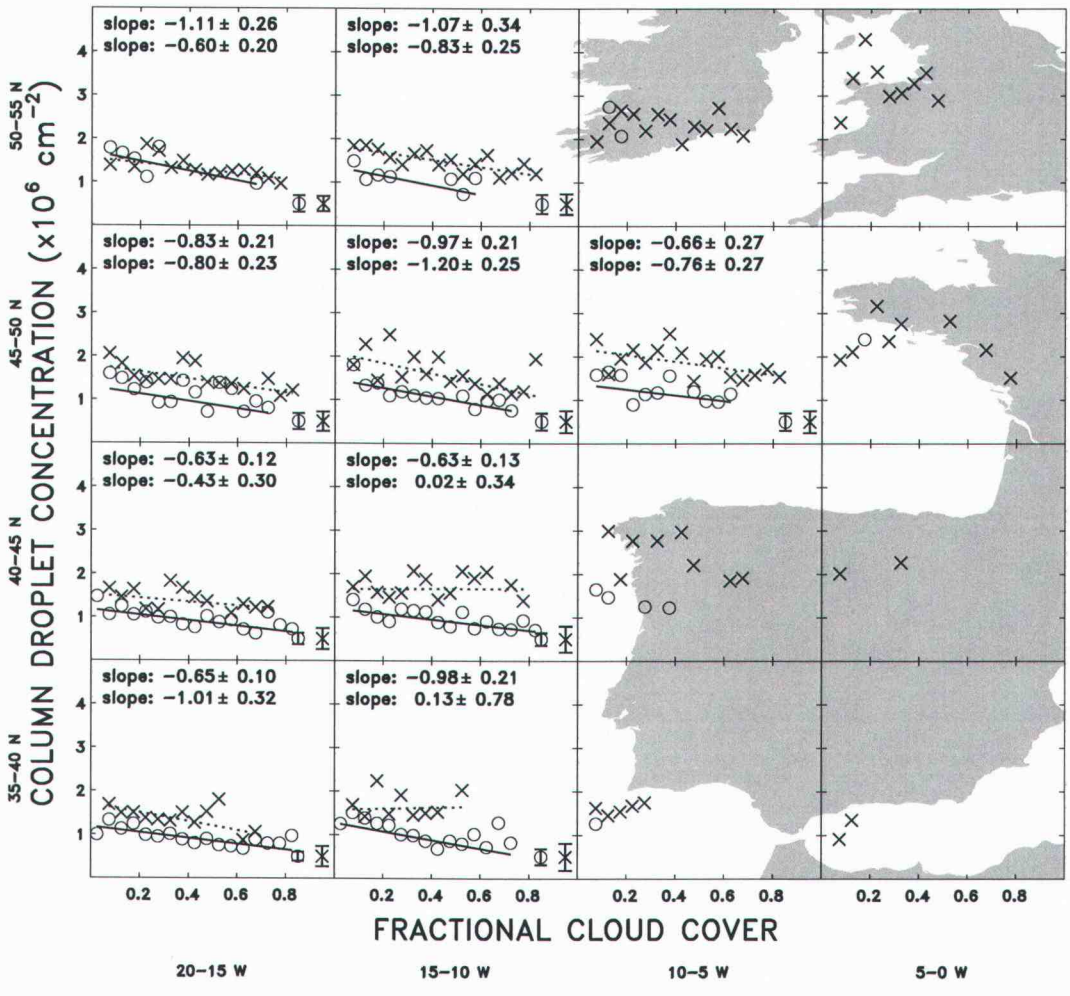

Figure 3.13. Same as Fig. 3.9, but for column droplet concentration (10^6 cm^{-2}).

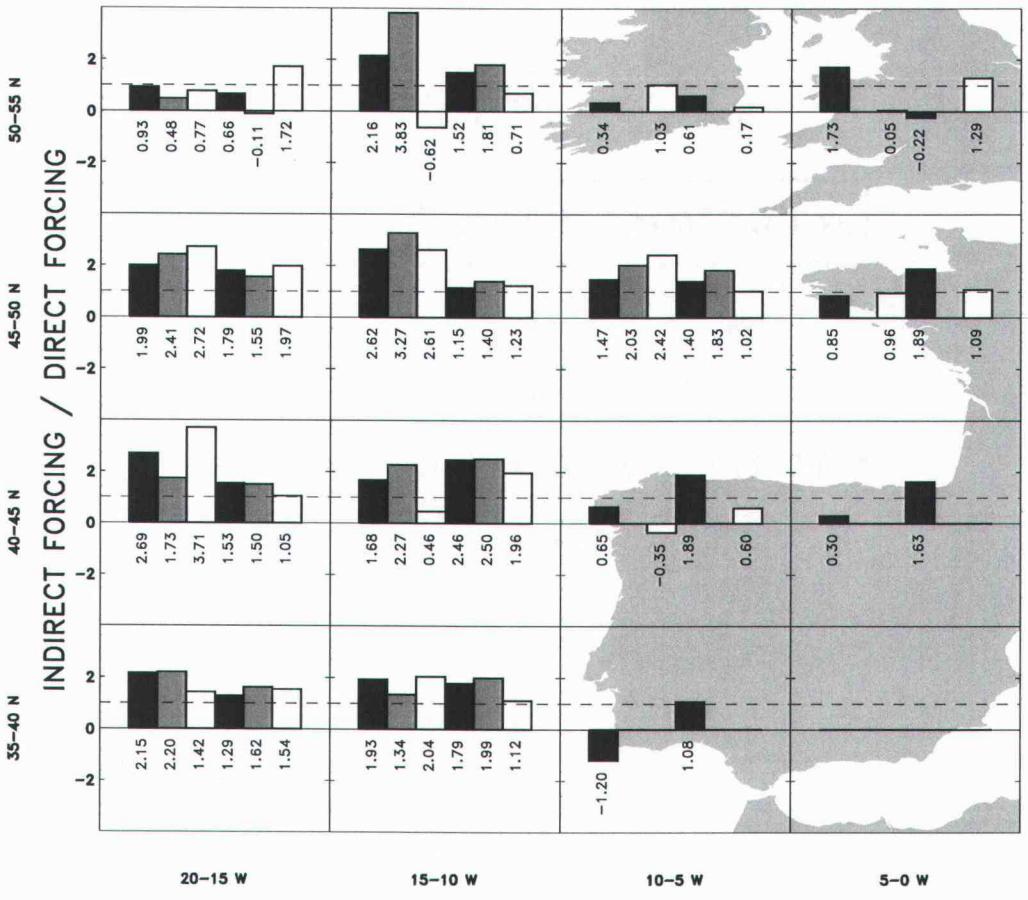

Figure 3.14. Ratio of indirect radiative forcing for overcast conditions to direct radiative forcing for cloud-free conditions. The three left-hand bars in each sub-panel are based on trends of cloud optical depth. The three right-hand bars in each sub-panel are based on trends of droplet effective radius and an assumption of fixed liquid water. The black bars use trends in cloud properties as a function of aerosol optical depth to calculate cloud optical depth. The gray bars are for the observations separated into clean clouds and polluted clouds and the trends in cloud properties as a function of fractional cloud cover (Figs. 3.9 and 3.10). The white bars are the results of MCT, which were calculated using the same method as used for the black bars. The dashed line shows the 1:1 line, where the indirect radiative forcing is equal to the direct radiative forcing.

Chapter 4
Effects of threshold retrievals on estimates of the aerosol indirect radiative forcing

4.1 Abstract

Empirical estimates of the aerosol indirect radiative forcing often rely on cloud properties derived from the application of thresholds to multispectral satellite imagery data. In such retrievals, pixels that surpass prescribed radiance thresholds are assumed to be overcast even if they are only partially cloud covered. The assumption leads to cloud optical depths that are underestimated and droplet radii that are overestimated. In addition, the changes in cloud optical depth and droplet radius for a given change in aerosol optical depth are overestimated with the threshold retrievals. A new retrieval scheme that accounts for fractional cloud cover within an imager pixel is used to estimate the enhancement in the indirect radiative forcing that arises from threshold cloud retrievals. The enhancement in estimates of the forcing prove to be relatively small, approximately 20%, on the order of the regional-scale variability in estimates of the forcing. If cloud liquid water is held fixed, the biases in droplet size and in the sensitivity of droplet size to changes in aerosol nearly cancel so that indirect radiative forcing estimates are almost the same for partly cloudy pixel and threshold retrievals.

4.2 Introduction

Many studies have sought to use satellite measurements to estimate the aerosol indirect radiative forcing [Kaufman and Nakajima, 1993; Kaufman and Fraser, 1997; Wetzel and Stowe, 1999; Nakajima et al., 2001; Seikiguchi et al., 2003; Quass et al. 2004]. While some of these studies applied measures of spatial

uniformity in infrared emission to ensure that the pixels being analyzed were overcast [Wetzel and Stowe, 1999; Nakajima et al., 2001] for the most part, the studies used threshold retrievals to derive the cloud properties. Such retrievals treat imager pixels that surpass radiance thresholds as being overcast, even though the pixels may be only partially cloud covered.

Recently, Coakley et al. [2005] developed a cloud property retrieval scheme that explicitly accounts for partly cloudy imager pixels. They showed that threshold retrievals overestimate droplet effective radius and underestimate cloud optical depth, liquid water path, and column number concentration. Matheson et al. [2005ab] used the partly cloudy pixel retrieval algorithm to investigate the aerosol indirect radiative forcing by examining changes in cloud properties in response to changes in aerosol optical depth. Here, aspects of the study are repeated using threshold retrievals for the cloud properties to determine how the threshold properties influence estimates of the aerosol indirect radiative forcing.

4.3 Data and methodology

The methodology used in the current study is described in Matheson et al. [2005a] and described here briefly. 4-km Global Area Coverage (GAC) radiances from the AVHRR aboard the *NOAA-14* satellite were analyzed for all daytime satellite passes for May-August 1995-1999 over the northeastern Atlantic. The region of analysis was bounded by 35°–55° N latitude and 0°–20° W longitude. Pixels over land were not used. Pixels that were within 40° of the sun's reflection, assuming specular reflection from a flat surface, were taken to have been affected by sun glint and were removed from further analysis.

A scene identification scheme was used to identify 4-km pixels as cloud-free, partially covered by clouds, completely overcast by clouds in a single layer, or containing clouds that were distributed in altitude. For cloud-free pixels, a scheme

developed for retrieving aerosol properties for the Indian Ocean Experiment (INDOEX) was used [Coakley et al. 2002].

For pixels that the scene identification scheme identified as being overcast by single-layered, low-level clouds, radiances at 0.64, 3.7 and 11 μm were used to retrieve 0.64-μm cloud optical depth, τ_c, droplet effective radius, R_e, and cloud altitude, z_c. Midlatitude summertime profiles of temperature, humidity, and ozone concentrations were used to estimate the absorption of sunlight and emission by atmospheric gases in the AVHRR channels. For partly-cloudy pixels, the pixel radiances were assumed to have a linear mixture of the radiances that would be seen if the pixels were either completely overcast or completely cloud-free, so that,

$$I = (1 - A_c) I_s + A_c I_c(\tau_c, R_e, z_c)$$

where I is the radiance observed by the satellite instrument, A_c is the fractional cloud cover for the pixel, I_s is the average radiance for the cloud-free portion of the pixel, and $I_c(\tau_c, R_e, z_c)$ is the average radiance for the cloud-covered portion of the pixel. With z_c given by the altitude retrieved for nearby pixels that were overcast, radiances at 0.64, 3.7, and 11 μm were used to derive A_C, τ_C, and R_e. Radiances in the cloud-free portions of the partly cloudy pixels were assumed to be equal to the mean of the radiances taken from nearby cloud-free pixels, or lacking sufficient nearby cloud-free pixels, from a monthly and regional climatology of cloud-free radiances. In turn, these retrieved properties were used to derive cloud liquid water path, $W = \frac{2}{3} R_e \tau_c \rho$, where ρ = 1 g cm^{-3} is the density of water, and column droplet concentration, $N_c = \frac{\tau_c}{Q \rho R_e^2}$, where Q is the scattering efficiency, here taken to be 2.

In order to simulate threshold retrievals, radiances from pixels identified as partly cloudy that had a pixel-scale fractional cloud cover greater than 0.20 were used as inputs to the overcast retrieval scheme to calculate a new set of cloud properties assuming that the pixel was overcast. Because errors in retrievals of cloud properties in pixels that have a pixel-scale fractional cloud cover less than 0.20 are large, pixels with pixel-scale fractional cloud cover less than 0.20 were removed from the data for both the partly cloudy pixel and threshold schemes. Of all pixels that contained clouds from single-layered, low-level cloud systems that had a fractional cloud cover greater than 0.20, 56.2% were identified as being overcast. The average pixel-scale cloud cover of the partly cloudy pixels was 0.67.

Pixel-scale observations for each satellite pass were mapped into 1° □ 1° latitude-longitude regions. The cloud screening rules described in Matheson et al. [2005a] were used to ensure that the clouds in the 1° latitude-longitude regions selected for analysis were all part of a single-layered, low-level cloud system. In addition the region had to contain sufficient numbers of cloudy and cloud-free pixels to allow reliable determination of the average cloud and aerosol properties within the region. For the partly cloudy retrieval scheme, the pixel-scale cloud properties were weighted by the pixel-scale fractional cloud cover to calculate the average properties.

The means of the 1□latitude-longitude regions were gathered into 5° □ 5° latitude-longitude regions in order to increase the number of samples exhibiting relatively homogeneous aerosol and cloud properties and to avoid, to the extent possible, the effects of geographic gradients in the cloud and aerosol properties observed for the northeastern Atlantic. Within each 5□region the 5^{th} and 95^{th} percentiles of the 1° latitude-longitude overpass means of all cloud and aerosol properties were calculated. With the exception of fractional cloud cover, which ranges from 0 to 1, if the mean value of an aerosol or cloud property for a 1° region from a single satellite overpass was outside the 5^{th} and 95^{th} percentiles for a particular 5° region for the five-year period, that 1° mean was considered an outlier

and all aerosol and cloud properties for that 1° region and overpass were eliminated.

Matheson et al. [2005b] demonstrated that the means and standard deviations of the means for the 1° cloud and aerosol properties within the 5° regions were consistent from year to year and that the inter-annual variability was much smaller than the day-to-day variability. The year-to-year consistency of the cloud and aerosol properties justified combining all five years of data into a single ensemble for each 5□region.

4.4 Collocated aerosol optical depths and cloud properties

Figures 4.1-4.3 show properties of low-level, single-layered clouds associated with aerosol optical depth. The cloud properties in each 5° latitude-longitude regions were divided into 0.05 wide bins of the 0.55-μm aerosol optical depth. The mean and standard error of the overpass means were calculated for each aerosol bin, where the standard error is the standard deviation divided by the square-root of the number of independent samples, in this case, the number of satellite overpasses that contributed observations to that bin. Bins with overpass means from fewer than 10 separate satellite overpasses were excluded. The slope and standard deviation of the slope for the trends were estimated from a linear fit to the bin means weighted by the inverse of the standard errors of the bin means [Bevington, 1969]. One 5° latitude-longitude region had bin-means from fewer than five bins, which was considered insufficient for calculating trends, and was left blank in the figures. In Figs. 4.1-4.3, the circles are the results for the partly cloudy pixel retrievals and the crosses are the results for the threshold retrievals.

The cloud optical depths retrieved by the threshold scheme are smaller than those retrieved by the partly cloudy scheme (Fig. 4.1). The mean cloud optical depth presented in Fig. 4.1 is 6.0 for the threshold retrievals and 7.2 for the partly cloudy pixel retrievals. In most of the 5° latitude-longitude regions, cloud optical

depth increased as aerosol optical depth increased. The mean slope, weighting the 15 regions equally, is 4.1 per unit change in aerosol optical depth for the partly cloudy pixel retrievals and 4.4 for the threshold retrievals, that is, the threshold retrievals amplify the change in cloud optical depth for a given change in aerosol loading by about 10%.

Droplet effective radii retrieved by the threshold retrieval scheme are generally larger than those retrieved by the partly cloudy pixel retrieval scheme (Fig. 4.2). The mean droplet radius in Fig. 4.2 is 12.6 μm for the threshold retrievals and 11.2 μm for the partly cloudy pixel retrievals. Because droplet number concentration is proportional to τ_c / R_e^2, droplet number concentration is also underestimated by the threshold retrievals. The 1° latitude-longitude mean of column number concentration is 0.91×10^6 cm^{-2} for the threshold retrievals and 1.45×10^6 cm^{-2} for the partly cloudy pixel retrievals. Droplet effective radius decreased as aerosol optical depth increased in most of the 5° latitude-longitude regions (Fig. 4.2). The mean slope, weighting the 15 regions equally, is –5.7 μm per unit change in aerosol optical depth for the partly cloudy pixel retrievals and –6.5 μm for the threshold retrievals.

Twomey's first estimates of the aerosol indirect radiative forcing assumed fixed cloud liquid water amounts [Twomey, 1974]. Albtrecht [1989] suggested that cloud liquid water would increase with increasing aerosol burden owing to the suppression of drizzle. In many of the 5° regions, particularly in the coastal regions, cloud liquid water decreased with increasing aerosol burden. Air masses with larger aerosol burdens probably originated over the continent and were therefore likely to be dryer than the less polluted, oceanic air masses. Ackerman et al. [2004] suggest that when the air in the free troposphere above the clouds is sufficiently dry, polluted clouds should lose liquid water, as appears to occur in the results shown in Fig. 4.3.

The average trend in Fig. 4.3 is –3.2 g/m^2 per unit aerosol optical depth for the partly cloudy pixel retrievals and –0.8 g/m^2 for the threshold retrievals. The

standard error of the errors of the slopes for the partly cloudy retrievals is 4.2 g/m^2, so the difference in the means of the slopes between the partly-cloudy and threshold retrievals is not statistically significant. On the other hand, 5 of the fifteen 5° latitude-longitude regions, using the partly cloudy pixel results, have downward slopes greater than twice the error of the slopes, here taken to be a measure of statistical significance. Because its biases in cloud properties tend to preserve the estimates of cloud liquid water, the threshold retrievals show 3 of the fifteen 5° regions having downward slopes greater than twice the error of the slopes. Evidently, clouds can lose liquid water as aerosol optical depth increases but the threshold retrievals appear to underestimate this loss of liquid water.

4.5 Radiative forcing estimates

As 0.55-μm aerosol optical depth increases, threshold retrievals of cloud optical depth increase more and threshold retrievals of droplet effective radius decrease more than do the partly-cloudy pixel retrievals of these properties. These trends enhance the apparent strength of the aerosol indirect effect when, in fact, they are caused by biases in the threshold retrievals. To investigate the impact of these trends on radiative forcing estimates, top of the atmosphere fluxes were calculated in each of the 5□latitude-longitude regions using a broadband radiative transfer model that accounts for scattering and absorption by gases, aerosols, and clouds [Coakley et al., 2002].

The radiative transfer model was run twice without clouds to determine the direct radiative forcing for cloud-free conditions, once with a small amount of aerosols and once with a larger amount of aerosols. The 0.55-μm aerosol optical depths were chosen to be 0.15 and 0.25 in order to measure the response of the system to a 0.1 change in aerosol optical depth. The difference in the top of the atmosphere fluxes between these two cases is taken to be the direct radiative forcing. The radiative transfer model was then run twice with overcast clouds

overlying the aerosol to determine the indirect radiative forcing for overcast conditions, once with a cloud optical depth for clean clouds overlying the small amount of aerosols and again for polluted clouds overlying the larger amount of aerosol. The difference in the top of the atmosphere fluxes between these cases is the aerosol indirect radiative forcing for overcast conditions. The cloud optical depths were calculated using the given aerosol optical depths and the trend lines in Fig. 4.1. These calculations were performed with the results of both the partly cloudy pixel and the threshold retrieval schemes. The results of these radiative forcing calculations are presented as the squares in Figure 4.4. The entire set of calculations was repeated using the same aerosol optical depths, but using the linear trends from Fig. 4.2 and an assumption of fixed cloud liquid water. Results from these calculations are presented as the pluses in Fig. 4.4.

The means of the forcings using the observed trends in cloud optical depth, weighting all 15 regions equally, were –5.3 W/m^2 for the partly cloud pixel retrievals and –6.6 W/m^2 for the threshold retrievals, an increase of 22%. The mean bias and RMS deviation were –1.3 and 2.9 W/m^2 respectively. The change in reflectivity of a cloud is approximately proportional to $\Delta\tau_c/\tau_c$ so that although $\Delta\tau_c$ is only 10% larger in the threshold retrievals, τ_c is 18% smaller, creating the 22% bias in radiative forcing when using the threshold retrievals.

For the methods that allow liquid water to vary, the ratios of indirect forcing for overcast conditions to direct forcing for cloud-free conditions are 1.4 for the partly cloudy pixel retrievals and 1.7 for the threshold retrievals. Matheson et al. [2005b] used the partly cloud pixel retrievals to measure the changes in cloud optical depth for a measured change in fractional cloud cover for clean and polluted clouds. They found a ratio of indirect to direct forcing of 2.2. Using threshold retrievals bias estimates of the aerosol indirect radiative forcing, this bias is larger than the standard error of the radiative forcing estimates of the fifteen 5° latitude-longitude regions.

The means of the forcings when liquid water was held fixed were –5.4 W/m^2 and –5.5 W/m^2 for the partly cloudy pixel and threshold retrievals respectively. The mean bias was –0.1 W/m^2 and the RMS deviation was 1.2 W/m^2. The change in cloud optical depth for fixed liquid water is approximately proportional to $\Delta R_e / R_e$. Although ΔR_e increased approximately 15 % for the threshold retrievals, R_e also increased by about 12%. The bias in droplet effective radius and in the sensitivity of droplet radius to changes in aerosol optical depth in the threshold retrievals nearly cancel each other in the estimates of aerosol indirect radiative forcing.

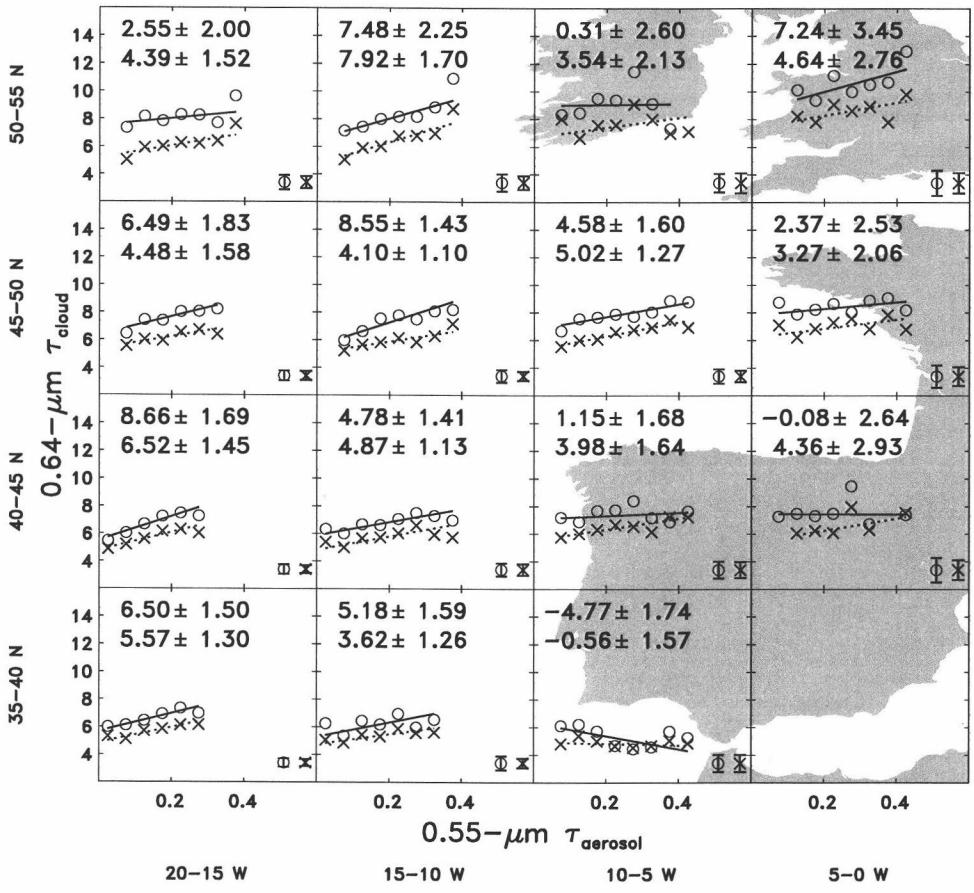

Figure 4.1. Means of overpass averaged 0.64-μm cloud optical depth for 1□ latitude-longitude regions binned for each 0.05 interval of 0.55-μm aerosol optical depth. Each sub-panel contains observations for that 5□□ 5□latitude-longitude region. Circles are for the partly cloudy pixel retrievals, crosses are for the threshold retrievals. Error bars in the lower right corner are the RMS of the standard error for the data points. The solid (dashed) line is a linear fit to the bin means of the circles (crosses) inversely weighted by the standard error. Also given are the mean and standard deviation estimated for the slope of the linear fit to the circles (upper) and crosses (lower). Results for the partly cloudy pixel retrievals are the same as Matheson et al. [2005b].

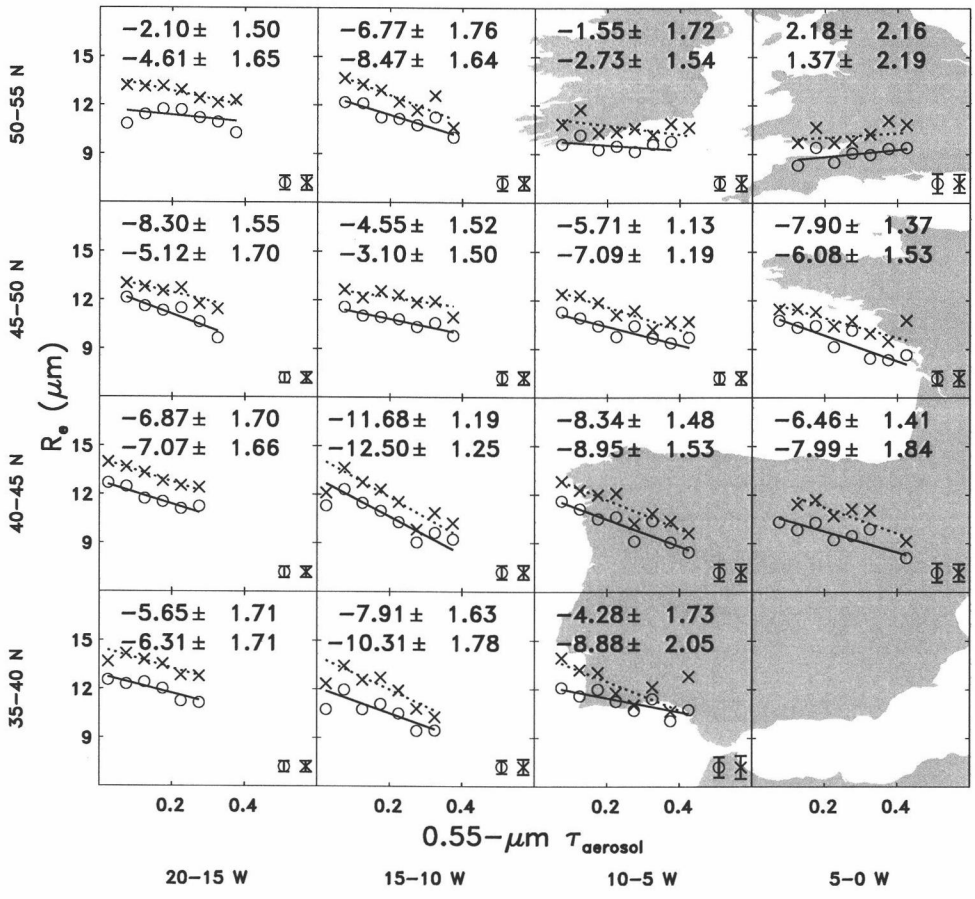

Figure 4.2. Same as Fig. 4.1, but for droplet effective radius (μm).

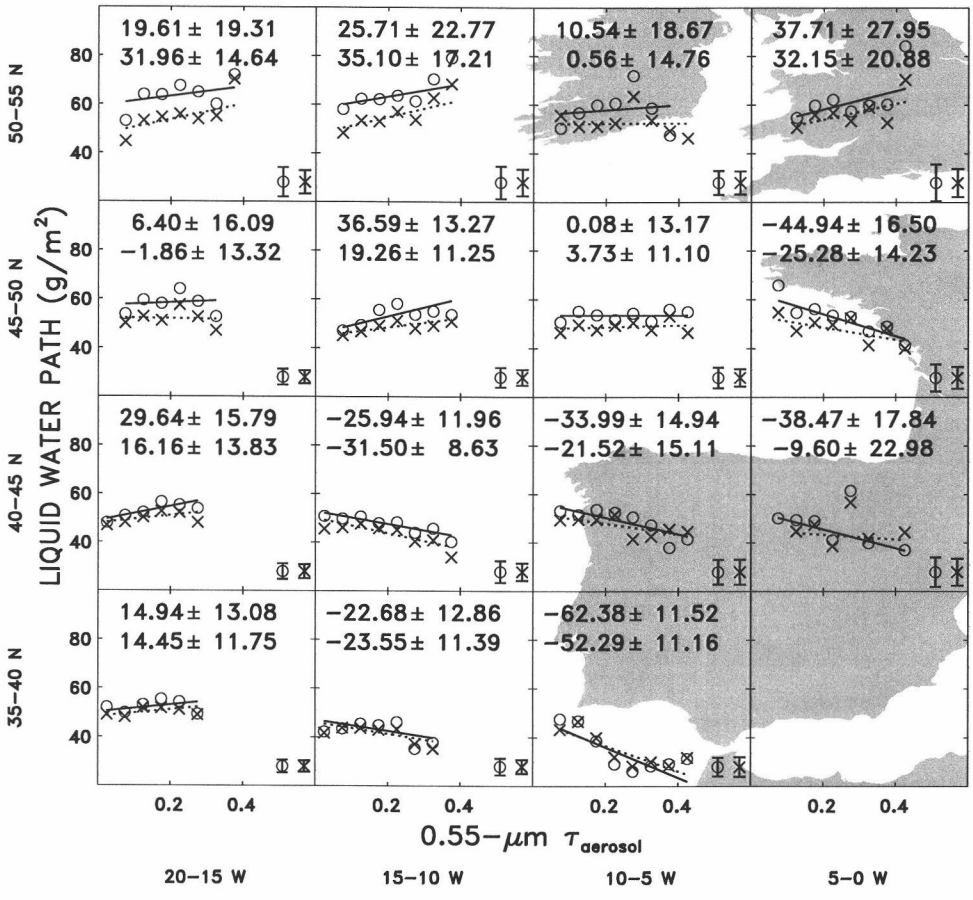

Figure 4.3. Same as Fig. 4.1, but for liquid water path (g/m^2).

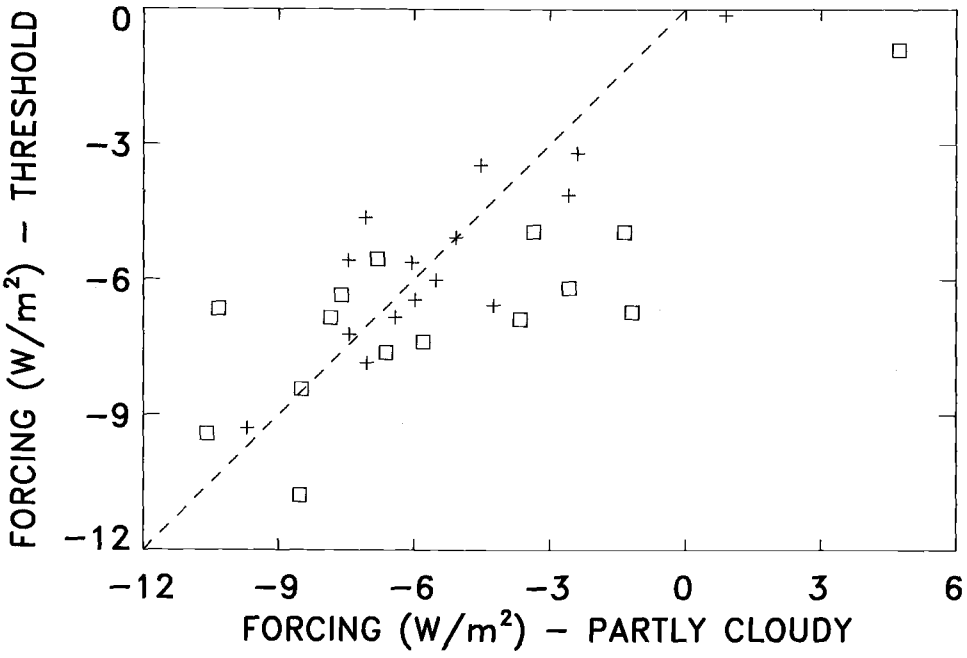

Figure 4.4. Radiative forcing estimates for overcast conditions (W/m^2) based on partly cloud pixel and threshold retrievals for an increase of 0.55-μm aerosol optical depth of 0.1 (from 0.15 to 0.25). Squares are the forcings using the changes in cloud optical depth taken from the linear fits in Fig. 4.1. Pluses are the forcings using the changes in droplet effective radius taken from the linear fits in Fig. 4.2 and assuming a constant liquid water path.

Chapter 5
Conclusion

5.1 Introduction

The largest uncertainty in predicting the magnitude of human impact on climate is the lack of scientific understanding concerning the aerosol indirect radiative forcing (IPCC, 2001). This thesis has described an improved methodology for using satellite observations to estimate the magnitude of aerosol indirect radiative forcing. In addition, the study identified situations that might be falsely attributed to the effect of aerosols on clouds.

5.2 Advancements in methodology

AVHRR observations over the northeastern Atlantic were used to derive aerosol optical depth and cloud properties for single-layered, low-level clouds. Cloud and aerosol properties were associated if they were from the same $1° \times 1°$ latitude-longitude region and the same satellite overpass. Because the observations were nearly simultaneous and within close spatial proximity, the observed cloud properties were likely to be influenced by the nearby aerosol. Some previous studies compared observations on different days or from widely spaced geographic locations. In addition, the 1° latitude-longitude observations were composited within the associated $5° \times 5°$ latitude-longitude regions. Constraining the data to small regions limited the influence of large-scale geographic trends. Smaller regions would have been preferable, but the smaller number of cases in each region would have decreased the statistical confidence in the results. Many previous studies have composited their data into much larger regions, even producing globally averaged results.

Only the Wetzel and Stowe (1999) study and the work reported in this study used multiple years of data. For the summertime north Atlantic, inter-annual variability of the means of cloud properties were much smaller than day-to-day variability, allowing five years of data do be combined into a single ensemble of cases. The five-fold increase in data over the one-year study improved statistical confidence in the results. The larger ensemble also allowed for the separation of the data into "clean" and "polluted" cases. Cloud properties were compared against fractional cloud cover for both the clean and polluted cases. The clean and polluted cases were clearly distinguishable, providing evidence for the Twomey effect. The cloud properties of both the clean and polluted cases exhibited trends with fractional cloud cover, showing that there are changes in clouds that are not necessarily being caused by an increase in aerosol burden.

Another innovation was the use of the newly available partly-cloud pixel retrieval scheme. Previous studies had used threshold retrieval schemes to retrieve cloud properties. Threshold retrievals are known to produce biased results for the cloud properties. Estimates of the radiative forcing using the results from the threshold retrieval scheme were larger in magnitude than those based on the partly cloudy pixel scheme. The bias in radiative forcing estimates caused by using threshold retrievals is larger than the standard error of the radiative forcing estimates in the 15 different 5° latitude longitude regions, indicating that the bias has statistical significance.

5.3 Associated cloud and aerosol properties

In general, clouds responded to aerosols as would be expected on the basis of the Twomey Effect. As aerosol optical depth increased, droplet number concentration and cloud optical depth increased while droplet effective radius decreased. This behavior was found both when the cloud properties were correlated with aerosol optical depth and when the clean clouds were compared to

the polluted clouds. On the other hand, cloud properties varied in systematic ways when the data set was divided into "clean" and "polluted" cases based on the 40th and 60th percentiles of aerosol optical depth. Droplet effective radius and liquid water path increased and column droplet concentration decreased with increasing cloud cover for both the clean and polluted clouds. When investigating aerosol indirect radiative forcing, changes in cloud properties that are caused by the Twomey Effect need to be distinguished from changes due to other causes.

Cloud liquid water remained constant or decreased as cloud optical depth increased contrary to the prediction that increased aerosol optical depth will suppress drizzle and increase the liquid water content of the clouds (Albrecht, 1989). It was suggested that air masses with large aerosol concentrations are associated with dry, continental air and air masses with small aerosol concentrations are associated with moist, oceanic air. The amount of moisture being entrained through the cloud tops can affect liquid water content (Ackerman et al., 2004). The role of moisture in the air mass above the cloud and changes in cloud properties as fractional cloud cover changes must be disentangled from the role of changing aerosol burden in order to improve estimates of aerosol indirect radiative forcing.

Aerosol optical depth appeared to increase as fractional cloud cover increased. A number of explanations were given for this finding including: cloud contamination, the swelling of aerosol particles in the high humidity environments near clouds, increased illumination of the aerosols by sunlight reflected from the sides of clouds, increased particle production near clouds, and in-cloud processing of aerosol particles. Cloud optical depth also increased as fractional cloud cover increased. Because both cloud and aerosol optical depth increase as fractional cloud cover increased, some of the increase seen in cloud optical depth as aerosol optical depth increased may not be due to the Twomey effect, but may be due to thermodynamic processes, such as elevated relative humidity, affecting both he aerosols and the clouds.

Estimates of the aerosol indirect radiative forcing were made using a broadband radiative transfer model. The changes in cloud properties were calculated using: 1) the observed changes in cloud optical depths far a prescribed change in aerosol optical depth, 2) changes in cloud optical depths for measured changes in fractional cloud cover between clean and polluted clouds, 3) the observed changes in droplet effective radii for a prescribed change in aerosol optical depth and an assumption of fixed liquid water, and 4) changes in droplet effective radii for measured changes in fractional cloud cover between clean and polluted clouds and an assumption of fixed liquid water. Aerosol indirect radiative forcing for overcast conditions was found to be 1.4 to 2.2 times larger than the direct radiative forcing for cloud-free conditions depending on which of the four methods was used to calculate changes in cloud properties. These results are similar to the results of Kaufman and Fraser (1997), who studied the effects of smoke on low-level clouds over the Amazon, but smaller than the ratios given by Sekiguchi et al. (2003), who calculated an indirect forcing for overcast conditions that was 3.0 to 4.5 times larger than the direct radiative forcing for cloud-free conditions.

In order to investigate possible biases introduced into the radiative forcing calculations using threshold retrievals, radiative forcing estimates were made using both the partly cloudy pixel and threshold retrievals. When cloud liquid water was held constant, the radiative forcing estimates based on the threshold retrievals were not significantly biased when compared to the forcing estimates using the partly cloudy pixel retrievals. When liquid water was allowed to vary, the ratios of indirect to direct radiative forcing were 1.4 for the partly cloud pixel retrievals and 1.7 for the threshold retrievals. In this case, threshold retrievals bias the estimates of the aerosol indirect radiative forcing by about 20%. In chapter 3, the liquid water was allowed to vary and the partly cloudy pixel retrievals were used, but two methods were used for estimating changes in cloud optical depth: 1) using the trends in cloud optical depth associated with aerosol optical depth and 2) using the changes in cloud optical depth between the "clean" and "polluted" data sets. The ratios for indirect to direct forcing using these two methods were 1.4 and 2.2,

respectively. Using threshold retrievals introduces a relatively small error when compared with the range of forcings estimated by different methods of calculating changes in cloud optical depth for a given change in aerosol burden.

5.4 Future work

The research presented in this thesis focused on clouds and aerosols over the northeastern Atlantic for May-August, 1995-1999. These years were chosen because they were all observed by *NOAA-14* and calibration between satellites was not an issue. Careful calibration between *NOAA-14* and other AVHRR satellites could extend the temporal coverage of the analysis. The results of this thesis should be compared to instruments with finer resolution, such as the Moderate Resolution Imaging Spectroradiometer (MODIS), to determine if the results are dependant of the spatial scales of the observations.

The results for clouds and aerosols over the northeastern Atlantic should be compared to results from the other major regions of marine stratocumulus: the north Pacific off the California coast, the southern Atlantic off the coast of southern Africa, the southern Pacific off the coast of Peru and the Indian Ocean west of Australia. These later two regions would be interesting for studying the natural variability of clouds with aerosol optical depth held fixed, because these regions have little anthropogenic aerosol.

It has been assumed in these studies that clouds and aerosols within in the same $1° \times 1°$ latitude-longitude region are interacting. It is possible, however, that the clouds and aerosols occur at different levels in the atmosphere and are not interacting. A profiling instrument, such as the lidar instrument to be launched on the *CALIPSO* satellite, will help assess the heights of the cloud and aerosol layers and whether the clouds and aerosols are likely to be interacting. Such an instrument will also improve screening of the data for thin cirrus clouds.

In much of this thesis, two cloud or aerosol properties were compared while allowing all other properties to take on any values. This method was slightly refined by dividing the data into clean and polluted parts, which partially constrained the range aerosol optical depths. Relationships between two properties, say aerosol optical depth and droplet effective radius, should be explored while other properties, such as cloud altitude and fractional cloud cover, are held constant. Such a study would require a data set much larger than that used for this thesis.

Bibliography

Abshire, J.B., J.C. Smith, and B.E. Schutz, 1998: The geoscience laser altimeter system (GLAS). *American Institute of Physics (AIP) Conf. Proc.*, **240**, 33-37.

Ackerman, A.S., O.B. Toon, D.E. Stevens, A.J. Heymsfield, V. Ramanathan, E.J. Welton, 2000: Reduction of tropical cloudiness by soot. *Science*, **288**, 1042-1047.

Ackerman, A.S., O.B. Toon, D.E. Stevens, and J.A. Coakley, Jr., 2003: Enhancement of cloud cover and suppression of nocturnal drizzle in stratocumulus polled by haze. *Geophys. Res. Lett.* **30**(7), doi:10.1029/2002GL016634.

Ackerman, A.S., M.P. Kirkpatrick, D.E. Stevens, and O.B. Toon, 2004: The impact of humidity above stratiform clouds on indirect aerosol climate forcing. *Nature*, **432**, 1014-1017.

Albrecht, B.A., 1989: Aerosols, cloud microphysics, and fractional cloudiness. *Science*, **245**, 1227-1230.

Albrecht, B.A., C.S. Bretherton, D. Johnson, W.H. Scubert, and A.S. Firsch, 1995: The Atlantic stratocumulus transition experiment – ASTEX. *Bull. of Amer. Met. Soc.*, **76**, 889-904.

Anderson, T.L., R.J. Charlson, D.M. Winker, J.A. Ogren, and K. Holmén, 2003: Mesoscale variations of tropospheric aerosols. *J. Atmos. Sci.*, **60**, 119-136.

Bevington, P.R., 1969: *Data Reduction and Error Analysis for the Physical Sciences*. Mcgraw-Hill, New York.

Brenguier, J.-L., P.Y. Chuang, Y. Fouquart, D.W. Johnson, F. Parol, H. Pawlowska, J. Pelon, L. Schüller, F. Schröder, and J. Snider, 2000a: An overview of the ACE-2 CLOUDYCOLUMN closure experiment. *Tellus*, **52B**, 815-827.

Brenguier, J.-L., H. Pawlowska, L. Schüller, R. Preusker, J. Fischer, and Y. Fouquart, 2000b: Radiative properties of boundary layer clouds: Droplet effective radius versus number concentration. *J. Atmos. Sci.*, **57**, 803-821.

Bréon, F.-M., D. Tanré, S. Generoso, 2002: Aerosol effect on cloud droplet size monitored from satellite. *Science*, **295**, 834-838.

Clarke, A.D., et al. 2002: INDOEX aerosol: A comparison and summary of chemical, microphysical, and optical properties observed from land, ship, and aircraft. *J. Geophys. Res.*, **107**(D19), 8033, doi:10.10292001JD000572.

Coakley, J.A., Jr. and C.D. Walsh, 2002: Limits to the aerosol indirect radiative effect derived from observations of ship tracks. *J. Atmos. Sci.*, **59**, 668-680.

Coakley, J.A., Jr., W.R. Tahnk, A. Jayaraman, P.K. Quinn, C. Devaux, and D. Tanré, 2002: Aerosol optical depths and direct radiative forcing for INDOEX derived from AVHRR: Theory. *J. Geophys. Res.*, **107**(D19), doi:10.1029/2000JD000182.

Coakley, J.A., Jr., M.A. Friedman, and W.R. Tahnk, 2005: Retrievals of cloud properties for partly cloudy imager pixels. *J. Atmos. Oce. Tech.*, **22**, 3-17.

Feichter, J., E. Roeckner, U. Lohmann, B. Liepert, 2004: Nonlinear aspects of the climate response to greenhouse gas and aerosol forcing. *J. Climate*, **17**, 2384-2398.

Han, Q., W.B. Rossow, and A.A. Lacis, 1994: Near-global survey of effective droplet radii in liquid water clouds using ISCCP data. *J. Climate*, **7**, 465-497.

Han, Q., W.B. Rossow, J. Chou, and R.M. Welch, 1998: Global variation of column droplet concentration in low-level clouds. *Geophys. Res. Lett.* **25**, 1419-1422.

Harshvardhan, S.E. Schwartz, C.M. Benkovitz, and G. Guo, 2002: Aerosol influence on cloud microphysics examined by satellite measurements and chemical transport modeling. *J. Atmos. Sci.*, **59**, 714-725.

Hess, M., P. Koepke, and I. Schult, 1998: Optical properties of aerosols and clouds: The software package OPAC. *Bull. of Amer. Met. Soc.*, **79**, 831-844.

Ignatov, A., P. Minnis, N. Loeb, B. Wielicki, W. Miller, S. Sun-Mack, D. Tanré, L. Remer, I. Laszlo, and E. Geier, 2005: Two MODIS aerosol products over ocean on the Terra and Aqua CERES SSF datasets. *J. Atmos. Sci.*, **62**, 1008-1031.

Intergovernmental Panel on Climate Change (IPCC), 2001: *Climate Change 2001: The Scietific Basis*, edited by J.T. Houghton et al., Cambridge Univ. Press, New York, New York.

Johnson, D.W., S. Osborne, R. Wood, K. Suhre, R. Johnson, S. Businger, P.K. Quinn, A. Wiedensohler, P.A. Durkee, L.M. Russell, M.O. Andreae, C.

O'Dowd, K.J. Noone, B. Bandy, J. Rudolph, and S. Rapsomanikis, 2000: An overview of the Lagrangian experiments undertaken during the North Atlantic regional Aerosol Characterization Experiment (ACE-2). *Tellus*, **52B**, 290-320.

Kaufman Y.J. and T. Nakajima, 1993: Effect of Amazon smoke on cloud microphysics and albedo – Analysis from satellite imagery. *J. Appl. Meteor.*, **32**, 729-744.

Kaufman, Y.J. and R.S. Fraser, 1997: The effect of smoke particles on clouds and climate forcing. *Science*, **277**, 1636-1639.

Kidwell, K. B., 1995: *NOAA Polar Orbiter Data Users Guide* (Washington, D.C.: U.S. Department of Commerce, National Oceanic and Atmospheric Administration, National Environmental Satellite, Data, and Information Service, National Climatic Data Center, Satellite Date Services Division).

King, M.D., W.P. Menzel, Y.J. Kaufman, D. Tanré, B.-C. Gao, S. Platnick, S.A. Ackerman, L.A. Remer, R. Pincus, and P.A. Hubanks, 2003: Cloud and aerosol properties, precipitable water, and profiles of temperature and water vapor from MODIS. *IEEE Trans. Geosci. Remote Sensing*, **41**, 442-458.

Krüger, O. and H Grassl, 2002: The indirect effect over Europe. *Geophys. Res. Lett.* **29**(19), doi:10.1029/2001GL014081.

Kütz, S. and R. Dubois, 1997: Balloon-borne aerosol measurements in the planetary boundary layer: Particle production associated with a continental stratiform cloud. *Contributions to Atmospheric Physics*, **70**, 109-116.

Lelieveld, J. and J. Heintzenberg, 1992: Sulfate cooling effect on climate through in-cloud oxidation of anthropogenic SO_2. *Science*, **258**, 117-120.

Loeb N.G. and N. Manalo-Smith, 2004: Top-of-atmosphere direct radiative effect of aerosols over global oceans from merged CERES and MODIS observations. *J. Climate*, **18**, 3506-3526.

Lohmann U., and J. Feichter, 1997: Impact of sulfate aerosols on albedo and lifetime of clouds: A sensitivity study with the ECHAM4 GCM. *J. Geophys. Res.*, **102**(D12), 13,685-13,700.

Lohmann, U., J. Feichter, J. Penner, and R. Leaitch, 2000: Indirect effect of sulfate and carbonaceous aerosols: A mechanistic treatment. *J. Geophys. Res.*, **105**(D10), 12,193-12,206.

Lohmann, U., and G. Lesins, 2002: Stronger constraints on the anthropogenic indirect aerosol effect. *Science*, **298**, 1012-1015.

Matheson, M.A., J.A.Coakley, Jr., and W.R. Tahnk, 2005a: Aerosol and cloud property relationships for summertime stratiform clouds in the northeastern Atlantic from AVHRR Observations. *J. Geophys. Res.*, in press.

Matheson, M.A., J.A.Coakley, Jr., and W.R. Tahnk, 2005b: Multiyear AVHRR observations of summertime stratocumulus collocated with aerosols in the northeastern Atlantic. *J. Geophys. Res.*, submitted for publication.

Nakajima, T., A. Higurashi, K. Kawamoto, and J.E. Penner, 2001: A possible correlation between satellite-derived cloud and aerosol microphysical parameters. *Geophys. Res. Lett.* **28**, 1171-1174.

Nakajima, T., M. Sekiguhi, T. Takemura, I. Uno, A. Higurashi, D. Kim, B.J. Sohn, S.-N. Oh, T.Y. Nakajima, S. Ohto, I. Okada, T. Takamura, and K. Kawamoto, 2003: Significance of direct and indirect radiative forcings of aerosols in the East China Sea region. *J. Geophys. Res.*, **108**(D23), doi:10.1029/2002JD003261.

Platnick, S., P.A. Durkee, K. Nielson, J.P. Taylor, S-C. Tsay, M.D. King, R.J. Ferek, P.V. Hobbs, and J.W. Rottman, 2000: The role of background cloud microphysics in the radiative formation of ship tracks. *J. Atmos. Sci.* 57, 2607-2624.

Platnick, S., M.D. King, S.A. Ackerman, W.P. Menzel, B.A. Baum, J.C. Riédi, and R.A. Frey, 2003: The MODIS cloud products: Algorithms and examples from Terra. *IEEE Trans. Geosci. Remote Sens.*, **41**, 459-473.

Podgorny, I.A., 2003: Three-dimensional radiative interactions in a polluted broken cloud system. *Geophys. Res. Lett.*, **30**, 1771, doi:10.1029/2003GL017287.

Potter, G.L. and R.D. Cess, 2004: Testing the impact of clouds on the radiation budgets of 19 atmospheric general circulation models. *J. Geophys. Res.*, **109**(D2), D02106, doi:10.1029/2003JD004018.

Press, W.H., S.A. Teukolsky, W.T. Vetterling, and B.P. Flannery, 1994: *Numerical recipes in FORTRAN: The art of scientific computing, 2nd edition.* Cambridge University Press, New York, New York.

Quaas, J., O. Boucher, and F.-M. Bréon, 2004: Aerosol indirect effects in POLDER satellite data and the Météorologie Dynamique—Zoom (LMDZ)

general circulation model. *J. Geophys. Res.*, **109**(D8), D08205, doi:10.1029/2003JD004317, 2004.

Raes, F. T. Bates, F. McGovern, and M. Van Liedekerke, 2000: The 2nd aerosol characterization experiment (ACE-2): General overview and main results. *Tellus*, **52B**, 111-125.

Ramanathan, V., R.D. Cess, E.F. Harrison, P. Minnis, B.R. Barkstrom. E. Ahmad, and D. Hartmann, 1989: Cloud-radiative forcing and climate: Results from the Earth Radiation Budget Experiment. *Science*, **243**, 57-63.

Randall, D., M. Khairoutdinov, A. Arakawa, and W. Grabowski, 2003: Breaking the cloud parameterization deadlock. *Bull. Amer. Meteor. Soc*, **84**, 1547-1564.

Rotstayn, L.D., 1999: Indirect forcing by anthropogenic aerosols: A global climate model calculation of the effective-radius and cloud-lifetime effects. *J. Geophys. Res.*, **104**(D8), 9369-9380.

Rotstayn, L.D. and J.E. Penner, 2001: Indirect aerosol forcing, quasi forcing, and climate response. *J. Climate*, **14**, 2960-2975.

Schwartz, S.E., Harshvardhan, and C.M. Benkovitz, 2002: Influence of anthropogenic aerosol on cloud optical depth and albedo shown by satellite measurements and chemical transport modeling. *Proc. Nat. Acad. Sci.*, **99**, 1784-1798.

Seinfeld, J.H. and S.N. Pandis, 1998: *Atmospheric chemistry and physics: From air pollution to climate change.* John Wiley & Sons, Inc., New York, New York.

Sekiguchi, M., T. Nakajima, K. Suzuki, K. Kawamoto, A. Higurashi, D. Rosenfeld, I. Sano, S. Mukai, 2003: A study of the direct and indirect effects of aerosols using global satellite data sets of aerosol and cloud parameters. *J. Geophys. Res.*, **108**(D22), 4699, DOI:10.1029/2002JD003359.

Shibata, A., K. Imaoka, T. Koike, 2003: AMSR/AMSR-E level 2 and 3 algorithm developments and data validation plans of NASDA. *IEEE Trans. Geosci. Remote Sensing*, **41**, 195-203.

Suzuki, K., T. Nakajima, A. Numaguti, T. Takemura, K. Kawamoto, and A. Higurahi, 2004: A study of the aerosol effect on a cloud field with simultaneous use of GCM modeling and satellite observations. *J. Atmos. Sci.*, **61**, 179-194.

Szczodrak, M., P.H. Austin, and P.B. Krummel, 2001: Variability of optical depth and effective radius in marine stratocumulus clouds. *J. Atmos. Sci.*, **58**, 2912-2926.

Tahnk, W.R. and J.A. Coakley, Jr., 2001a: Improved calibration coefficients for *NOAA*-14 AVHRR visible and near-infrared channels. *Int. J. Remote Sens.*, **22**, 1269-1283.

Tahnk, W.R., and J.A. Coakley, Jr., 2001b: Updated calibration coefficients for *NOAA*-14 AVHRR channels 1 and 2. *Int. J. Remote Sens.* **22**, 3053-3057.

Twohy, C.H., M.D. Petters, J.R. Snider, B. Stevens, W. Tahnk, M. Wetzel, L. Russell, and F. Burnet, 2005: Evaluation of the aerosol indirect effect in marine stratocumulus clouds: Droplet size, liquid water path, and radiative impact. *J. Geophys. Res.*, **110**, D08203, DOI:10.1029/2004JD005116.

Twomey, S., 1974: Pollution and the planetary albedo. *Atmos. Env.*, **8**, 1251-1256.

Wetzel, M.A., and L.L. Stowe, 1999: Satellite-observed patterns in stratus microphysics, aerosol optical thickness, and shortwave radiative forcing. *J. Geophys. Res.*, **104**(D24), 31,287-31,299.

Winker, D.M., J.R. Pelon, and M.P. McCormick, 2003: The *CALIPSO* mission: Spaceborne lidar for observation of aerosols and clouds. *Lidar Remote Sensing for Industry and Environment Monitoring III., Proc. of* SPIE, **4839**, 1-11.